MELTING OF A VERTICAL ICE WALL BY NATURAL CONVECTION INTO PURE OR SALINE WATER

JIUNN-JIU LEE

NOTICE

The quality of this microfiche is heavily dependent upon the quality of the original thesis submitted for microfilming. Every effort has been made to ensure the highest quality of reproduction possible.

If pages are missing, contact the university which granted the degree.

Some pages may have indistinct print especially if the original pages were typed with a poor typewriter ribbon or if the university sent us a poor photocopy.

Previously copyrighted materials (journal articles, published tests, etc.) are not filmed.

Reproduction in full or in part of this film is governed by the Canadian Copyright Act, R.S.C. 1970, c. C-30. Please read the authorization forms which accompany this thesis.

THIS DISSERTATION HAS BEEN MICROFILMED EXACTLY AS RECEIVED

AVIS

La qualité de cette microfiche dépend grandement de la qualité de la thèse soumise au microfilmage. Nous avons tout fait pour assurer une qualité supérieure de reproduction.

S'il manque des pages, veuillez communiquer avec l'université qui a conféré le grade.

La qualité d'impression de certaines pages peut laisser à désirer, surtout si les pages originales ont été dactylographiées à l'aide d'un ruban usé ou si l'université nous a fait parvenir une photocopie de mauvaise qualité.

Les documents qui font déjà l'objet d'un droit d'auteur (articles de revue, examens publiés, etc.) ne sont pas microfilmés.

La reproduction, même partielle, de ce microfilm est soumise à la Loi canadienne sur le droit d'auteur, SRC 1970, c. C-30. Veuillez prendre connaissance des formules d'autorisation qui accompagnent cette thèse.

LA THÈSE A ÉTÉ MICROFILMÉE TELLE QUE NOUS L'AVONS REÇUE

MELTING OF A VERTICAL ICE WALL BY NATURAL CONVECTION INTO PURE OR SALINE WATER

by

Jiunn-Jiu Lee, B.Sc. ©

A Thesis submitted in partial fulfillment
of the requirements for the degree of
Master of Engineering

Faculty of Engineering & Applied Science
Memorial University of Newfoundland

August 1979

St. John's Newfoundland

PREFACE

The author would like to express his gratitude to his supervisor, Dr. N. W. Wilson for help and suggestions throughout the investigation, and also to the Dean of Graduate Studies, Dr. Frederick A. Aldrich for financial support during the research period in Memorial University of Newfoundland.

CONTENTS

ABSTRACT

A steady state two dimensional finite difference analysis is presented for the heat, mass and momentum transfer resulting from the initial portion of a semi-infinite vertical ice sheet melting into pure or saline water by natural convection. Fluid properties are assumed to be constant with the exception of the fluid density in the body force terms of the momentum equations.

Results of the analysis are presented for free stream temperatures from 0 °c to 24 °c and salinities from 0 ‰ to 35 ‰. They include streamlines, velocity profiles, temperature profiles, salinity profiles, local Nusselt numbers and mean Nusselt numbers for plate length of 0.7632 m. For pure water, calculated mean Nusselt numbers are favourably compared with existing data and analyses. For saline water, previous information not being available in the literature, the predicted results require verification.

Overall, the results show three distinct flow regimes: steady unidirectional upward flow, steady unidirectional downward flow, and dual flow. The solution method is convergent for the unidirectional regimes, and mostly non-convergent for dual flows. Since the solution method is capable of accounting for local recirculations, this suggests that the dual flow regime may be transitory in nature.

INTRODUCTION

If a vertical isothermal solid boundary is in contact with a surrounding real fluid which is at a temperature different from that of the wall, it is well known that a steady state fluid motion will occur near the wall. This motion is induced by the existence of a density distribution within the fluid as a result of the temperature differences between the wall and the fluid far from the wall. Basically, if the fluid near the wall is lighter than that further away, an upwards flow is induced near the wall. Similarly, if the fluid near the wall is heavier than that further away, a downwards flow is induced. In either case, if the fluid density either increases or decreases monotonically with increasing temperature, such free convective flows are amenable to boundary layer analyses such as can be found in many introductory heat transfer texts.

In many engineering applications, such free convective heat transfer phenomena are used with fluids which may exhibit density extrema. For example, environmentally exposed vertical surfaces may be in contact with fresh or saline water. Such water exhibits density extrema (see reference [1]) for salinities between 0 ‰ and 25.6 ‰ at atmospheric pressures. If the wall and fluid temperatures lie on alternate sides of the temperature at which the density extrema occurs, the simple boundary layer analysis is not directly applicable. Through one portion of the thermal boundary layer the bouyancy forces will be upwards, but through the other portion such forces will be

downwards, and a complicated flow structure may result. Essentially vertical ice surfaces in contact with water do occur in nature on the sides of icebergs, and on the underwater portion of metallic structures in a cold ocean environment. In such cases analysis is further complicated by the melting or fusion process which occurs at the ice-water interface. While the melting or fusion process can be approximated by appling a blowing or suction boundary condition at the interface, the resulting salinity distribution necessitates a further extension of such analyses.

Before further identifying the objectives of the present work, a review of the relevant literature is in order. As far as is known the first analytical solution concerned with the effect of the density maximum on natural convection was achieved by Merk [9], who consider heat transfer between a melting sphere of ice and adjacent pure water by using the integral momentum method. He predicted that in the neighbourhood of $T_\infty = 5\ ^\circ c$, the Nusselt number has a minimum and the direction of the flow changed from upwards at lower temperatures to downwards at higher temperatures. Further, he found that the effect of the melting is only appreciable for T_∞ greater than the inversion temperature and may be neglected for T_∞ less than the inversion temperature.

Dumore, Merk, and Prins [3] demonstrated experimentally for melting ice spheres a convective inversion occurred at $4.8\ ^\circ c$. The results indicated that the flow was upward when $T_\infty < 4.8\ ^\circ c$ and

downward when $T_\infty > 4.8\ ^\circ c$. A minimum Nusselt number at 5.5 °c was obtained by Tkachev [5] in his experimental work with vertical melting ice cylinders.

Ede [4] compared his experimental results for heat transfer from a heated vertical isothermal wall to cold pure water with the predictions made by Merk [9] and found them to be in reasonable agreement except in the region of low Nusselt number.

Both experiments and analyses on natural convection heat transfer in regions of maximum fluid density have been carried out by Schechter and Isbin [12]. They substantiated the findings of Dumore, Merk, and Prins [3] that there is a bidirectional flow in the boundary layer when heat is transferred from a vertical isothermal flat plate to cold water in the range of 4 °c.

Vanier and Tien [16] studied the influence of density inversion and melting on natural convection heat transfer from vertical surface for various wall and bulk temperature combinations. Their numerical boundary layer analysis indicated that for the case of $T_w = 0\ ^\circ c$ a dual flow exists near the wall and for $4.75\ ^\circ c < T_\infty < 6\ ^\circ c$ no solution was found. The effect of melting on the heat transfer rate was found to be small.

Schenk and Schenkels [13] measured natural convection heat transfer from an ice sphere in water for T_∞ from 0 to 10 °c and found that a dual flow exists in the range $4\ ^\circ c < T_\infty < 6\ ^\circ c$. In this complicated region, they observed upward flow near the wall and

downward flow at some distance away from the wall.

Vanier and Tien [18] also performed experiments with ice spheres melting in water from 0 to 20 °c and obtained a convective inversion at 5.35 °c.

The problem of natural convection heat transfer to a horizontal ice cylinder immersed in water was studied both theoretically and experimentally by Takeo Saitoh [14]. A minimum Nusselt number at above T_∞ = 6 °c was obtained.

Bendell and Gebhart [1] carried out experiments with vertical melting ice sheets in pure water at various values of T_∞. The experimentally determined heat-transfer results were found to be in good agreement with that from the boundary layer calculations of Gebhart and Mollendorf [5]. For the experimental investigation, a minimum Nusselt number in the range, 2.2 °c $\leq T_\infty \leq$ 25.2 °c, was found to occur at T_∞ = 5.6 °c. Meanwhile a net upflow and a net downflow were deduced from fluid temperature measurements when $T_\infty \leq$ 5.6 °c and $T_\infty \geq$ 5.5 °c respectively. For the theoretical analysis by using first order boundary layer approximations, the numerical solution in the range, 4 °c < T_∞ < 6.8 °c, was not obtainable.

Similar analyses based on [1] were made by Qureshi and Gebhart [11] for a vertical ice plate with a uniform flux condition in water.

Carey, Gebhart, and Mollendorf [2] reported a numerical result for laminar thermal natural convection to or from a vertical isothermal

surface in cold water wherein a density extremum arises. In pure water at atmospheric pressure, they found the flow is bidirectional for T_∞ between 4.75 °c and 5.98 °c and that convective inversion occurs at some T_∞ between 4.75 °c and 5.81 °c. Solutions could not be obtained for this range of temperatures.

In response to Griffin [7], R. G. Watts (1974) performed an experiment on flow patterns around a colored ice cube in saline water. For some ambient fluid temperature, he found the flow to be strongly upwards, except possibly very near the wall where there might have been a slight downward motion.

Wilson and Vyas [18] conducted experiments on the velocity profiles near a vertical ice surface melting into fresh water for $2\ ^{\circ}c \leq T_\infty \leq 7\ ^{\circ}c$. Their results indicated steady state motion upwards when the water temperature is below 4.7 °c and downwards when the water temperature is above 7 °c. For intermediate temperatures oscillatory bidirectional flow were observed.

The previous work can be summarized as follows:

1. All existing quantitative information pertains to the heat transfer from a non-melting isothermal surface to or from pure or saline water, or to a melting ice surface from pure water. In either case, dissipative or convective transport of salt has not been considered.

2. For ice melting into pure water, analyses based upon boundary

layer approximations adequately describe the flow patterns for temperatures yielding unidirectional upflow or unidirectional downflow. For intermediate water temperatures where bidirectional flows may exist, the boundary analyses have failed to yield satisfactory solutions.

3. In the bidirectional flow regime, the inadequacy of the steady state boundary layer analyses may be attributed to their inability in accounting for opposing flow directions within the boundary layers, or to a possible transient and oscillating nature of the flow, or to a combination of these effects.

In view of the above summary, the scope of the present work can be defined. Because of the occurrence of ice in contact with either pure or saline water in some circumstances, an analysis should be capable of accounting for the mass transfer of salt through the water. The analysis should be capable of yielding results for unidirectional upflow, unidirectional downflow, or bidirectional flow. Since steady bidirectional flow would imply that steady recirculation exists within the fluid adjacent to the ice sheet, the analytical model should be capable of readily accounting for such recirculations in such steady state flows. Then if solutions are still unobtainable, further work would be suggested in developing a transient analysis.

ANALYSIS

For constant fluid properties with the exception of density in the body force terms, the steady state laminar two dimensional continuity, momentum, and heat and mass transfer equations can be written as

$$\frac{\partial u}{\partial x} + \frac{\partial v}{\partial y} = 0 \tag{1}$$

$$\rho \left(u \frac{\partial u}{\partial x} + v \frac{\partial u}{\partial y} \right) = - \frac{\partial P}{\partial x} + \mu \left(\frac{\partial^2 u}{\partial x^2} + \frac{\partial^2 u}{\partial y^2} \right) \pm \rho g \tag{2}$$

$$\rho \left(u \frac{\partial v}{\partial x} + v \frac{\partial v}{\partial y} \right) = - \frac{\partial P}{\partial y} + \mu \left(\frac{\partial^2 v}{\partial x^2} + \frac{\partial^2 v}{\partial y^2} \right) \tag{3}$$

$$\rho \left(u \frac{\partial T}{\partial x} + v \frac{\partial T}{\partial y} \right) = \frac{k}{Cp} \left(\frac{\partial^2 T}{\partial x^2} + \frac{\partial^2 T}{\partial y^2} \right) \tag{4}$$

$$\rho \left(u \frac{\partial S}{\partial x} + v \frac{\partial S}{\partial y} \right) = \rho D \left(\frac{\partial^2 S}{\partial x^2} + \frac{\partial^2 S}{\partial y^2} \right) \tag{5}$$

In writing the above equations, Cartesian co-ordinate systems have been implied as shown in Figures 1(a) and 1(b). Thus, for dominant upward flow the gravitational force on a fluid element would be in the negative x direction and the $-\rho g$ term expressed in equation (2) would apply. If the dominant flow direction were downward, the co-ordinate system of Figure 1(b) would be employed along with the $+\rho g$ term in equation (2).

Gosman et al [6] describe a procedure of eliminating the pressure, P, from equations (2) and (3) by differention with respect to y and

x respectively and subtraction. As is described in Appendix A, their formulation when applied to equations (1) to (5) results in

$$\frac{\partial}{\partial x}\left(\omega\frac{\partial\psi}{\partial y}\right)-\frac{\partial}{\partial y}\left(\omega\frac{\partial\psi}{\partial x}\right)-\mu\left(\frac{\partial^2\omega}{\partial x^2}+\frac{\partial^2\omega}{\partial y^2}\right)-\frac{\partial}{\partial x}\left(\frac{u^2+v^2}{2}\right)\frac{\partial\rho}{\partial y}$$

$$+\frac{\partial}{\partial y}\left(\frac{u^2+v^2}{2}\right)\frac{\partial\rho}{\partial x}\pm g\frac{\partial\rho}{\partial y}=0 \qquad (6)$$

$$\frac{1}{\rho}\left(\frac{\partial^2\psi}{\partial x^2}+\frac{\partial^2\psi}{\partial y^2}\right)+\omega=0 \qquad (7)$$

$$\frac{\partial}{\partial x}\left(T\frac{\partial\psi}{\partial y}\right)-\frac{\partial}{\partial y}\left(T\frac{\partial\psi}{\partial x}\right)-\frac{k}{Cp}\left(\frac{\partial^2T}{\partial x^2}+\frac{\partial^2T}{\partial y^2}\right)=0 \qquad (8)$$

$$\frac{\partial}{\partial x}\left(S\frac{\partial\psi}{\partial y}\right)-\frac{\partial}{\partial y}\left(S\frac{\partial\psi}{\partial x}\right)-\rho D\left(\frac{\partial^2S}{\partial x^2}+\frac{\partial^2S}{\partial y^2}\right)=0 \qquad (9)$$

where the stream function, ψ, is defined by

$$\rho u=\frac{\partial\psi}{\partial y} \quad \text{and} \quad \rho v=-\frac{\partial\psi}{\partial x}$$

Vorticity, ω, is defined as

$$\omega=\frac{\partial v}{\partial x}-\frac{\partial u}{\partial y}$$

Inspection of equations (6), (7), (8), and (9) and the definitions of vorticity and stream function shows that a solution requires determination of the dependent variables, ω, ψ, T, S, and ρ over the (x,y) co-ordinate system in the region of interest. This necessitates the specification of an appropriate equation of state expressing the

density, ρ, in terms of T and S. The approach of Lafond [8] was employed in the present analysis. Namely, the density is expressed as follows:

$$\rho = \sigma_t + 1000 \tag{10}$$

where

$$\sigma_t = \Sigma_t + [\, \sigma_o + 0.1324 \,][\, 1 - A_t + B_t (\sigma_o - 0.1324) \,]$$

$$\Sigma_t = - \frac{(T - 3.98)^2}{503.57} \frac{T + 283}{T + 67.26}$$

$$A_t = T (4.7867 - 0.098185\, T + 0.0010843\, T^3) \times 10^{-3}$$

$$B_t = T (18.03 - 0.8164\, T + 0.01667\, T^2) \times 10^{-6}$$

$$\sigma_o = - 0.093 + 0.8149\, S - 0.000482\, S^2 + 0.0000068\, S^3$$

This density relationship is summarized in Figures 2 and 3.

In order to conclude the specification of the analysis, the associated boundary conditions should be considered. At the leading edge of the ice sheet, that is at the bottom of the plate for upflow or the top of the plate for downflow, the fluid is assumed to have no velocity in the direction along the plate. However, the fluid could be flowing in a direction normal to and towards the ice surface. If this is the case, the fluid would be flowing with zero shear stress and with a temperature and salinity equal to the values far removed from the wall. Thus, at $x = 0$ (except for $y = 0$)

$$\omega = 0$$

$$\psi = 0$$

$$T = T_\infty$$

$$S = S_\infty$$

Far removed from the wall, the fluid is at T_∞ and S_∞, and possesses a zero u component of velocity. In addition, $\frac{\partial u}{\partial y}$ is assumed to be zero and $\frac{\partial v}{\partial x}$ is assumed to be small enough to be negligible. Thus for large y

$$\omega = 0$$

$$\frac{\partial \psi}{\partial y} = \frac{\partial^2 \psi}{\partial y^2} = 0$$

$$T = T_\infty$$

$$S = S_\infty$$

Along the ice surface, for $y = 0$, the melting phenomena must be accounted for in the boundary conditions. The u-component of velocity is zero, but because of melting, the v-component is non-zero. Heat conduction into the ice is neglected for simplicity. (This corresponds to assuming that the ice is at its fusion temperature throughout). Therefore, the heat transferred to the ice by conduction through the fluid immediately adjacent to the ice can be equated, in the steady state, to the heat required to melt the ice. Thus, the local v-component of velocity can be expressed as

$$v = -\frac{k}{\rho L} \frac{\partial T}{\partial y}\bigg|_{y=0} \qquad (11)$$

Hence, if the temperature profile were known, the stream function could be evaluated along the ice sheet from

$$\psi = -\int_0^x \rho v \, dx \tag{12}$$

The steady state local salinity at the ice surface can be evaluated by equating the convection of salt away from the ice by the meltwater to the molecular diffusion of salt towards the ice. Thus

$$S_w = \frac{D}{v}\frac{\partial S}{\partial y}\bigg|_{y=0} \tag{13}$$

Once the wall salinity is known, the local fusion temperature can be evaluated using the relation from Neumann and Pierson [10].

$$T = -0.003 - 0.0527\, S - 0.00004\, S^2 \tag{14}$$

Obviously, equations (11), (13), and (14) are linked and must be solved iteratively. When this is done, the wall vorticity values may be found by applying equation (7).

If the analysis were based upon boundary layer equations, the boundary conditions described so far would be sufficient to describe the flow near the leading portion of the plate. That is, boundary conditions would then need to be specified only at the leading edge, at the ice surface and far removed in the direction normal to the plate. However, if a fully two dimensional solution is to be found, boundary conditions must be specified at the downstream end. This requires that the flow geometry be carefully specified.

Obviously, whatever method is to be used to solve equations (6) to (14), a solution can be expected only for finite values of the x co-ordinate. A number of choices for the flow geometry, therefore, exist. One could consider the flow near a vertical ice sheet of finite length immersed in water with all other solid boundaries or air-water interfaces far removed from the ice sheet. Another possibility would be to consider a vertical ice sheet immersed to a finite depth below a horizontal air-water interface in water of infinite depth. While downstream or closure boundary conditions could be written for either of these cases, the solutions so obtained would presumably depend upon the length of the immersed ice sheet, and hence may be lacking in generality. Each of the above cases very well might warrant investigation on its own merits, but the present work is more concerned with generality. To achieve this, a finite leading portion of a long vertical ice sheet has been considered. It is assumed that the ice sheet is immersed in water with all other boundaries far removed from the ice surface, and that the ice sheet is much longer than the leading portion over which a solution will be found. This implies that the length of the region of interest of the plate may be arbitrarily chosen provided the x-direction gradients of ω, ψ, T, S and ρ are not varying too appreciably at that point. Then the closure boundary values for these variables can be found by extrapolation from the interior of the region of interest. The implications and validation of this procedure is found later in the report.

For the present, the boundary conditions discussed above and

summarized in figures 4(a) and 4(b) provide sufficient information to permit the simultaneous solution of equations (6) to (10) if an appropriate solution method can be found. Equation (10) is algebraic whereas equations (6) to (9) can be classified as elliptic partial differential expressions. Because of their complexity, direct analytical solution of the equations is not possible, and the application of numerical methods is necessary. In broad terms, a numerical solution can be obtained by approximating the differential equations and the boundary conditions by either finite element or finite difference techniques and solving the resulting set of approximate equations. Such techniques are described in detail in the literature and their characteristics can be summarized briefly. In both cases the region of interest is discretized and the equations are integrated by approximate methods over small discrete areas. This results in the case of the finite element method, in sets of simultaneous linear equations normally in the form of banded matrices which can be solved on a digital computer using appropriate matrix techniques. A characteristic feature, therefore, is that large amounts of computer storage may be necessary with relatively small execution times for a particular problem. In the case of finite differences, iterative methods have been devised which result in lower computer storage requirements with longer execution times. Because of the availability of a PDP 11/60 computer with modest storage facilities but free time within the Faculty of Engineering and Applied Science, finite difference methods were chosen for the present work.

Basically, the scheme developed by Gosman et al [6] was employed as is outlined in Appendix B. This consisted of approximating all terms in equations (6) to (9), with exception of the convection terms as identified in Appendix B, by central differences with the " upwind differences " discussed by Gosman et al being employed for the convection terms. The basic computer programme given in reference [6] could have been employed in the present work with appropriate modification to incorporate the boundary conditions. However, this programme was written in a general form to permit calculation for a wide range of problems for laminar or turbulent flows in Cartesian or polar cylindrical co-ordinates. If applied to the present case without substantial modification, the programme would calculate many parameters during each iteration even though the values would not change from iteration to iteration. In view of this, an abbreviated version of the programme had been written by Wilson [19] for the simple case of laminar flow over a flat plate. This version was limited to considering ω and ψ only with constant fluid properties for a variable grid in Cartesian co-ordinates. It featured storage of the bulk of the intermediate parameters and dependent variables on a disk with a minimum number of variables being stored in the computer memory at any one time. A suitable scheme was incorporated to transfer information between the computer memory and the mass storage device. The net result was that a large number of grid lines could be considered with a limit being imposed by the capacity of the disk rather than that of the computer memory. The execution time was minimized by calculating all

constants on a once-and-for all basis in a seperate programme which was run to supply initial values to the data file on the disk. As part of development of the coursework material of reference [19] the programme had been tested against that of Gosman et al and yielded identical results for identical conditions.

The pair of programmes from reference [19] were modified to incorporate equations for temperature, salinity, and density and to include the boundary conditions for the present case. This resulted in the computer programmes listed in Appendix C. These programmes incorporate the 51 by 41 node grid values listed in Table 1(b).

A typical run was conducted by first specifying the T_∞, and S_∞ values to the initialization programme in order to create a working data file on the disk. The main programme was then run until it had converged, that is, until each of the ω, ψ, T, and S values changed by less than 0.0001 of the reference values. For vorticity and stream functions, reference values were arbitrarily chosen as 10., and for temperature and salinity, the free stream values were employed. Results were then plotted using various programmes, and transferred to another disk for storage. Typically, a run would require about 800 iterations which required about 4 hours to process. While this time seems excessive by the standards of a large computer facility, it should be recognized that the computations were performed on a minicomputer without a high speed processor. Of the various facilities available for this work, the hands on control over the programmes and the plotting facility more than offset the disadvantage of long execution times.

RESULTS AND DISCUSSION

Before presenting the numerical results in detail, the validity of the finite difference approximation must be established. Two main aspects of this analysis require attention - namely, the appropriateness of the grid utilized and the boundary conditions applied at the downstream end. As is described below, suitable procedures could be devised to examine each of these aspects and thereby to validate the results.

First of all, a grid of arbitrary mesh size was chosen as shown in Table 1(a). Tables 1(b), 1(c) and 1(d) show other grids with the same spacing in the y-direction but the plate length increased to 1.731 m, the same spacing in the y-direction but half spacing in the x-direction, and the original spacing in the x-direction but half spacing in the y-direction, respectively. The programmes were run for fresh water at $T_\infty = 4\ ^0c$ with the previously described boundary conditions for each case. The streamline patterns obtained are as shown in Figures 6(a) to 6(d). Inspection of Figures 6(a) and 6(b) shows that the 25 by 41 node grid gives the same streamlines as the 51 by 41 node grid. Since the y-direction spacings and the first 25 x-direction spacings are identical in both of these cases, the solution has been shown to be insensitive to the location at which the downstream boundary condition is applied. Furthermore, if these extrapolative boundary conditions were erroneous, shifting the location of their application would significantly alter the results obtained over the

leading portion of the plate. Since this has not occurred, it is concluded that the downstream boundary conditions are acceptable for either grid.

In Figure 6(c) the x-direction grid spacing is twice as fine as in Figure 6(a) and the y-direction grid spacings are identical. Since the stream function solutions are identical, it can be concluded that the x-direction spacing of Table 1(a) is sufficient to describe the flow phenomena. Similarily, the y-direction spacing of Figure 6(d) is twice as fine as that of Figure 6(a) while the x-direction spacings are identical. The good agreement between the resulting streamline patterns vindicates the use of the y-direction spacing of Table 1(a).

From the above tests, it is concluded that the 25 by 41 node grid can be utilized for the analysis and that the downstream boundary conditions are appropriate. The various implications of the results can now be examined in detail.

For the fresh water case, the salinity was set equal to zero throughout the field and the melt interface temperature was set to zero . The resulting streamline patterns for representative temperatures are presented in Figures 7(a) to 7(f) for a portion of the flow field from the ice wall, which is along the x-axis, to $y = 0.020$ m. Inspection of Figure 7(a), for example, shows that for $T_\infty \doteq 1\ ^0c$ fluid is entrained far from the wall most strongly at the lower end of the plate. That is $\frac{\partial \psi}{\partial x}$ is greater for small values of x than for large values if $y = 0.020$ m. Since $v = -\frac{1}{\rho}\frac{\partial \psi}{\partial x}$, the fluid at

large distances from the plate flows essentially normal to and towards the ice surface. For any constant values of x, the v component of velocity decreases for decreasing values of y and u component of velocity increases. Thus, in this case, fluid is drawn towards the ice surface and then essentially pumped upwards by the buoyancy forces. The behaviour of the streamlines immediately adjacent to the ice surface could be examined in detail to yield information concerning the melt velocity, v, at y = 0. This is examined in detail later. For the present, the effect of varying T_∞ on the streamline patterns can be readily examined except for the near wall regions.

If Figures 7(a) and 7(b) are compared, the effect of increasing the free stream temperature can be determined for temperatures well below 4 °c which is approximately the temperature of the density maximum in fresh water. Generally, for the increased temperature, the streamlines are more closely crowded together over the whole of the flow field. This corresponds to a more vigorous entrainment and pumping action. This trend was found, by running the programme for numerous cases, to be valid for temperatures in the range $0 < T_\infty \leq 2.50$ °c. If T_∞ is increased beyond 2.50 °c, the streamlines become progressively further spread apart indicating overall lower fluid velocities. This results from the relatively low buoyancy forces which exist in the outer portion of the thermal boundary layer for values of T_∞ approaching or surpassing 4 °c. Figure 7(c) demonstates this, and also represents the maximum value of T_∞ for which stable solutions could be obtained for upflow with fresh water.

For $4.50 < T_\infty < 5.73$ °c, converged solutions could not be obtained for either upflow or downflow. The programme was run for up to 1200 iterations, and it was observed to yield results which oscillated. Various grid configurations and degrees of under-relaxation were employed to obviate this difficulty but all attempts were unsuccessful. In general, two dimensional finite difference schemes such as the present work can oscillate for steady state flow conditions if the grid or the boundary conditions are insufficient to describe the phenomena, or if the flow field itself is truly oscillatory. The present analysis is capable of describing steady state recirculations as is discussed below pertaining to Figure 7(d). The temperature range through which the present solution was non-convergent corresponds approximately to that in which the analysis of Bendell and Gebhart fails to obtain solutions. It also corresponds to the range in which the experimental data of Wilson and Vyas showed continual oscillations in the velocity distributions near a melting ice wall. Therefore, it is speculated that for $4.50 < T_\infty < 5.73$ °c the flow is oscillatory in nature. Obviously, further work is required to fully investigate this range of temperature.

For $T_\infty = 5.73$ °c, a solution could be found with the streamline patterns as shown in Figure 7(d). Because of the high free stream temperature, the fluid far from the ice wall is significantly lighter than that near the wall. Therefore, the fluid nearer the wall flows generally downwards. In the region very close to the wall ($y < 0.003$ m), the fluid density increases with increasing y resulting in a localized region of upflow. Hence the $\psi = -0.002$ streamline shows upflow near

the wall, and a turning point followed by downflow further from the wall. The sharpness of the turning point in this streamline is partially attributable to the algorithm used for producing the streamline contours from the stream function data available at the nodes. (Linear interpolations were used over a rectangle enclosed by four adjacent nodes). In order to more adequately describe this turning point an excessively fine grid would be required.

In Figures 7(e) and 7(f), the streamline patterns for T_∞ = 14.0 °c and 24.0 °c are presented. In these cases, the near wall upflowing region has disappeared because of the increased shear forces resulting from the more vigorous downflow.

The velocity profiles at a distance of x = 0.5029 m along the plate are summarized for selected free temperatures in Figure 8(a) where positive velocities indicate upflow. For T_∞ = 2.5 °c the maximum velocity is greater than at 1 °c and the maximum velocity occurs nearer the wall. At 4.50 °c the peak velocity is decreased due to the decreased net buoyancy forces, and the maximum has shifted towards the wall. For T_∞ = 5.73 °c, a slight upwards velocity is indicated near the wall with a wide downflowing region away from the wall. As T_∞ is further increased, the downwards flow increases substantially with the position of the maximum velocity shifting towards the wall.

The melt velocity distributions (v at y = 0) along the ice surfaces are summarized in Figure 8(b). Generally, for each of the ranges $0 < T_\infty \leq 4.50$ and $T_\infty \geq 5.73$ °c the melt velocity is highest at

the leading edge of the plate and decreases with increasing x. Also for each range, the melt velocity increases with increasing T_∞. At T_∞ = 5.73 °c when recirculation is present, the melt velocity is higher at the leading edge than at T_∞ = 4.50 °c. For increasing x it then falls below that of the lower temperature because of the lower near wall upwards flowing portion of the longitudinal flow. The u component of velocity can be determined for any value of x by $u = \frac{1}{\rho}\frac{\partial \psi}{\partial y}$. Typical velocity pofiles at selected positions along the ice surface are shown for selected temperatures in Figures 9(a) to 9(d). For T_∞ = 4.50 °c the velocity profiles are wholly upward flowing with both the maximum longitudinal velocity and the boundary layer thickness increasing for increasing distances along the plate. This same trend was observed for all profiles for $0 < T_\infty < 4.50$ °c. For T_∞ = 5.73 °c the dominant flow direction is downwards with a small region near the wall possessing upwards velocities. Both of the local velocity maxima and the recirculating boundary layer thickness increase with increasing x. As the value of T_∞ is increased beyond 5.73 °c the upwards flowing portion of the boundary layer progressively decreases in magnitude and thickness until it disappears at T_∞ = 6.00 °c as is shown in Figure 9(c). At this value of T_∞ the viscous forces exerted by the outer portion of the flow are just sufficient to overcome the upwards buoyancy forces in the fluid near the wall. For higher free stream temperatures the viscous forces become progressively more dominant and the velocity profiles take on shapes such as those of Figure 9(d) in which the upwards near wall buoyancy effects are no longer visible.

Typical temperature profiles are summarized for x = 0.5029 m in Figure 10. The trends in thermal boundary layer thickness can be described as follows: For $T_\infty < 2.5\ ^\circ c$ the thickness progressively decreases and then increases for $2.5 < T_\infty < 4.50\ ^\circ c$ with increasing temperature. For $5.73 < T_\infty < 24.0\ ^\circ c$ the thermal boundary layer thickness progressively decreases for increasing temperature. The growth of the thermal boundary layers is shown for $T_\infty = 4.54\ ^\circ c$ and $5.87\ ^\circ c$ in Figures 11(a) and 11(b) respectively.

The local Nusselt number, Nu_x, can be defined as

$$Nu_x = \frac{hx}{k} = -\frac{x}{Tw - T_\infty} \left.\frac{\partial T}{\partial y}\right|_{y=0}$$

If $\left.\frac{\partial T}{\partial y}\right|_{y=0}$ is evaluated numerically by a second order approximation, the Nusselt number variation along the plate can be determined for various free stream water temperatures as is shown in Figure 12. In many applications the mean heat transfer coefficient, $\bar{h}$, over a length , ℓ, of a plate is of interest. It is determined from

$$\bar{h} = \frac{1}{\ell} \int_0^{\ell} h\, dx$$

For the present analysis the above integration was performed numerically to permit the calculation of the mean Nusselt number values presented in Figure 13. The present analysis is in reasonable agreement with the experimental data.

The findings so far indicate that the analysis is basically valid

for fresh water for temperatures in the ranges $4.50 \geq T_\infty \geq 5.73$ °c. Improvements could possibly be made to improve the agreement with experimental data in this range, and further work is indicated to investigate the non-convergence of the programme for $4.50 < T_\infty < 5.73$ °c. However, the results presented so far are satisfactory to vindicate extension of the analysis to the saline water case for which no information is presently available in the literature.

For $S_\infty = 5$ ‰, the streamline patterns for selected temperatures are presented in Figures 14(a) to 14(e). Figure 14(a) shows that as was the case for fresh water for $T_\infty = 1$ °c, fluid is entrained horizontally far from the wall most strongly at the lower edge of the plate. Because of the low free stream temperature, which is far below the temperature of the density maximum, 2.93 °c, the fluid far from the ice wall is significantly heavier than that near the wall. Therefore, the fluid near the wall flows upwards. Comparison with Figure 7(a) shows that the increased salinity results in more closely spaced streamlines which indicates a more vigourous entrainment and pumping action. Upflow was found to exist for $0 < T_\infty \leq 3.87$ °c as is shown in Figures 14(a), 14(b) and 14(c). As the temperature was increased from 1 °c to 3 °c the streamlines become more closely crowded as is seen by comparing Figures 14(a) and 14(b). If the temperature is increased beyond 3 °c the streamlines become less closely spaced due to the decline in the buoyancy forces in the outer portion of the boundary layer. This trend continued up to $T_\infty = 3.87$ °c for which the streamline pattern is shown in Figure 14(c).

As was the case for fresh water, a range of temperatures was found for which converged solutions could not be obtained. For S_∞ = 5 %, the same oscillatory behaviour was found in running the computer programme for temperatures in the range of $3.87 < T_\infty < 20.85$ °c. It is noted that the range of instability has widened as a result of the increased salinity.

Solutions could be obtained for $T_\infty \geq 20.85$ °c and streamline patterns are shown in Figures 14(d) and 14(e). Since the fluid density is significantly greater near the wall than the density far away, vigourous downflow results with the greatest entrainment at the upper end of the plate.

The velocity profiles at x = 0.5029 m are summarized for selected free stream temperatures in Figure 15. For T_∞ = 3 °c the maximum velocity is greater than at 1 °c and the maximum velocity occurs nearer the wall. At 3.87 °c the peak velocity is decreased slightly and it has shifted towards the wall. As T_∞ increases to 20.85 °c, the critical temperature of dominant downflow where converged solution could be found, it shows that the flow is purely downward. The magnitude of the downward velocities is seen to increase with increasing temperature and the position of the velocity maximum shifts towards the wall.

Typical temperature profiles at x = 0.5029 m are summarized in Figure 16. Since the local temperature of the plate is given by equation (14) in which the salinity of the ice surface can vary along the plate, negative values of Tw are seen. For $T_\infty < 3$ °c, the thermal

boundary layer thickness progressively decreases and then increases for $3 < T_\infty < 3.87$ °c with increasing temperature. For $20.85 < T_\infty < 24$ °c, the thickness progressively decreases for increasing temperature.

The salinity profiles at x = 0.5029 m for selected temperatures are summarized in Figure 17(a). It is clear that the concentration boundary layer is thinner than the thermal boundary layer and the hydrodynamic boundary layer. This can be observed by comparing Figure 17(a) to Figures 16 and 15. Figure 17(b) shows the variation of the wall salinity, Sw, along the plate for various free stream temperatures. It is seen that for values of T_∞ in which upflow is dominant, the wall salinity increases very sharply near the leading edge and then more slowly with increasing distance along the plate. In this range, increases in the free stream temperature lead to overall decreases in the wall salinity. For T_∞ values in the higher range which produces downflow, the wall salinity values are very much reduced by the higher convective action. In addition, near the leading edge, the wall salinities rise rapidly to a maximum value and then decrease slowly with increasing x.

In Figure 18 the local Nusselt number variations along the plate are presented for various free stream temperatures. For $T_\infty \leq 3$ °c the local heat transfer rates increase with increasing temperature, and then decrease in the range $3 < T_\infty \leq 3.87$ °c. For the downflow region the local heat transfer rates increase with increasing temperature.

For $T_\infty = 2$ °c, selected streamline patterns are presented for

differing salinities in Figures 19(a), 19(b) and 19(c). If these figures are compared the effect of increasing the salinity can be established. The streamlines are more closely crowded together. This implies that as salinity increases, the fluid velocity along the plate is increased.

The velocity profiles at x = 0.5029 m are summarized for selected free stream salinities in Figure 20. For high salinity the maximum velocity is greater than at low salinity and the maximum velocity occurs nearer the wall. The variation of the temperature profiles evaluated at x = 0.5029 m is shown for different free stream salinities in Figure 21. As the salinity is increased the thermal boundary layer becomes thinner, the fusion temperature at the ice wall decreases and $\frac{\partial T}{\partial y}$ increases at y = 0. Hence, the heat transfer or melting rate increases.

Typical salinity profiles at x = 0.5029 m are summarized in Figure 22. In the region very close to the wall (y < 0.001 m), the gradient of salinity in y direction at high salinity is greater than at low salinity. This phenomenon is the dominant factor which affects the density gradients and produces increased buoyancy forces.

In Figure 23, the variations for Nu_x along the plate for selected free stream salinities are presented. For a given value of x, especially at a large distance from the leading edge, the Nu_x at high salinity is greater than at low salinity.

For T_∞ = 22 °c, solutions could be obtained only for $S_\infty \leq 5$ ‰.

Typical streamline patterns are presented in Figures 24(a), 24(b) and 24(c). The streamlines are spread apart successively more widely spaced towards the downstream end for the increased free stream salinity indicating a decreased fluid velocity along the plate. Figure 25 demonstrates this and also that the peak velocity is slightly removed from the ice surface for increasing salinities. The variation of temperature profiles evaluated at $x = 0.5029$ m for selected free stream salinities is not appreciable as shown in Figure 26.

The salinity profiles at $x = 0.5029$ m are summarized for selected free stream salinities in Figure 27 for $y = 0.01$ m. In the region very close to the wall ($y < 0.0007$ m), the gradient of salinity in y direction at 5 ‰ is nearly the same as at 3 ‰. For $0.0007 < y < 0.002$ m, the slope is increased for the higher fluid salinity. Figure 28 shows the Nu_x distributions for selected free stream salinities. The local Nusselt number is decreased successively with increasing salinity especially at higher values of x.

Finally, the overall heat transfer results are summarized in Figure 29 for selected salinities in the range $0 \leq S_\infty \leq 35$ ‰. For upflow the overall heat transfer increases markedly with increasing salinity. The temperature range for stable solutions is broadened to the extent that for $S_\infty > 5$ ‰ stable solutions could not be found for $T_\infty \leq 24.0$ °C.

CONCLUSIONS

1. A finite-difference technique is developed for predicting the steady state natural convection heat and mass transfer to a vertical ice flat plate immersed in fresh or saline water.

2. The results show three distinct flow regimes: dominant upward flow, dominant downward flow and a dual flow region. The analysis does not yield stable results for all combinations of salinity and temperature, and further work is suggested to investigate this problem.

3. The calculated streamfunction shows that near the wall there exists a noted upward flow in the dominant downward flow region for fresh water for $5.73 \leq T_\infty \leq 6.00$ °c.

4. The buoyancy caused by density differences resulting from the salinity gradient is stronger than that from the temperature gradient.

5. As a result of the temperature and salinity exchange, it is noted that in dominant upward flow the Nusselt number at high salinity is higher than at low salinity, while in dominant downward flow the Nusselt number at high salinity is lower than at low salinity.

6. For fresh water, the results indicate that the calculated values of overall heat transfer in dominant upflow region are slightly higher than the experimental data of Bendell and Gebhart.

7. In order to improve the results and overcome the difficulties where the steady state solution would not converge for fresh or saline

water , a transient analysis is needed for future research.

NOMENCLATURE

C_p	:	Constant pressure specific heat, J/(kg ^{0}c)
D	:	Diffusion coefficient, m^2/s
g	:	Acceleration of gravity, m/s^2
I	:	Grid number in x direction
J	:	Grid number in y direction
k	:	Thermal conductivity, W/(m ^{0}c)
L	:	Specific internal energy per unit mass, J/kg
Nu_x	:	Local Nusselt number
$\overline{Nu}$	:	Mean Nusselt number
P	:	Pressure, kg/(m s^2)
Pr	:	Prandtl number
S	:	Local salinity of fluid, ‰ or g/kg
Sc	:	Schmidt number
S_∞	:	Bulk salinity of fluid, ‰ or g/kg
Sw	:	Salinity of plate, ‰ or g/kg
T	:	Local temperature of fluid, ^{0}c
T_∞	:	Bulk temperature of fluid, ^{0}c
Tw	:	Temperature of plate, ^{0}c
u,v	:	Velocities in x and y directions, m/s
x,y	:	Cartesian co-ordinates
X,Y	:	Body forces in x and y directions, $kg/(m\ s)^2$
ρ	:	Local density of fluid, kg/m^3
μ	:	Dynamic viscosity, kg/(m s)
ψ	:	Stream function, kg/(m s)
ω	:	Vorticity, s^{-1}

REFERENCES

[1] Bendell, M.S. and B. Gebhart, " Heat Transfer and Ice-melting in ambient Water near Its Density Extremum ", International Journal of Heat and Mass Transfer, Vol. 19, pp 1081-1087, 1976

[2] Carey, V.P., B. Gebhart and J.C. Mollendorf, " Buoyancy Force Reversals in Vertical Natural Convection Flows in Cold Water ", 1979

[3] Dumore, J.M., H.J. Merk and J.A. Prins, " Heat Transfer from Water to Ice by Thermal Convection ", Nature, Lond., Vol. 172, pp 460-461, 1953

[4] Ede, A.J., " The Influence of Anomalous Expansion on Natural Convection in Water ", Appl. Sci. Res., Vol. 5, pp 458-460, 1955

[5] Gebhart, B. and J.C. Mollendorf, " Buoyancy-induced Flows in Water under Conditions in which Density Extremum may Arise ", Journal of Fluid Mechanics, Vol. 87, pp 673-708, 1978

[6] Gosman, W.M.Pun, A.K. Runchal, D.B. Spalding and M. Wolfshtein, " Heat and Mass Transfer in Recirculating Flows ", Academic Press, London and New York, 1969

[7] Griffin, O.M., " Heat, Mass and Momentum Transfer during the Melting of Glacial Ice in Sea Water ", Journal of Heat Transfer, Trans. ASME, Series c, Vol. 95, No. 3, pp 317-323, 1973

[8] Lafond, E.C., " Processing Oceanographic Data ", U.S. Navy Electronics Laboratory, H.O.Pub. No. 614, U.S. Navy Hydrographic Office, Washington, D.C., pp 91, 1951

[9] Merk, H.J., " The Influence of Melting and Anomalous Expansion on the Thermal Convection in Laminar Boundary Layers ", Appl. Sci. Res., Vol. 4, pp 435-452, 1953

[10] Neumann, G. and W.J. Pierson, Jr., " Principles of Physical Oceanography ", Englewood Cliffs. NJ. Prentice-Hall, 1966

[11] Qureshi, Z.H. and B. Gebhart, " Vertical Natural Convection with a Uniform Flux Condition in Pure and Saline Water at the Density Extremum ", Six International Heat Transfer Conference, Toronto, Canada, Vol. 2, Aug. 7-11, 1978

[12] Schechter, R.S. and H.S. Isbin, " Natural-convection Heat Transfer in Regions of Maximum Fluid Density ", A.I.Ch.E., J14, pp 81-89, 1958

[13] Schenk, J. and F.A.M. Schenkels, " Thermal Free Convection from Ice Sphere in Water ", Appl. Sci. Res., Vol. 19, pp 465-476, 1968

[14] Takeo Saitoh, " Natural Convection Heat Transfer from a Horizontal Ice Cylinder ", Appl. Sci. Res., Vol. 32, pp 429-451, 1976

[15] Tkachev, A.G., " Heat Exchange in Melting and Freezing of Ice ", Problems of Heat Transfer during a Change of State, A Collection of Articles, AEC-TR-3405, Translated from a Publication of the State Power Press, Moscow-Leningrad, pp 169-178, 1953

[16] Vanier, C.R. and C. Tien, " Effect of Maximum Density and Melting on Natural Convection Heat Transfer from a Vertical Plate ", Chemical Engineering Progress Symposium Series, Vol. 64, pp 240-254, 1968

[17] Vanier, C.R. and C. Tien, " Free Convection Melting of Ice Spheres ", America Institute of Chemical Engineers Journal, Vol. 16, pp 76-82, 1970

[18] Wilson, N.W. and B.D. Vyas, " Velocity Profiles near a Vertical Ice Surface Melting into Fresh Water ", Trans. ASME, Journal of Heat Transfer, Vol. 101, No. 2, pp 313-317, 1979

[19] Wilson, N.W., " Course Notes in Advanced Fluid Mechanics ", Faculty of Engineering and Applied Science, Memorial University of Newfoundland, 1978

LIST OF TABLES

Table 1(a) Mesh Sizes of Grid for 25 by 41 Node Grid

I	x (m)	J	y (m)
1	0.00000	1	0.00000
2	0.00953	2	0.00050
3	0.02120	3	0.00100
4	0.03530	4	0.00160
5	0.05260	5	0.00220
6	0.07380	6	0.00292
7	0.09950	7	0.00364
8	0.13100	8	0.00450
9	0.16900	9	0.00536
10	0.20540	10	0.00640
11	0.24260	11	0.00744
12	0.27980	12	0.00868
13	0.31690	13	0.00992
14	0.35410	14	0.01142
15	0.39130	15	0.01292
16	0.42850	16	0.01471
17	0.46570	17	0.01650
18	0.50290	18	0.01865
19	0.54010	19	0.02080
20	0.57720	20	0.02340
21	0.61440	21	0.02600
22	0.65160	22	0.02910
23	0.68880	23	0.03220
24	0.72600	24	0.03590
25	0.76320	25	0.03960
		26	0.04400
		27	0.04840
		28	0.05380
		29	0.05920
		30	0.06560
		31	0.07200
		32	0.07970
		33	0.08740
		34	0.09670
		35	0.10600
		36	0.11550
		37	0.12500
		38	0.13750
		39	0.15000
		40	0.16250
		41	0.17500

Table 1(b) Mesh Sizes of Grid for Testing

With 51 by 41 Node Grid

I	x (m)	I	x (m)	J	y (m)
1	0.00000	41	1.35900	1	0.00000
2	0.00953	42	1.39600	2	0.00050
3	0.02120	43	1.43300	3	0.00100
4	0.03530	44	1.47000	4	0.00160
5	0.05260	45	1.50800	5	0.00220
6	0.07380	46	1.54500	6	0.00292
7	0.09950	47	1.58200	7	0.00364
8	0.13100	48	1.61900	8	0.00450
9	0.16900	49	1.65700	9	0.00536
10	0.20540	50	1.69400	10	0.00640
11	0.24260	51	1.73100	11	0.00744
12	0.27980			12	0.00868
13	0.31690			13	0.00992
14	0.35410			14	0.01142
15	0.39130			15	0.01292
16	0.42850			16	0.01471
17	0.46570			17	0.01650
18	0.50290			18	0.01865
19	0.54010			19	0.02080
20	0.57720			20	0.02340
21	0.61440			21	0.02600
22	0.65160			22	0.02910
23	0.68880			23	0.03220
24	0.72600			24	0.03590
25	0.76320			25	0.03960
26	0.80040			26	0.04400
27	0.83760			27	0.04840
28	0.87480			28	0.05380
29	0.91200			29	0.05920
30	0.94920			30	0.06560
31	0.98630			31	0.07200
32	1.02350			32	0.07970
33	1.06070			33	0.08740
34	1.09790			34	0.09670
35	1.13510			35	0.10600
36	1.17230			36	0.11550
37	1.21020			37	0.12500
38	1.24740			38	0.13750
39	1.28460			39	0.15000
40	1.32180			40	0.16250
				41	0.17500

Table 1(c) Mesh Sizes of Grid for Testing with 49 by 41 Node Grid

I	x (m)	I	x (m)	J	y (m)
1	0.00000	41	0.61440	1	0.00000
2	0.00476	42	0.63300	2	0.00050
3	0.00953	43	0.65160	3	0.00100
4	0.01536	44	0.67020	4	0.00160
5	0.02120	45	0.68880	5	0.00220
6	0.02825	46	0.70740	6	0.00292
7	0.03530	47	0.72600	7	0.00364
8	0.04395	48	0.74460	8	0.00450
9	0.05260	49	0.76320	9	0.00536
10	0.06320			10	0.00640
11	0.07380			11	0.00744
12	0.08665			12	0.00868
13	0.09950			13	0.00992
14	0.11525			14	0.01142
15	0.13100			15	0.01292
16	0.15000			16	0.01471
17	0.16900			17	0.01650
18	0.18720			18	0.01865
19	0.20540			19	0.02080
20	0.22400			20	0.02340
21	0.24260			21	0.02600
22	0.26120			22	0.02910
23	0.27980			23	0.03220
24	0.29835			24	0.03590
25	0.31690			25	0.03960
26	0.33550			26	0.04400
27	0.35410			27	0.04840
28	0.37270			28	0.05380
29	0.39130			29	0.05920
30	0.40990			30	0.06560
31	0.42850			31	0.07200
32	0.44710			32	0.07970
33	0.46570			33	0.08740
34	0.48430			34	0.09670
35	0.50290			35	0.10600
36	0.52150			36	0.11550
37	0.54010			37	0.12500
38	0.55865			38	0.13750
39	0.57720			39	0.15000
40	0.59580			40	0.16250
				41	0.17500

Table 1(d) Mesh Sizes of Grid for Testing

with 25 by 81 Node Grid

I	x (m)	J	y (m)	J	y (m)
1	0.00000	1	0.00000	41	0.02600
2	0.00953	2	0.00025	42	0.02755
3	0.02120	3	0.00050	43	0.02910
4	0.03530	4	0.00075	44	0.03065
5	0.05260	5	0.00100	45	0.03220
6	0.07380	6	0.00130	46	0.03405
7	0.09950	7	0.00160	47	0.03590
8	0.13100	8	0.00190	48	0.03775
9	0.16900	9	0.00220	49	0.03960
10	0.20540	10	0.00256	50	0.04180
11	0.24260	11	0.00292	51	0.04400
12	0.27980	12	0.00328	52	0.04620
13	0.31690	13	0.00364	53	0.04840
14	0.35410	14	0.00407	54	0.05110
15	0.39130	15	0.00450	55	0.05380
16	0.42850	16	0.00493	56	0.05650
17	0.46570	17	0.00536	57	0.05920
18	0.50290	18	0.00588	58	0.06240
19	0.54010	19	0.00640	59	0.06560
20	0.57720	20	0.00692	60	0.06880
21	0.61440	21	0.00744	61	0.07200
22	0.65160	22	0.00806	62	0.07585
23	0.68880	23	0.00868	63	0.07970
24	0.72600	24	0.00930	64	0.08355
25	0.76320	25	0.00992	65	0.08740
		26	0.01067	66	0.09205
		27	0.01142	67	0.09670
		28	0.01217	68	0.10135
		29	0.01292	69	0.10600
		30	0.01382	70	0.11075
		31	0.01471	71	0.11550
		32	0.01561	72	0.12025
		33	0.01650	73	0.12500
		34	0.01758	74	0.13125
		35	0.01865	75	0.13750
		36	0.01973	76	0.14375
		37	0.02080	77	0.15000
		38	0.02210	78	0.15625
		39	0.02340	79	0.16250
		40	0.02470	80	0.16875
				81	0.17500

Table 2 $\overline{Nu}$ of Different S_∞ as a Function of T_∞ for a Length, 0.5029 m, of a Vertical Plate

S_∞ = 0 %		S_∞ = 5 %		S_∞ = 10 %	
T_∞	$\overline{Nu}$	T_∞	$\overline{Nu}$	T_∞	$\overline{Nu}$
		0.00	100.4	0.00	131.9
0.25	104.5	0.25	127.6	0.25	153.8
0.50	119.2	1.00	162.9	1.00	189.7
1.00	135.9	2.00	182.2	2.00	210.6
2.00	149.6	2.50	185.9	2.50	214.5
2.50	151.3	3.00	186.5	2.90	215.7
3.00	150.5	3.50	184.1	3.20	214.7
4.00	140.8	3.80	180.3	3.24	214.6
4.50	130.0	3.87	178.6	3.27	214.3
5.73	89.3				
5.74	91.8				
5.76	94.9				
5.80	99.9				
5.86	106.0				
5.87	107.2				
6.00	116.4				
7.00	156.0				
10.00	216.8				
14.00	268.8	20.85	265.7		
20.00	324.4	21.00	270.0		
22.00	339.6	22.00	285.6		
24.00	353.5	24.00	308.7		

Table 2 $\overline{Nu}$ of Different S_∞ as a Function of T_∞ for a Length, 0.5029 m, of a Vertical Plate (Continued)

S_∞ = 17 %		S_∞ = 25 %		S_∞ = 35 %	
T_∞	$\overline{Nu}$	T_∞	$\overline{Nu}$	T_∞	$\overline{Nu}$
0.25	193.2	1.25	275.6	2.10	343.9
0.50	206.9	1.50	282.3	2.30	347.3
1.00	226.5	2.00	292.6	2.50	350.5
2.00	248.2	2.30	297.0	3.00	356.9
2.50	253.6	2.75	302.2	3.50	361.6
2.80	255.4	2.80	302.6	3.73	363.3
2.90	256.1	2.85	303.1	3.80	363.7
		2.90	303.5	3.84	364.0

LIST OF FIGURES

15 Velocity Profiles of Different T_∞ for S_∞ = 5 ‰ at x = 0.5029 m

16 Temperature Profiles of Different T_∞ for S_∞ = 5 ‰ at x = 0.5029 m

17(a) Salinity Profiles of Different T_∞ for S_∞ = 5 ‰ at x = 0.5029 m
(b) Salinity Profiles of Different T_∞ for S_∞ = 5 ‰ at y = 0.0000 m

18 Nu_x of Different T_∞ as a Function of x for S_∞ = 5 ‰

19(a) Streamlines for T_∞ = 2 °c, S_∞ = 0 ‰
(b) Streamlines for T_∞ = 2 °c, S_∞ = 10 ‰
(c) Streamlines for T_∞ = 2 °c, S_∞ = 25 ‰

20 Velocity Profiles of Different S_∞ for T_∞ = 2 °c at x = 0.5029 m

21 Temperature Profiles of Different S_∞ for T_∞ = 2 °c at x = 0.5029 m

22 Salinity Profiles of Different S_∞ for T_∞ = 2 °c at x = 0.5029 m

23 Nu_x of Different S_∞ as a Function of x for T_∞ = 2 °c

24(a) Streamlines for T_∞ = 22 °c, S_∞ = 0 ‰
(b) Streamlines for T_∞ = 22 °c, S_∞ = 3 ‰
(c) Streamlines for T_∞ = 22 °c, S_∞ = 5 ‰

25 Velocity Profiles of Different S_∞ for T_∞ = 22 °c at x = 0.5029 m

26 Temperature Profiles of Different S_∞ for T_∞ = 22 °c at x = 0.5029 m

27 Salinity Profiles of Different S_∞ for T_∞ = 22 °c at x = 0.5029 m

28 Nu_x of Different S_∞ as a Function of x for T_∞ = 22 °c

29 $\overline{Nu}$ Over a Length, 0.7632 m, of a Vertical Plate for Selected Salinities

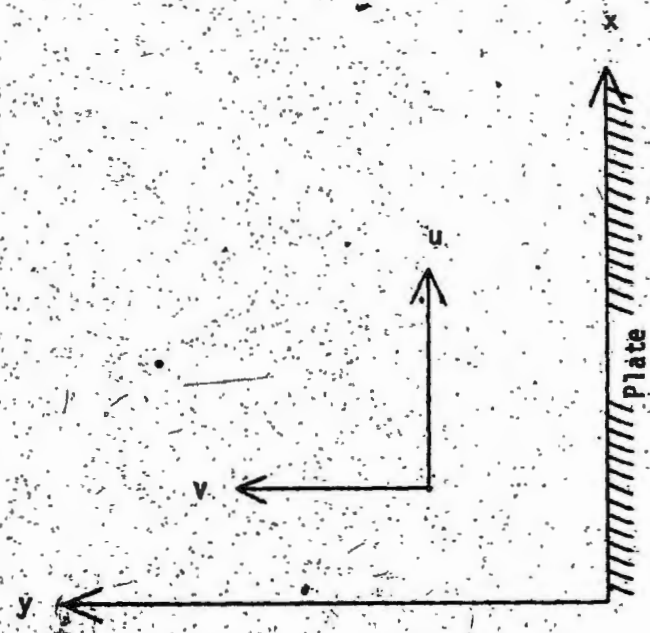

(a) For Dominant Upflow

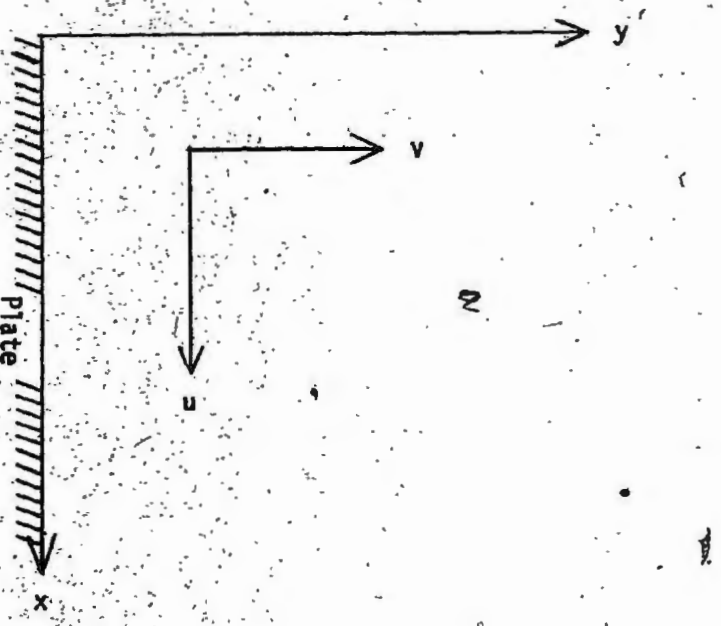

(b) For Dominant Downflow

Figure 1 Coordinate Systems

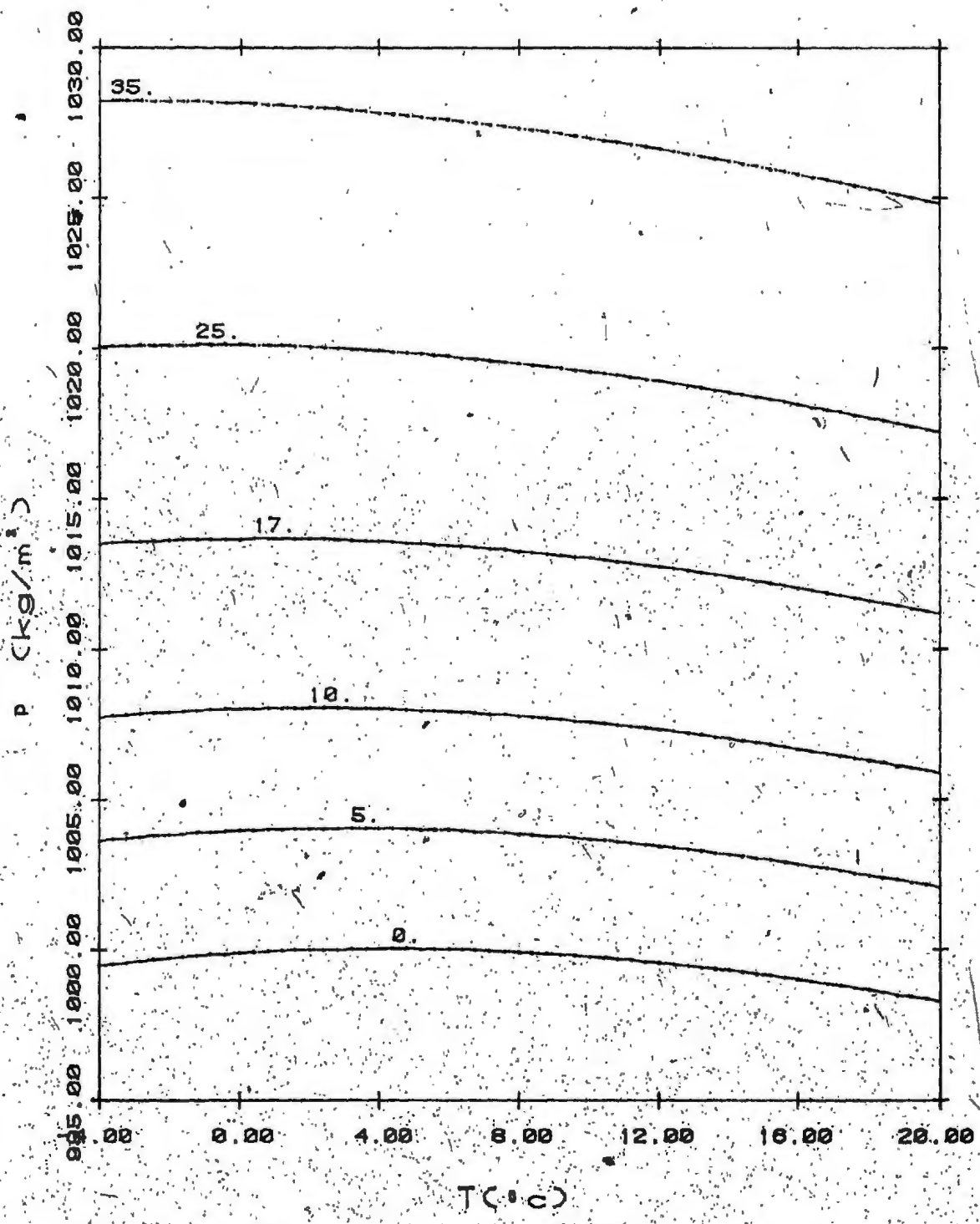

Figure 2 Density of Fresh Water and of Saline Water as a Function of Temperature

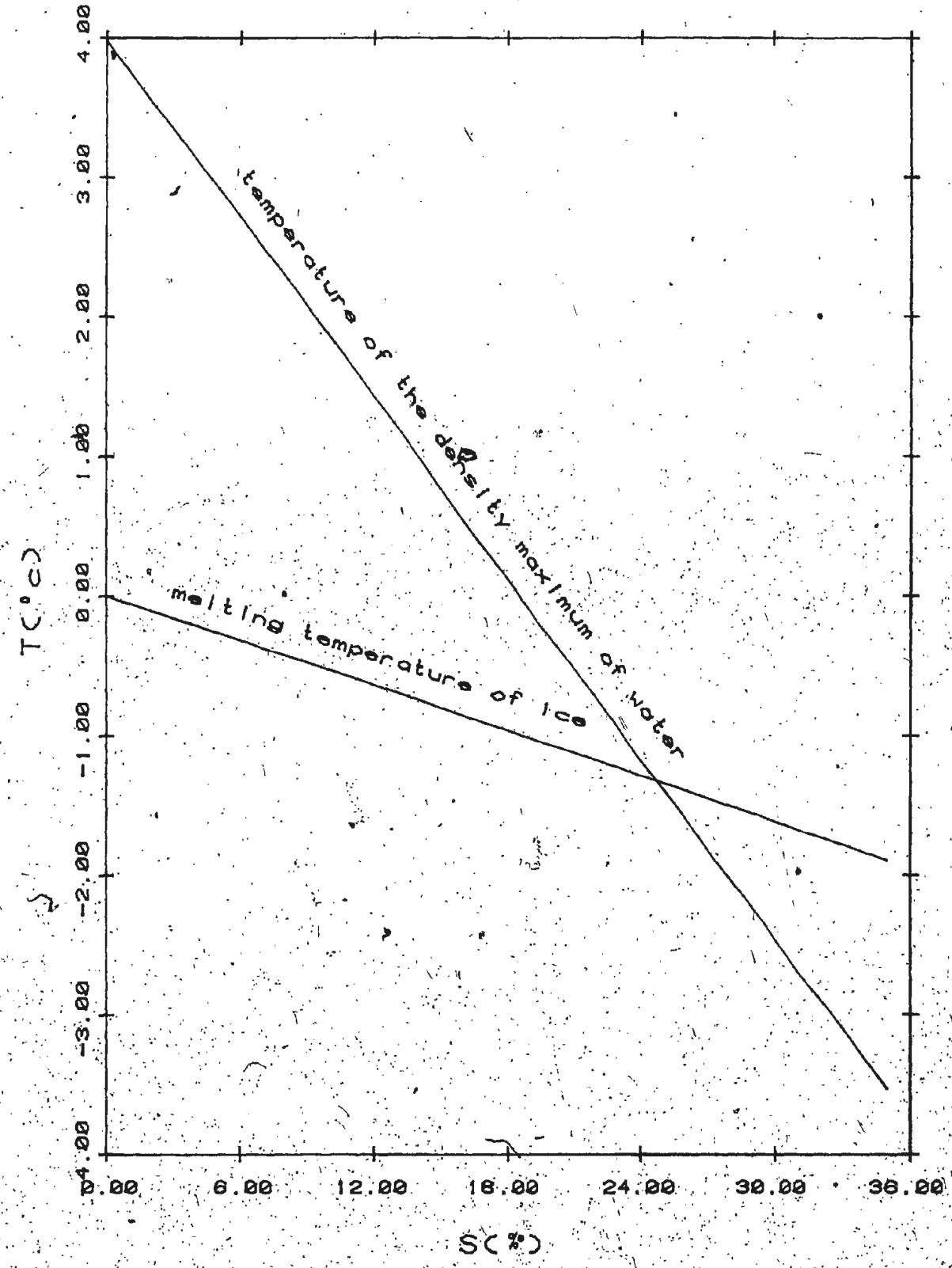

Figure 3 Melting Temperature of Ice and Temperature Density Maximum of Water as a Function of Salinity at Atmospheric Pressure

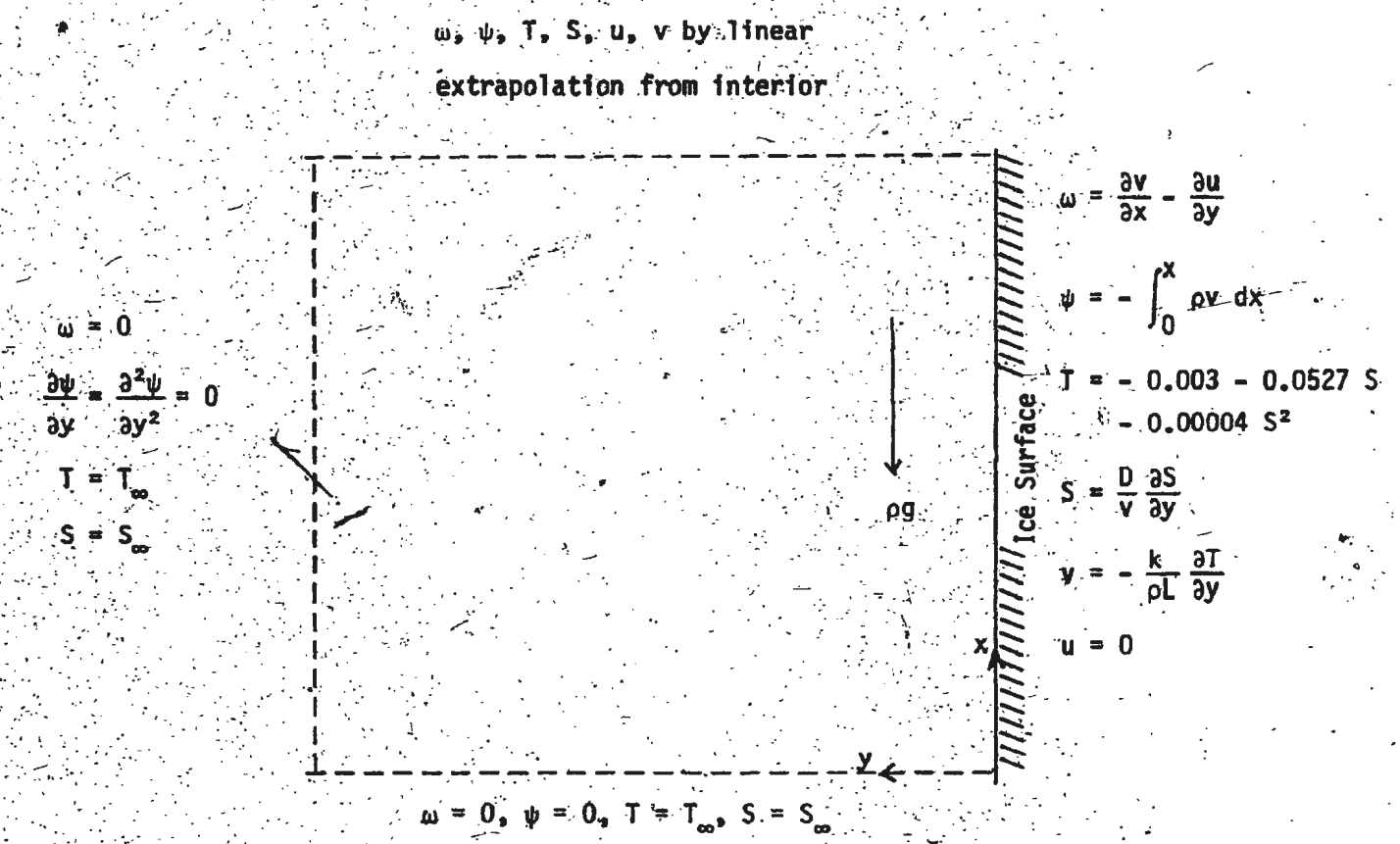

Figure 4(a) Boundary Conditions for Dominant Upflow

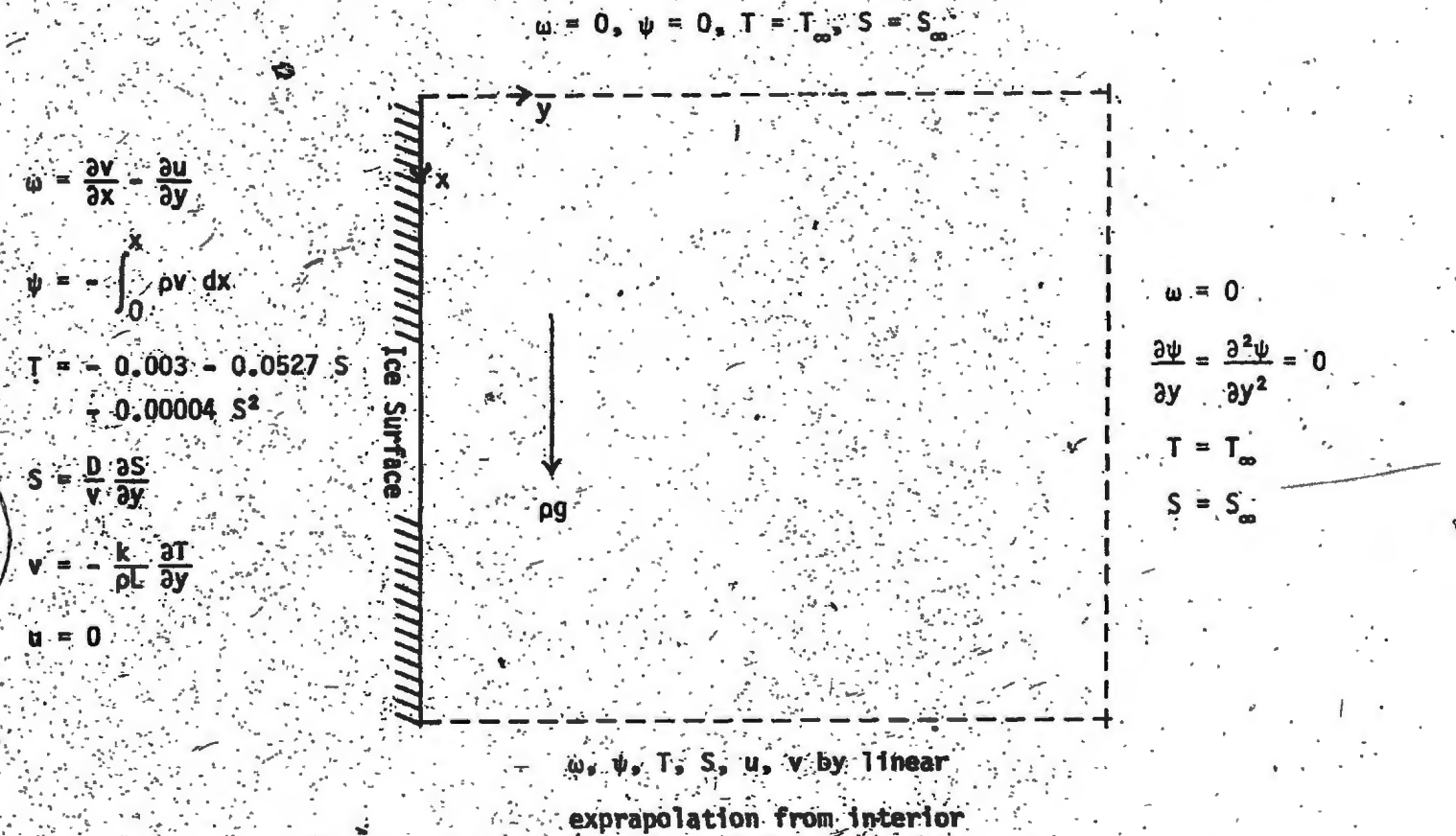

Figure 4(b) Boundary Conditions for Dominant Down flow

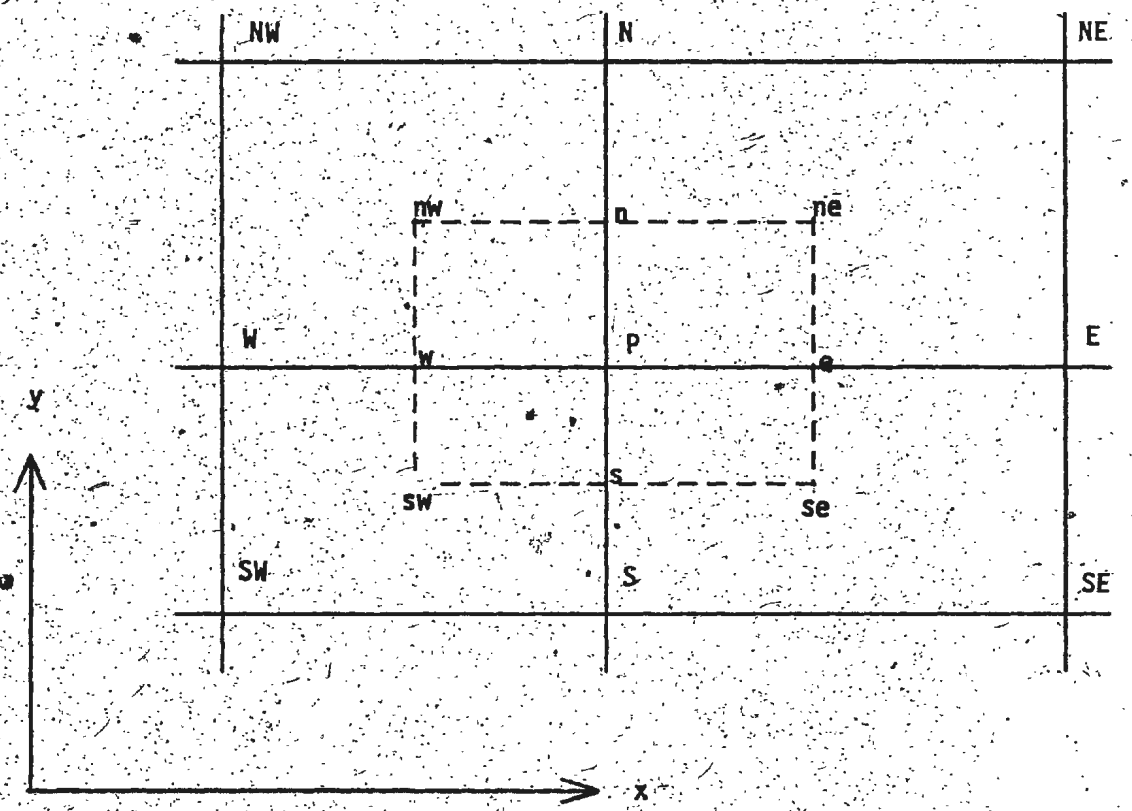

Figure 5 Rectangular Grid Model Used for Integration

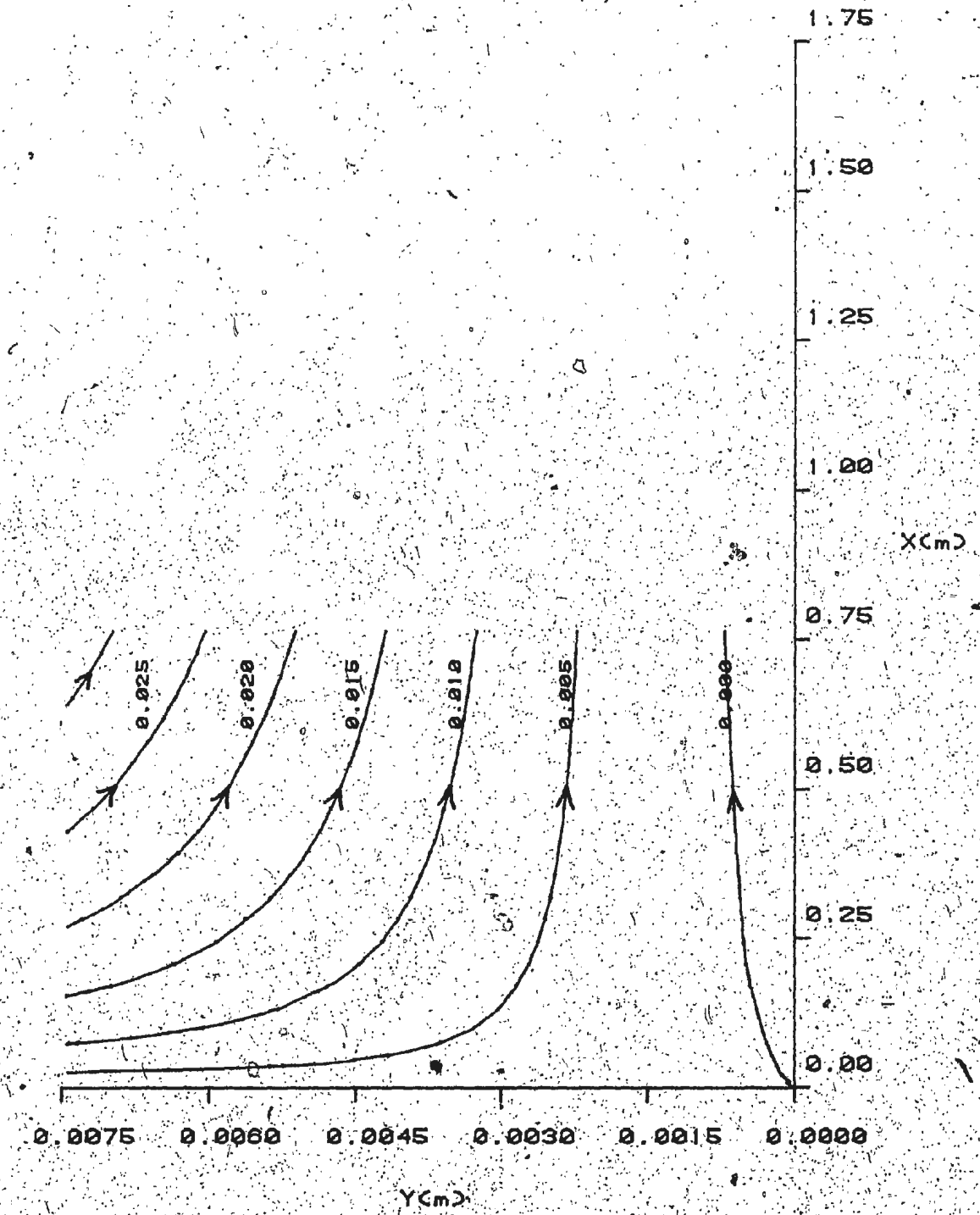

Figure 6(a) Streamlines for T_∞ = 4.00 °C, S_∞ = 0.0 ‰ with 25 by 41 Node Grid

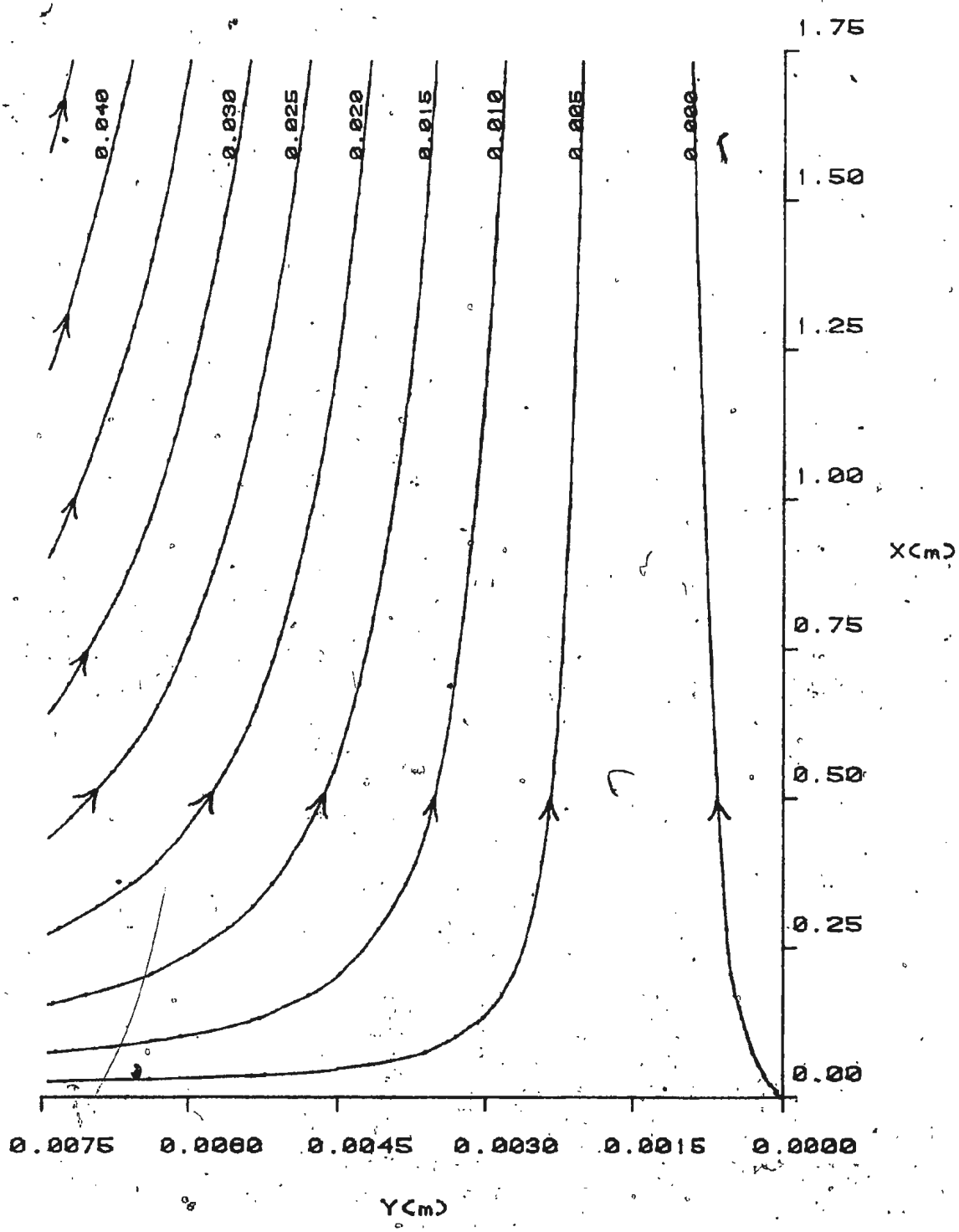

Figure 6(b) Streamlines for T_∞ = 4.00 °C, S_∞ = 0.0 ‰ with 51 by 41 Node Grid

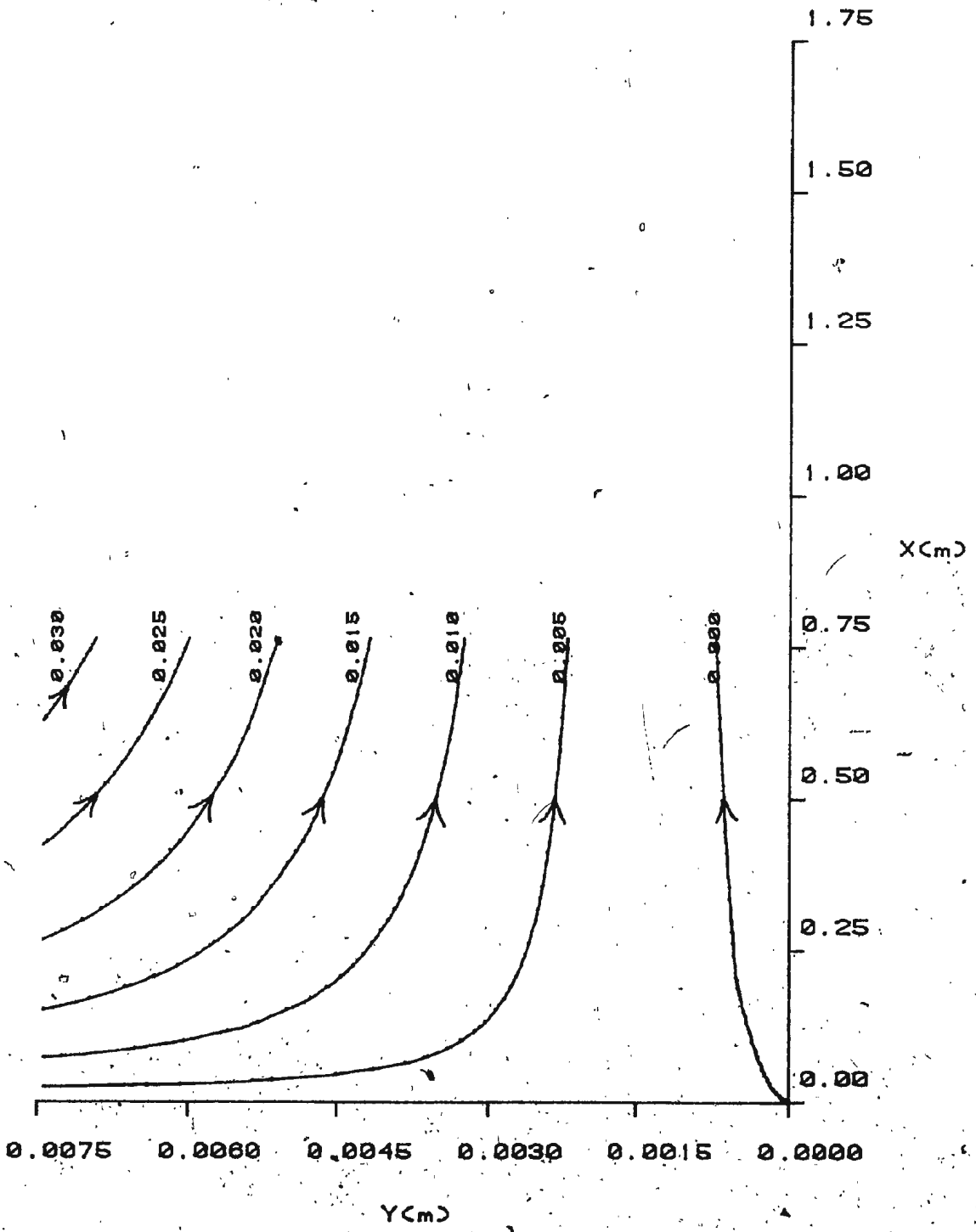

Figure 6(c) Streamlines for T_∞= 4.00 °C, S_∞= 0.0‰ with 49 by 41 Node Grid

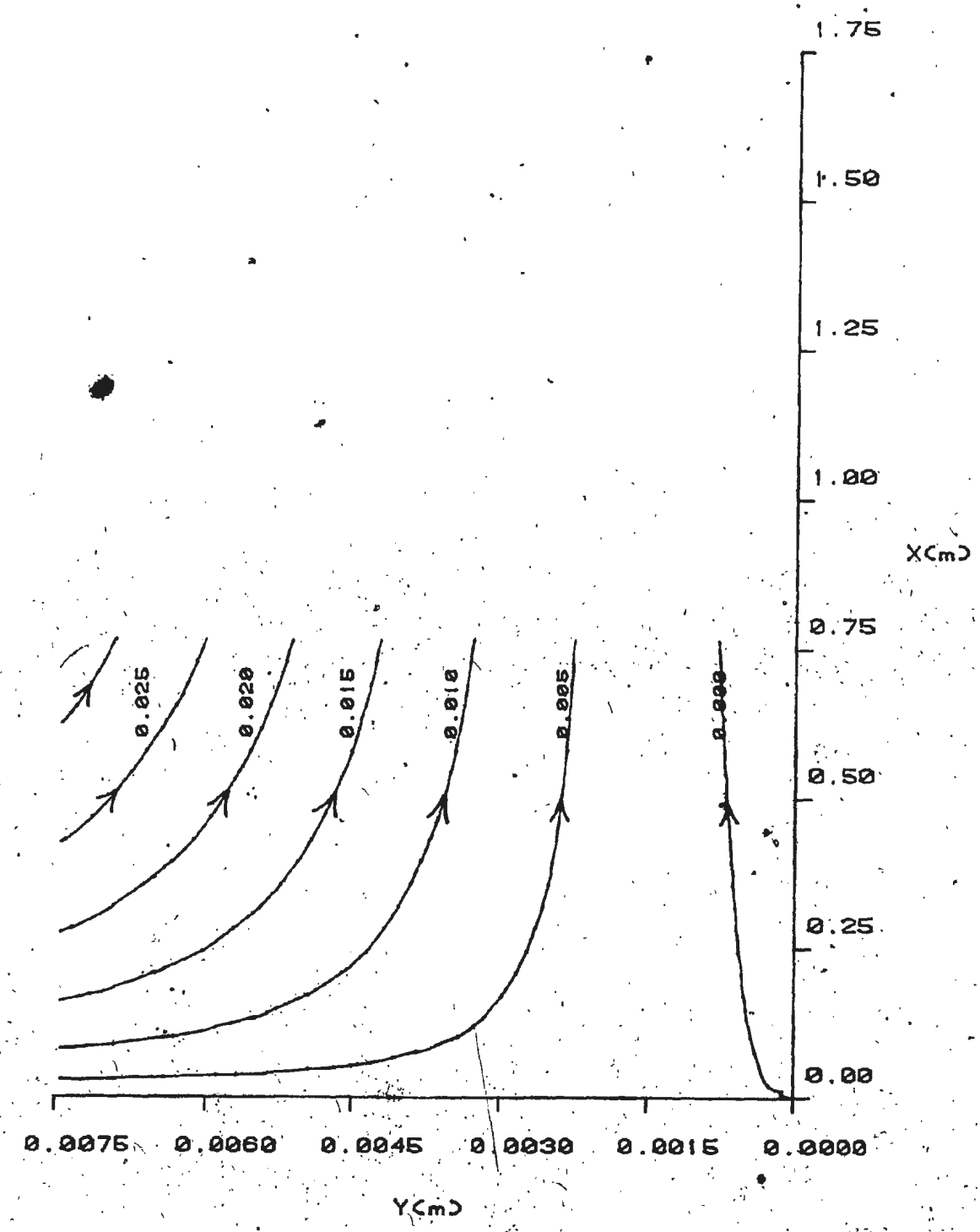

Figure 6(d) Streamlines for T_∞= 4.00 °C, S_∞= 0.0 ‰ with 25 by 81 Node Grid

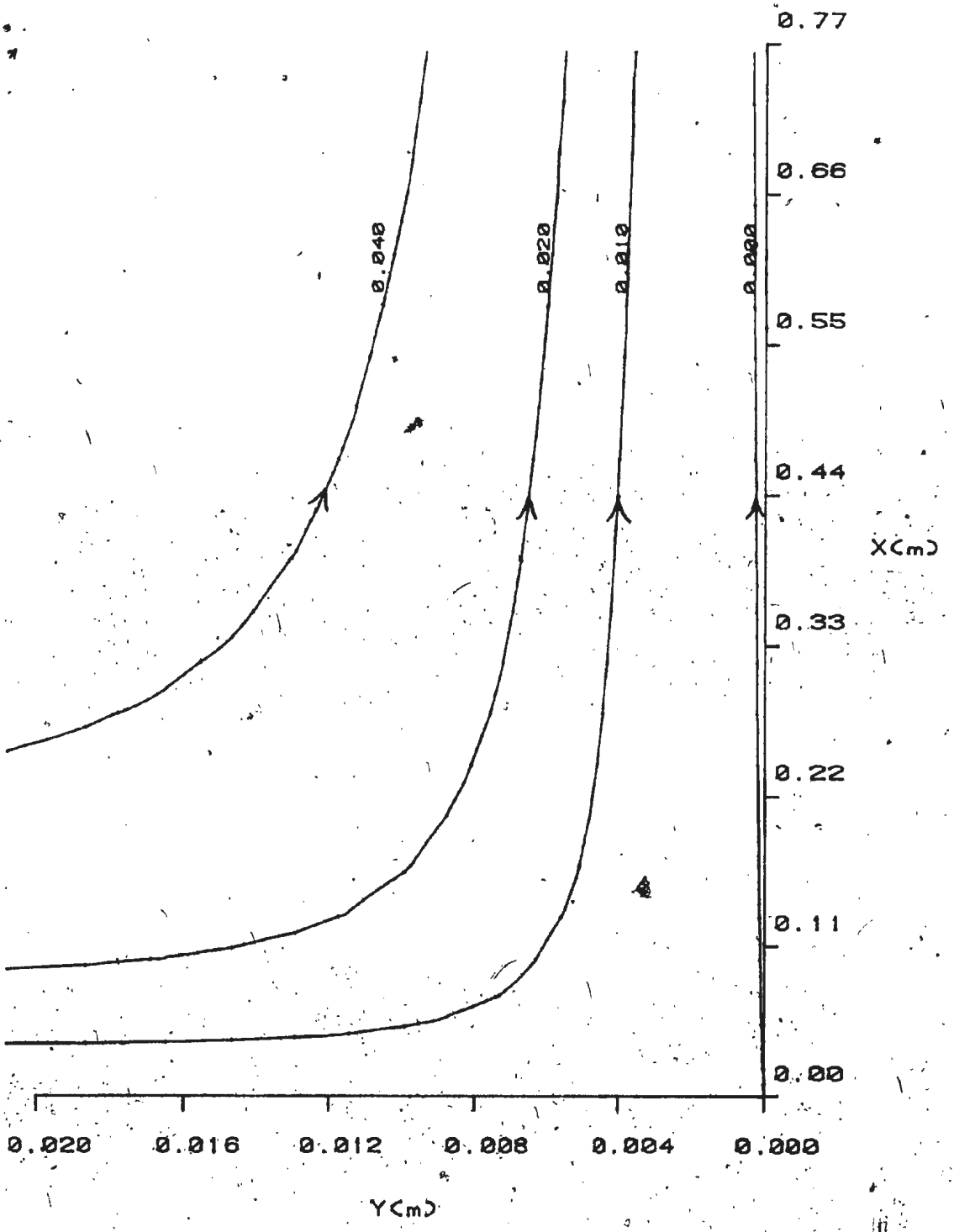

Figure 7(a) Streamlines for T_∞= 1.00 °C, S_∞= 0.0 ‰

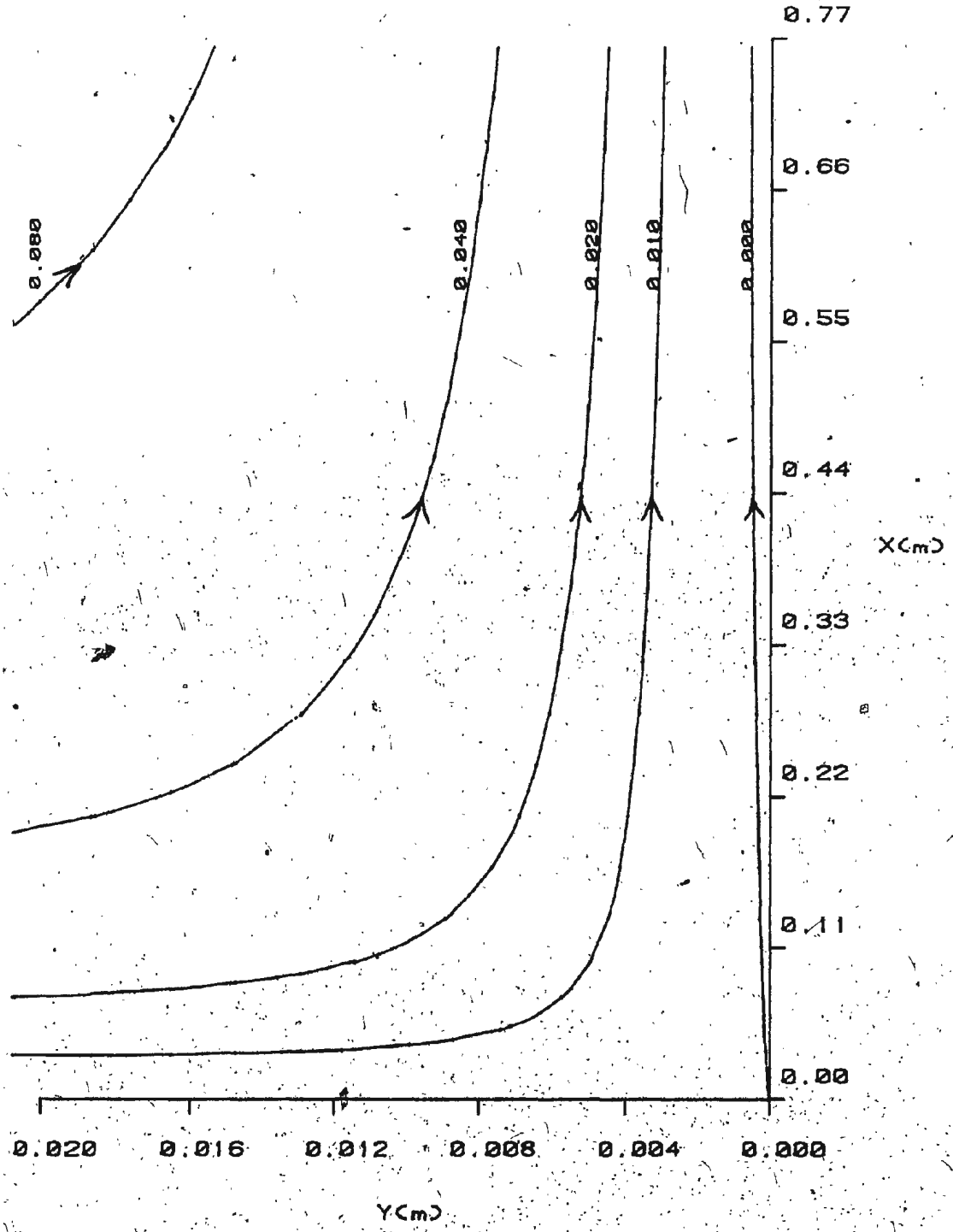

Figure 7(b) Streamlines for T_∞ = 2.50 °c, S_∞ = 0.0‰

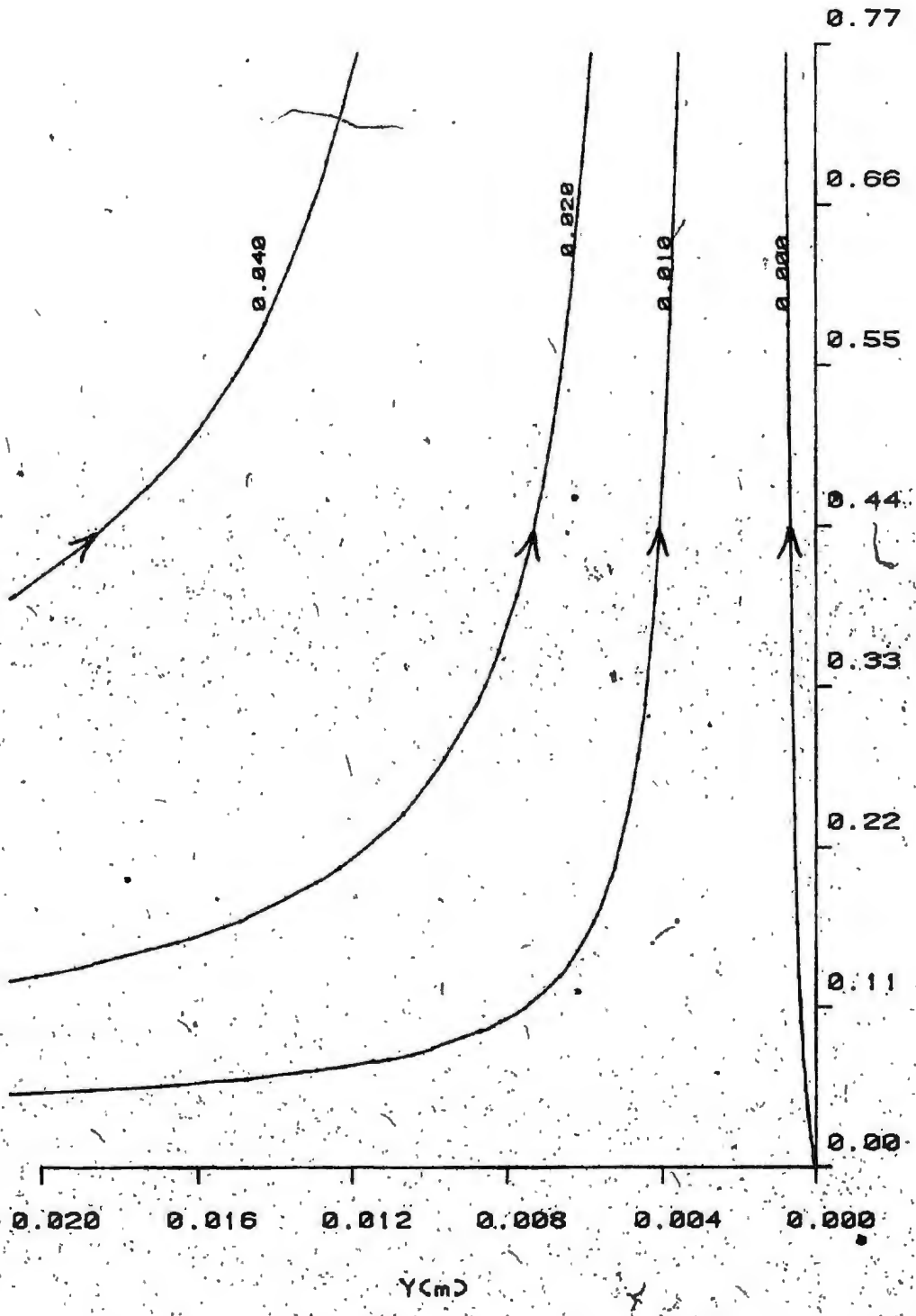

Figure 7(c) Streamlines for T_∞ = 4.50 °C, S_∞ = 0.0‰

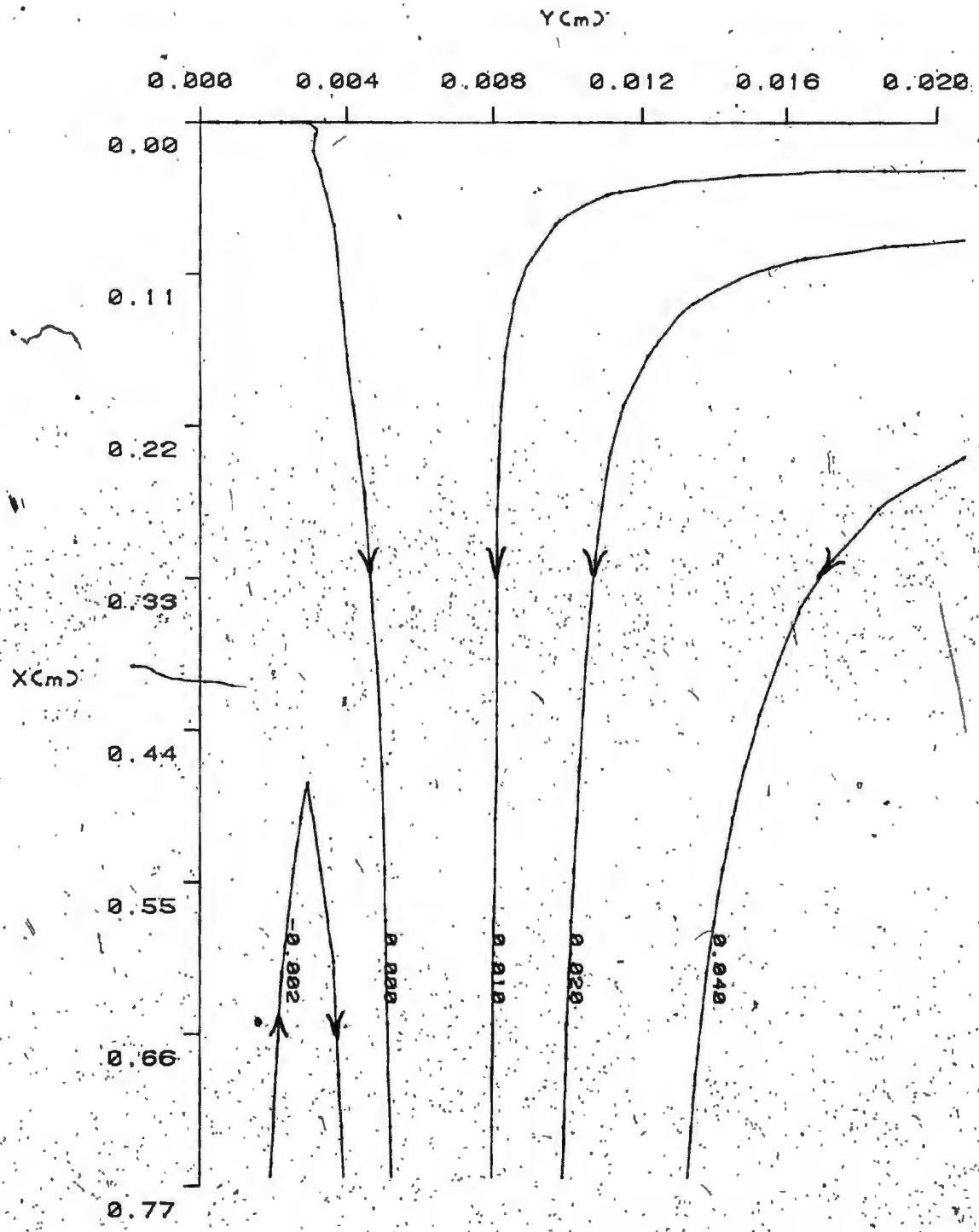

Figure 7(d) Streamlines for T_∞= 5.73 °c, S_∞= 0.0 ‰

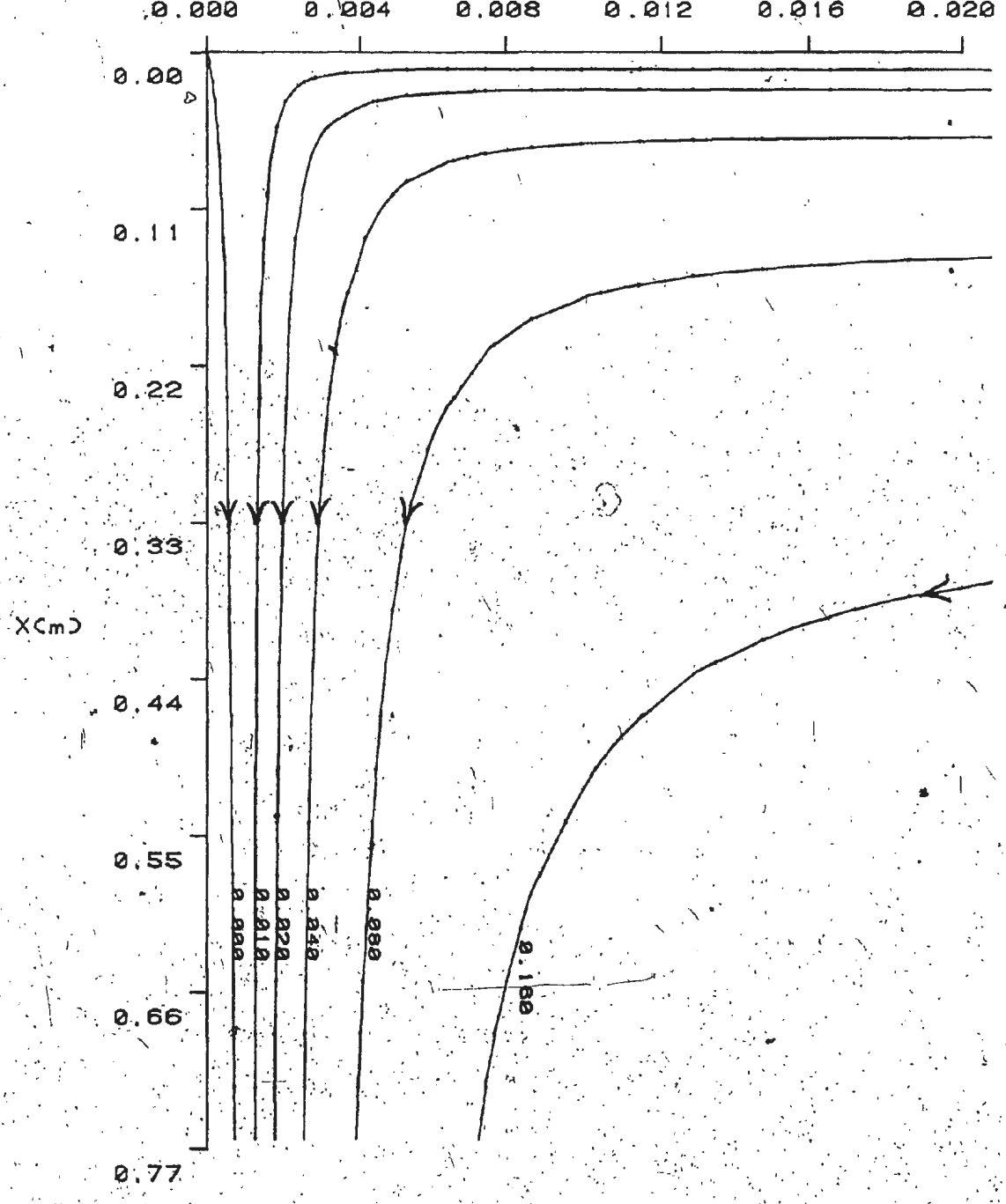

Figure 7(e) Streamlines for $T_\infty = 14.00\,^{\circ}C$, $S_\infty = 0.0\%$

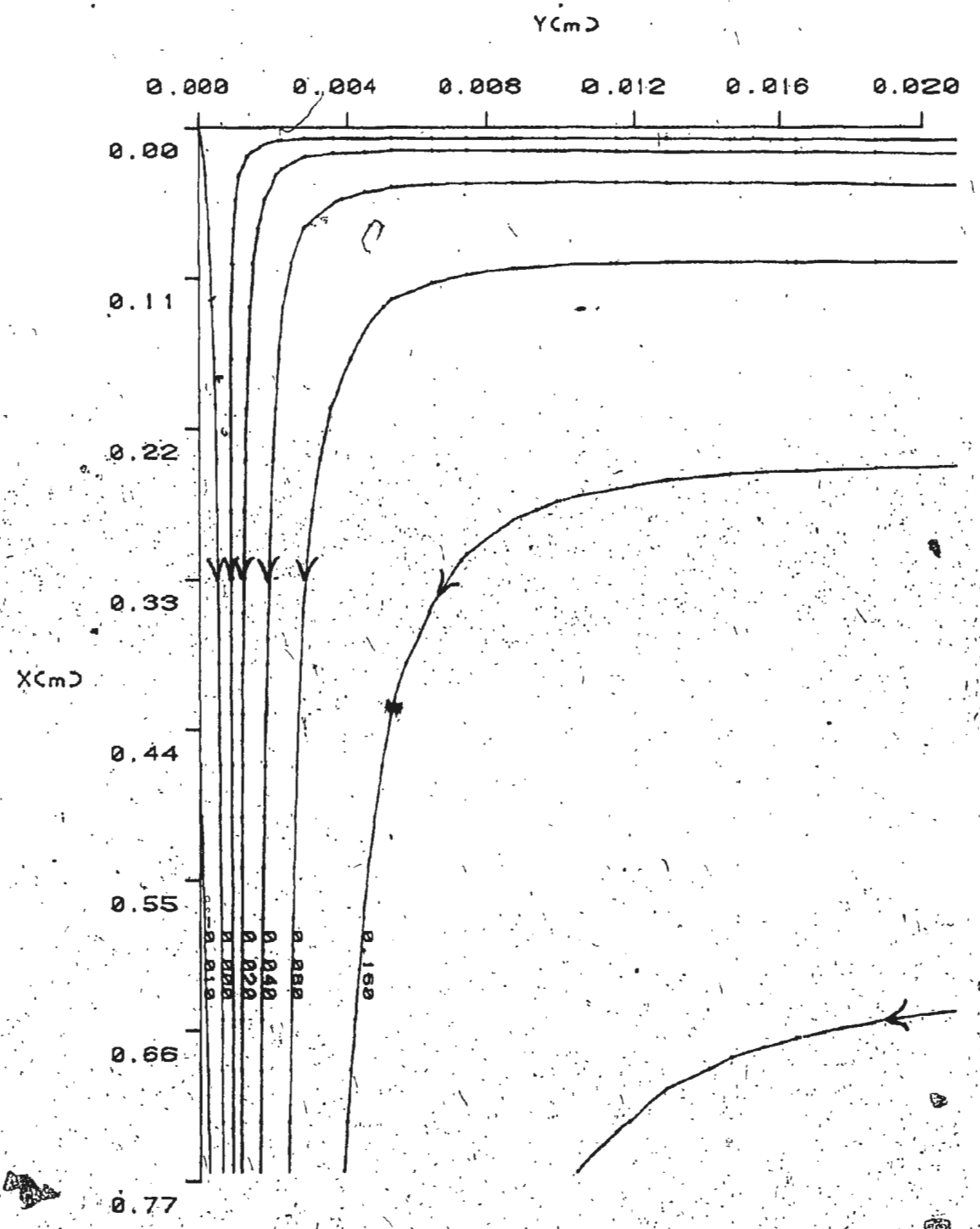

Figure 7(f) Streamlines for $T_\infty = 24.00\,^{\circ}C$, $S_\infty = 0.0\,\%$

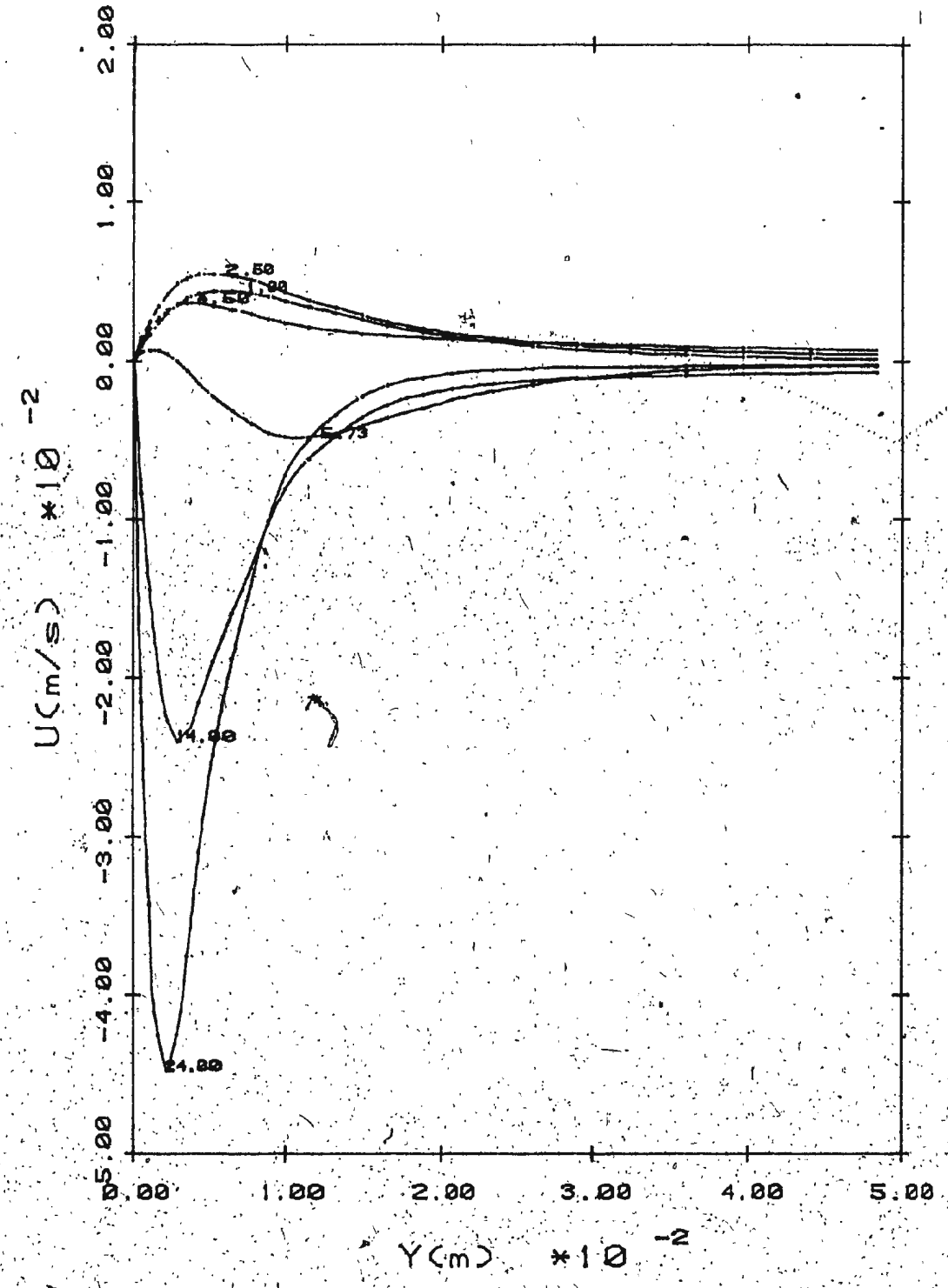

Figure 8(a) Velocity Profiles of Different T_∞ for S_∞= 0.% at x= 0.0528 m

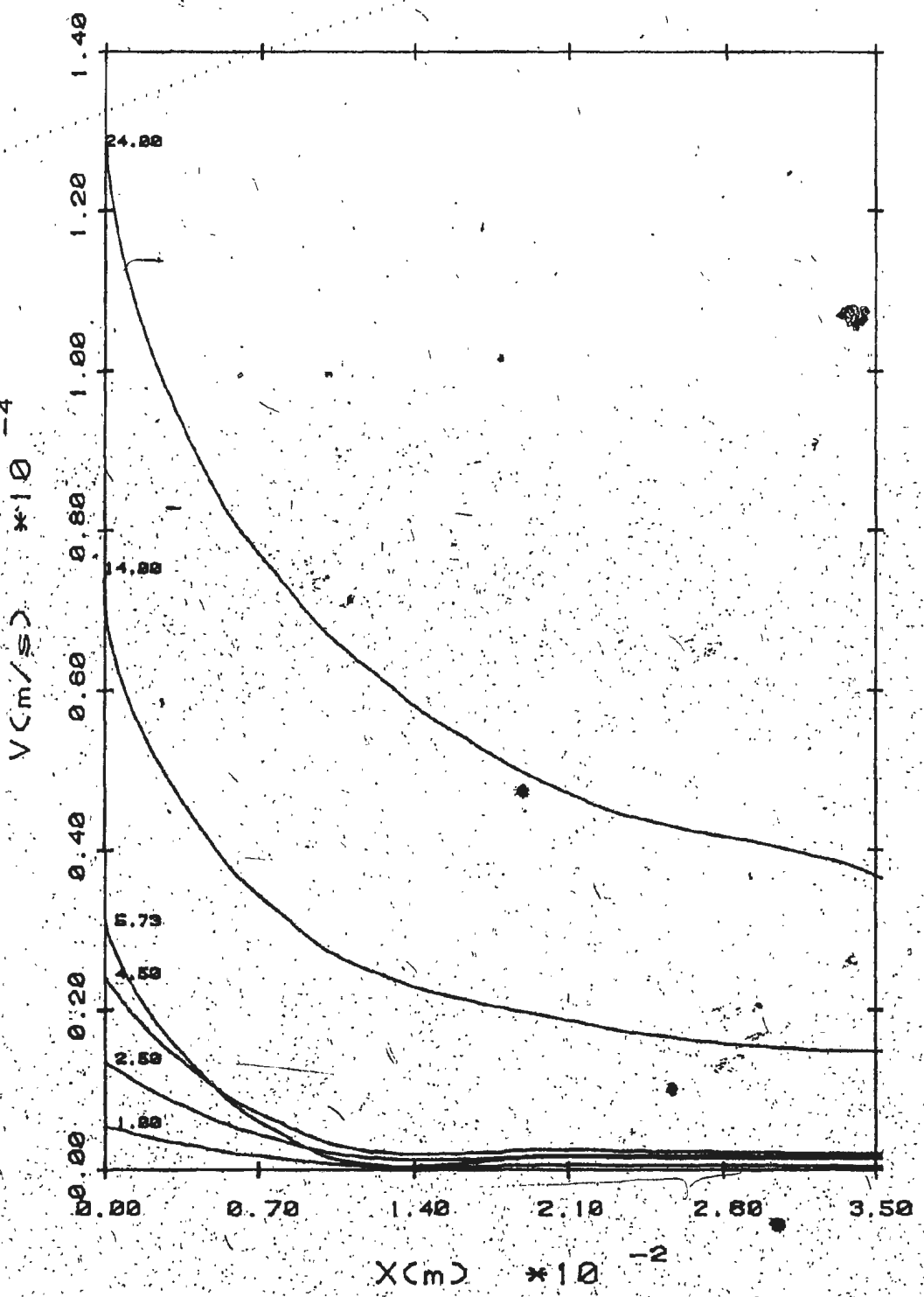

Figure 8(b) Melt Velocities of Different T_∞ for $S_\infty = 0.\%$ at $y = 0.$ m

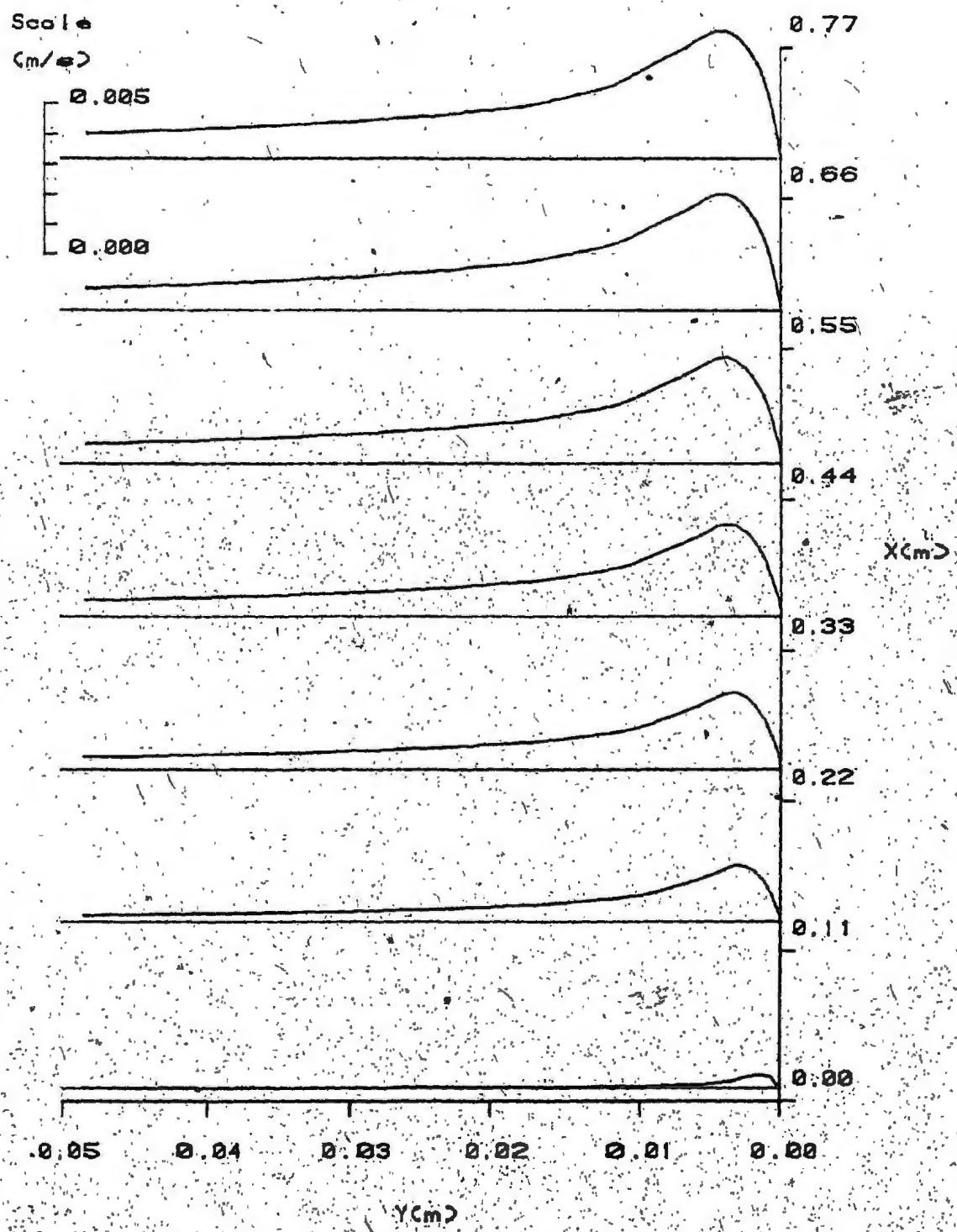

Figure 9(a) Velocity Profiles for T_∞ = 4.50 °C, S_∞ = 0.‰

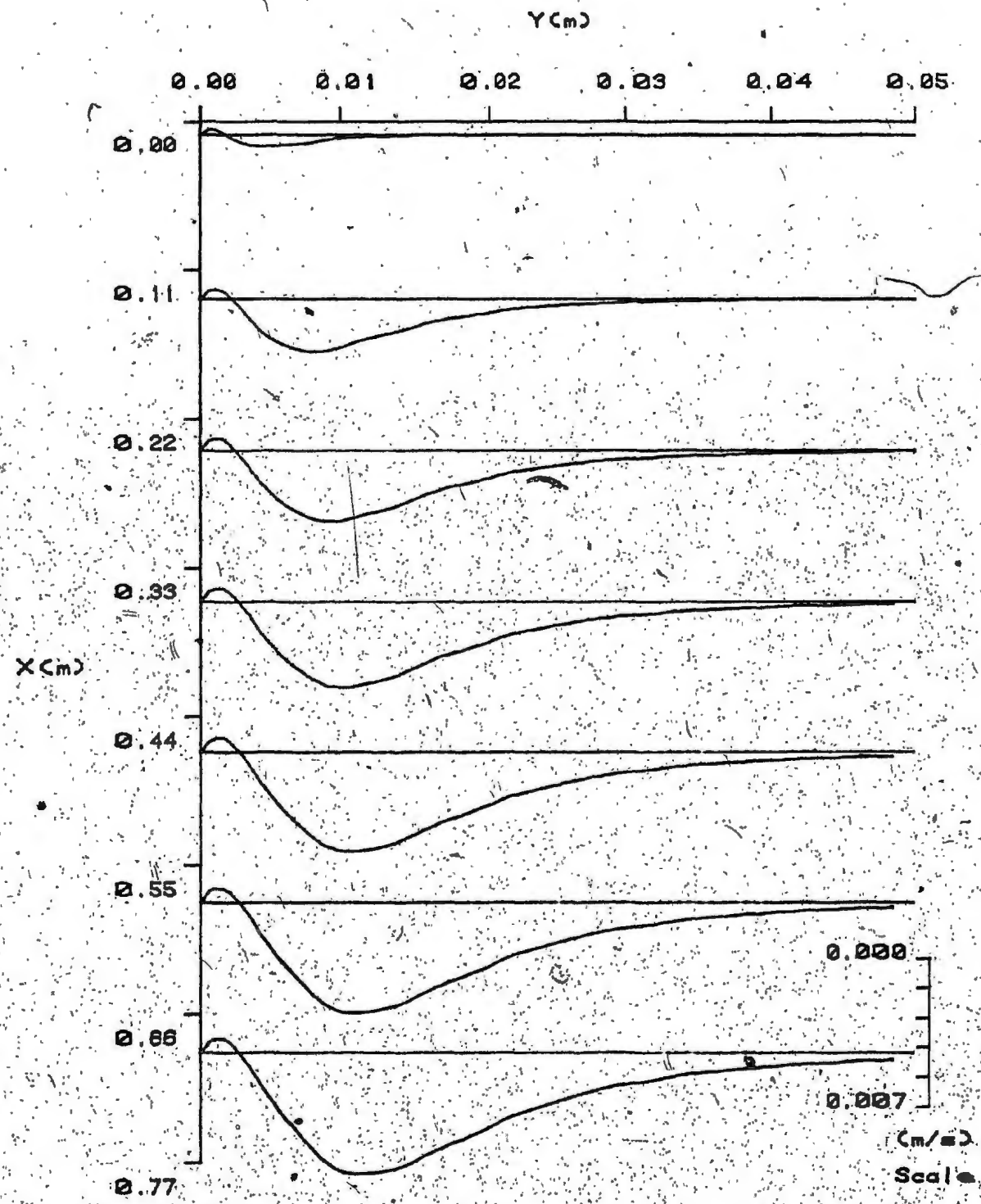

Figure 9(b) Velocity Profiles for $T_\infty = 5.73^\circ C$, $S_\infty = 0.\%$

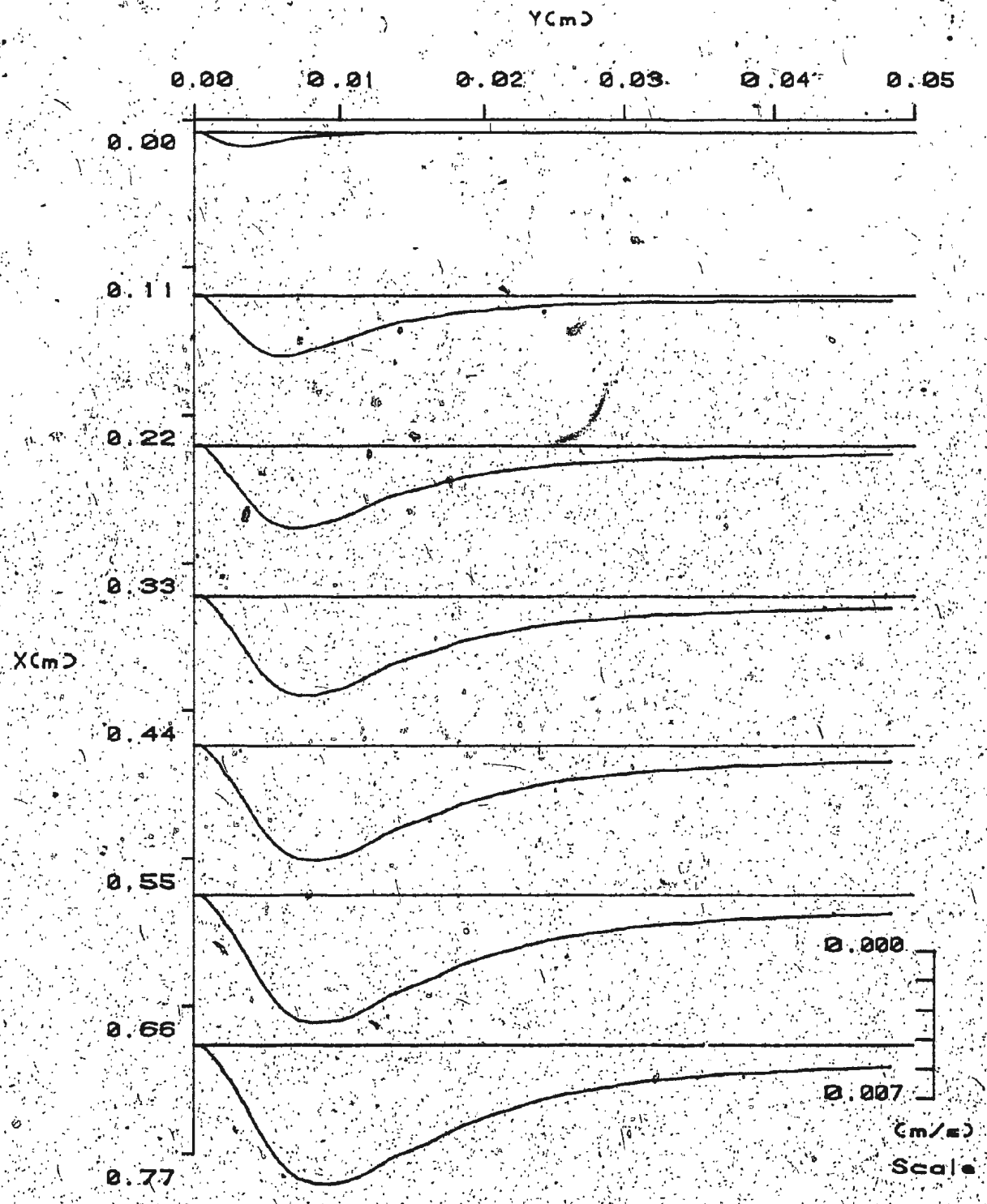

Figure 9(c) Velocity Profiles for T_∞ = 6.00 °c, S_∞ = 0. ‰

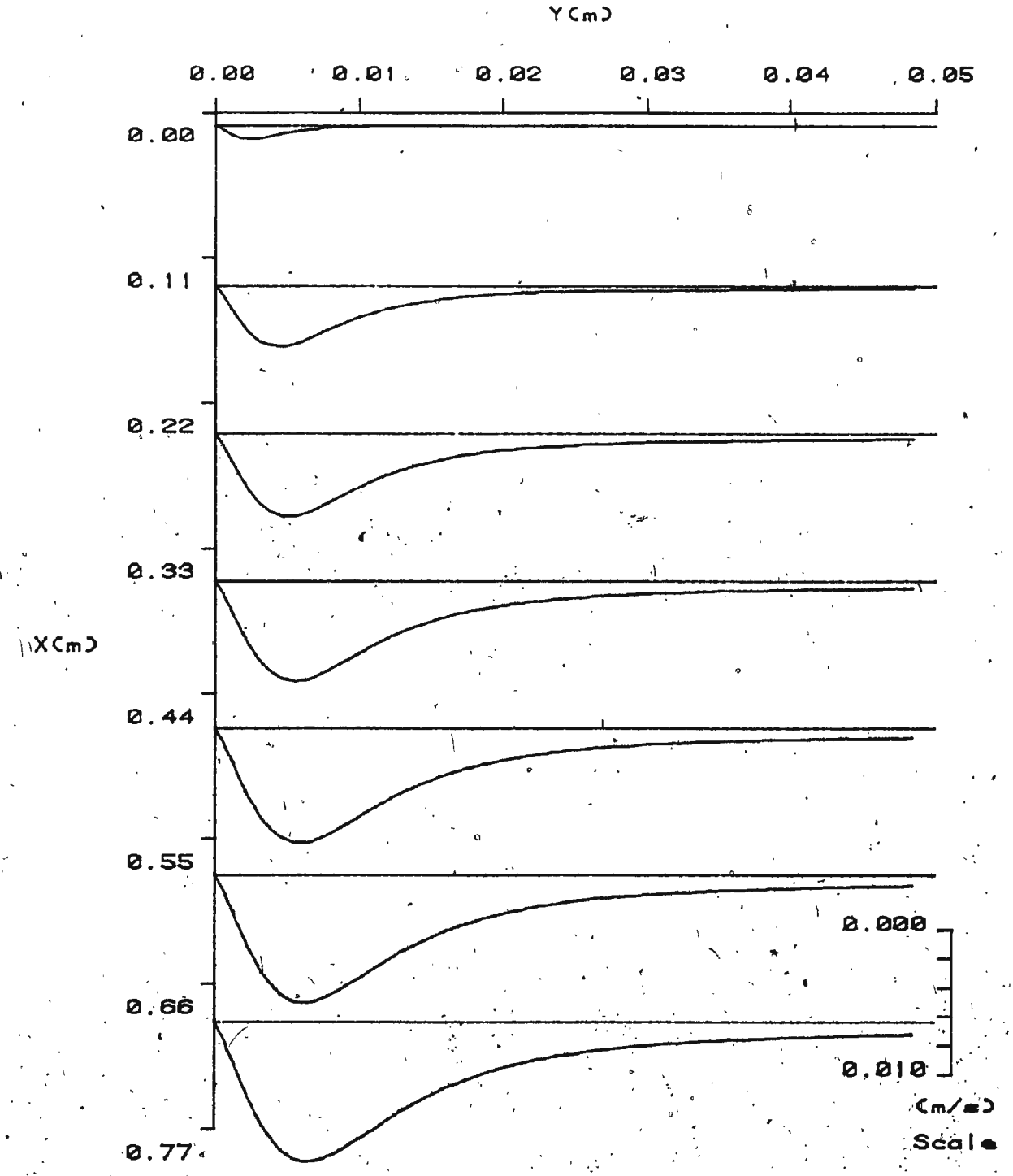

Figure 9(d) Velocity Profiles for T_∞ = 7.00 °C, S_∞ = 0. ‰

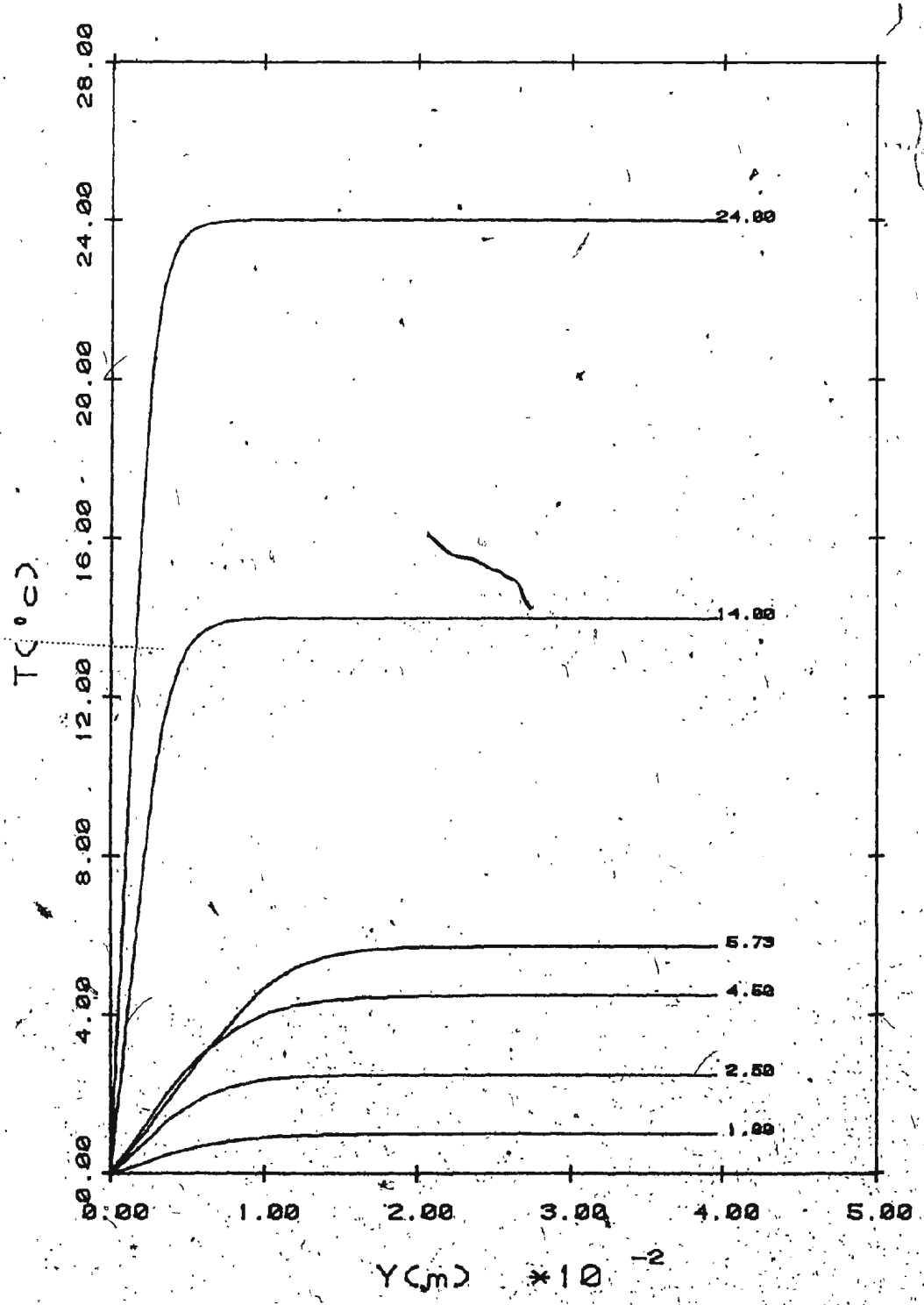

Figure 10 Temperature Profiles of Different T_∞ for S_∞ = 0.% at x= 0.5029 m

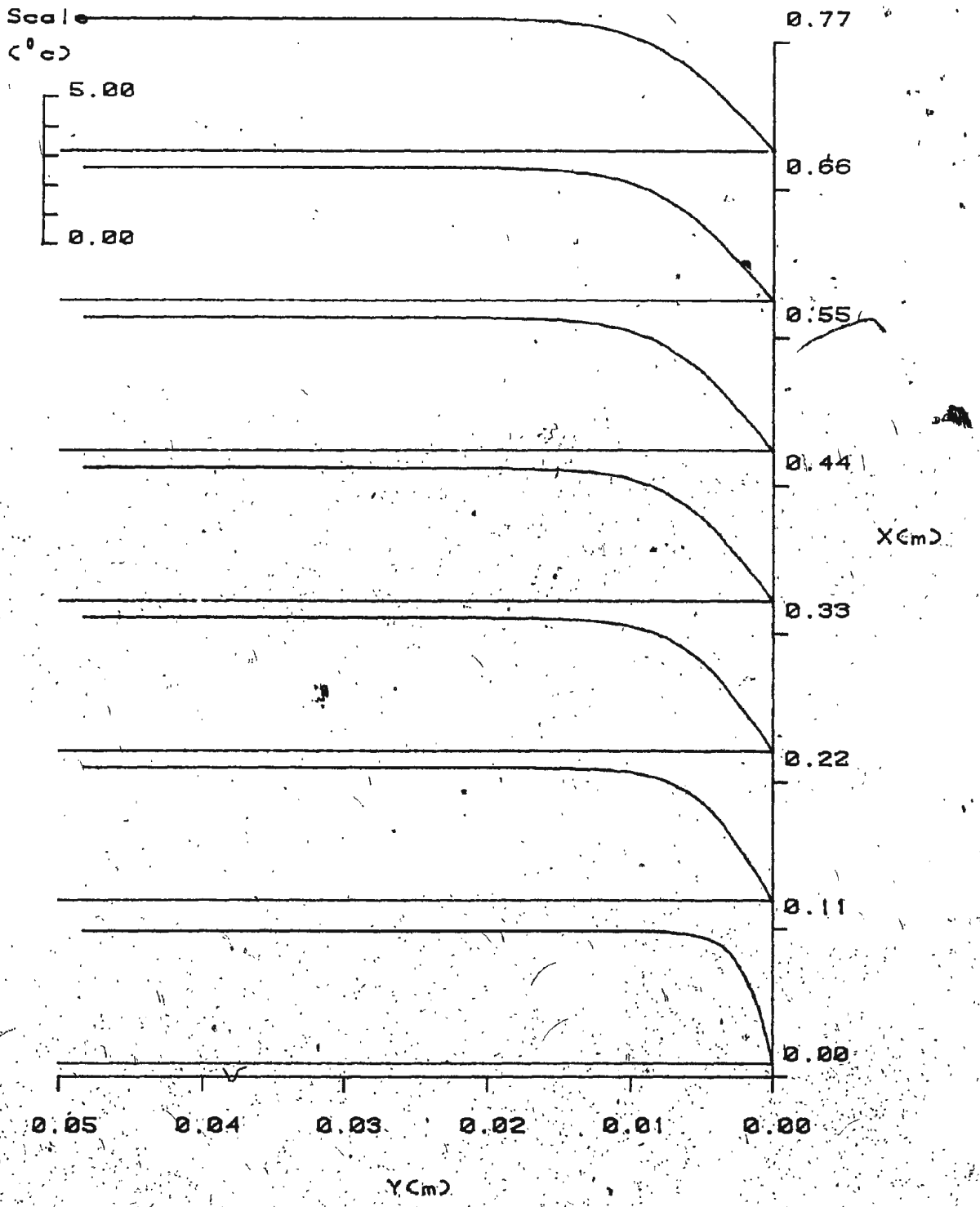

Figure 11(a) Temperature Profiles for T_∞ = 4.50°c, S_∞ = 0.%

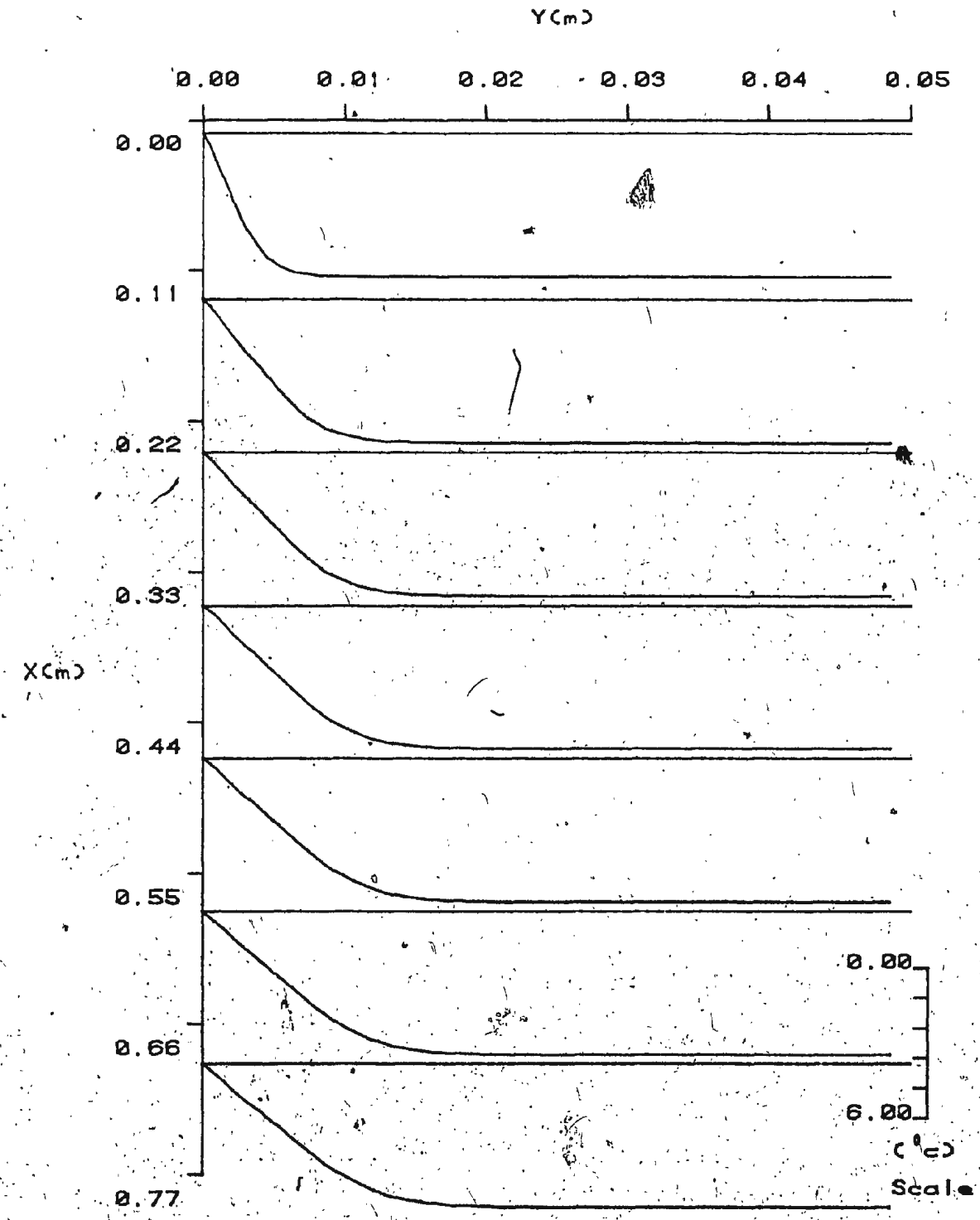

Figure 11(b) Temperature Profiles for T_∞ = 5.73°C, S_∞ = 0.‰

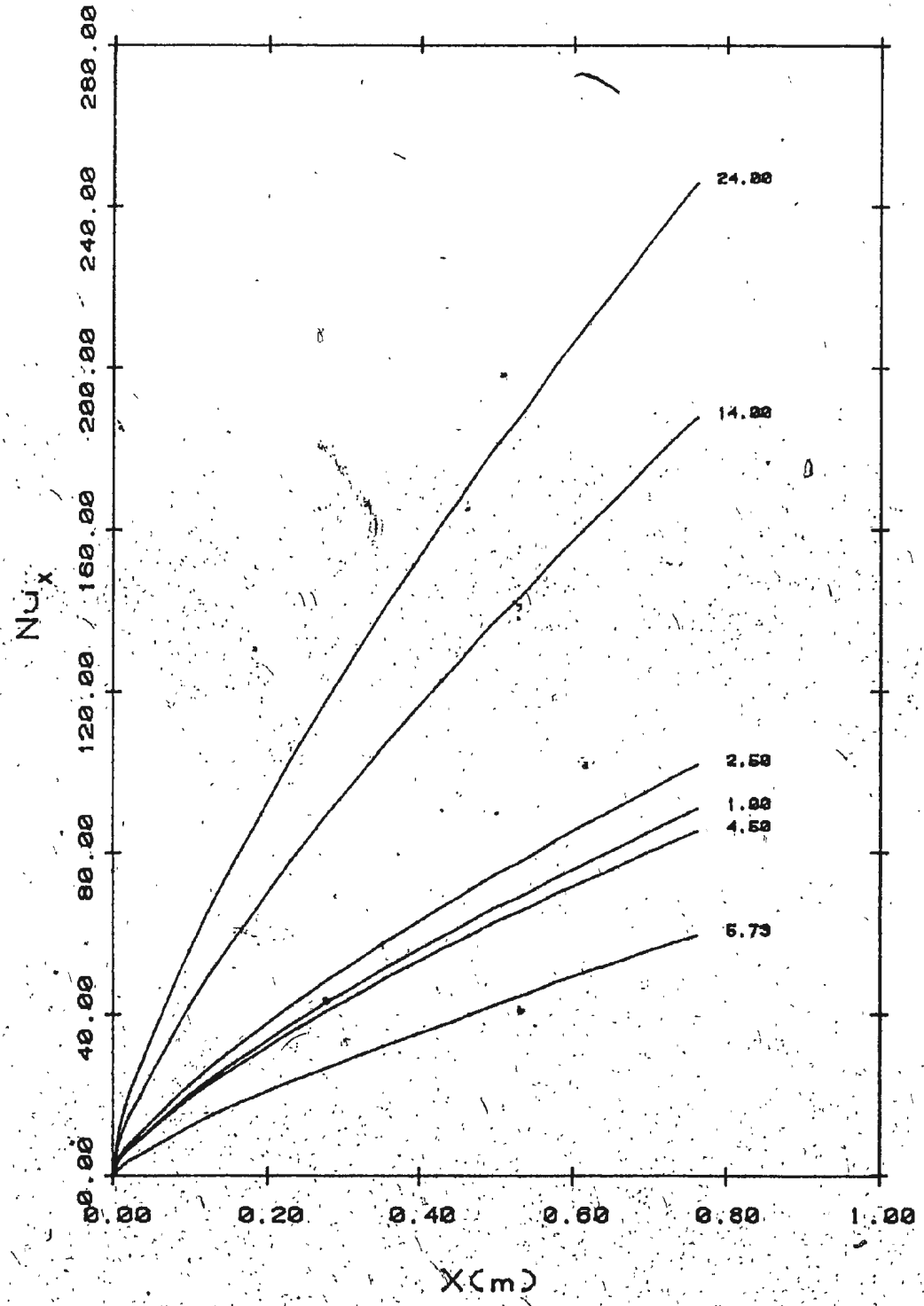

Figure 12 Nu_x of Different T_∞ as a Function of x for S = 0.9

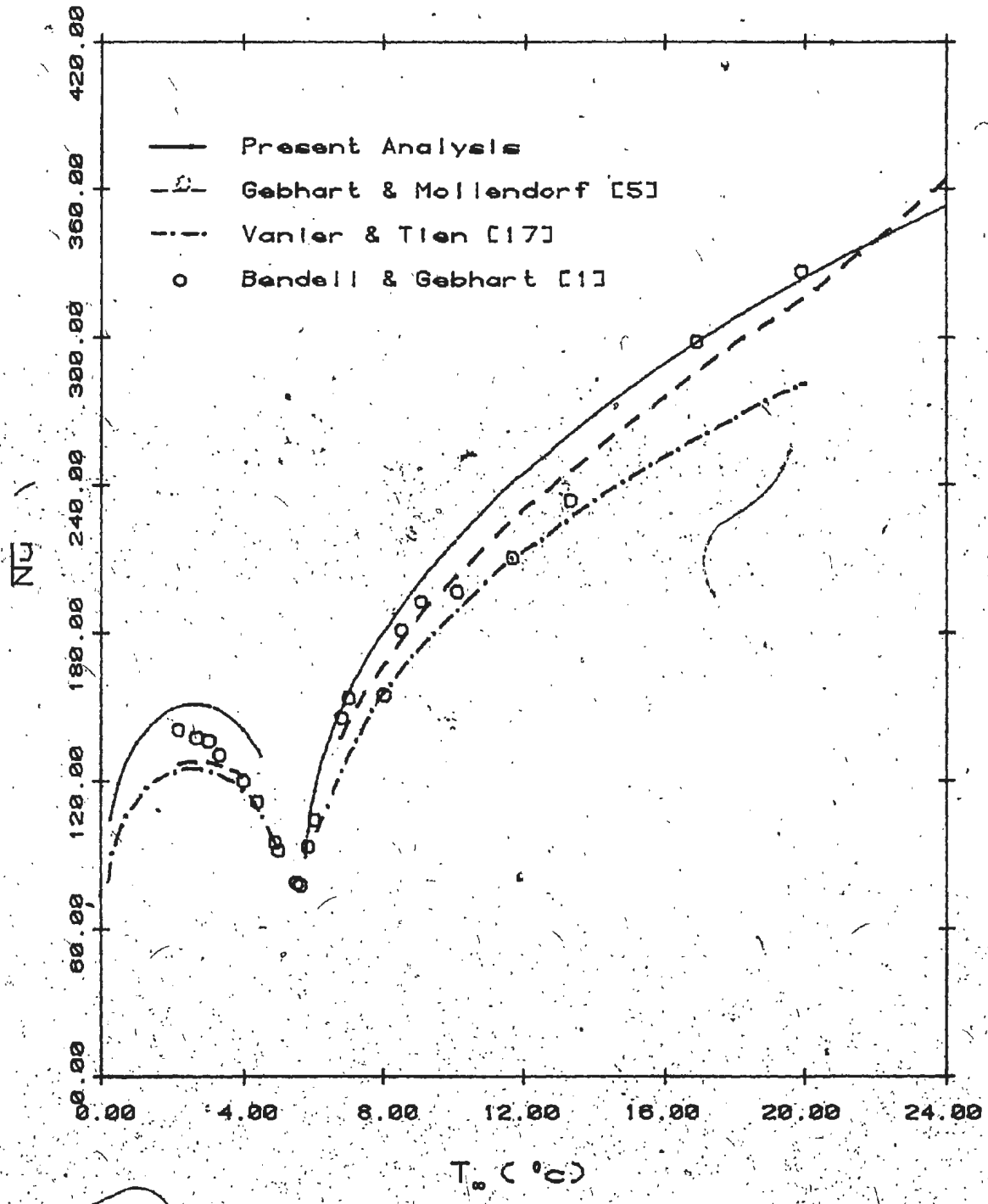

Figure 13 $\overline{Nu}$ Over a Length, 0.7632 m, of a Vertical Plate for Zero Salinity

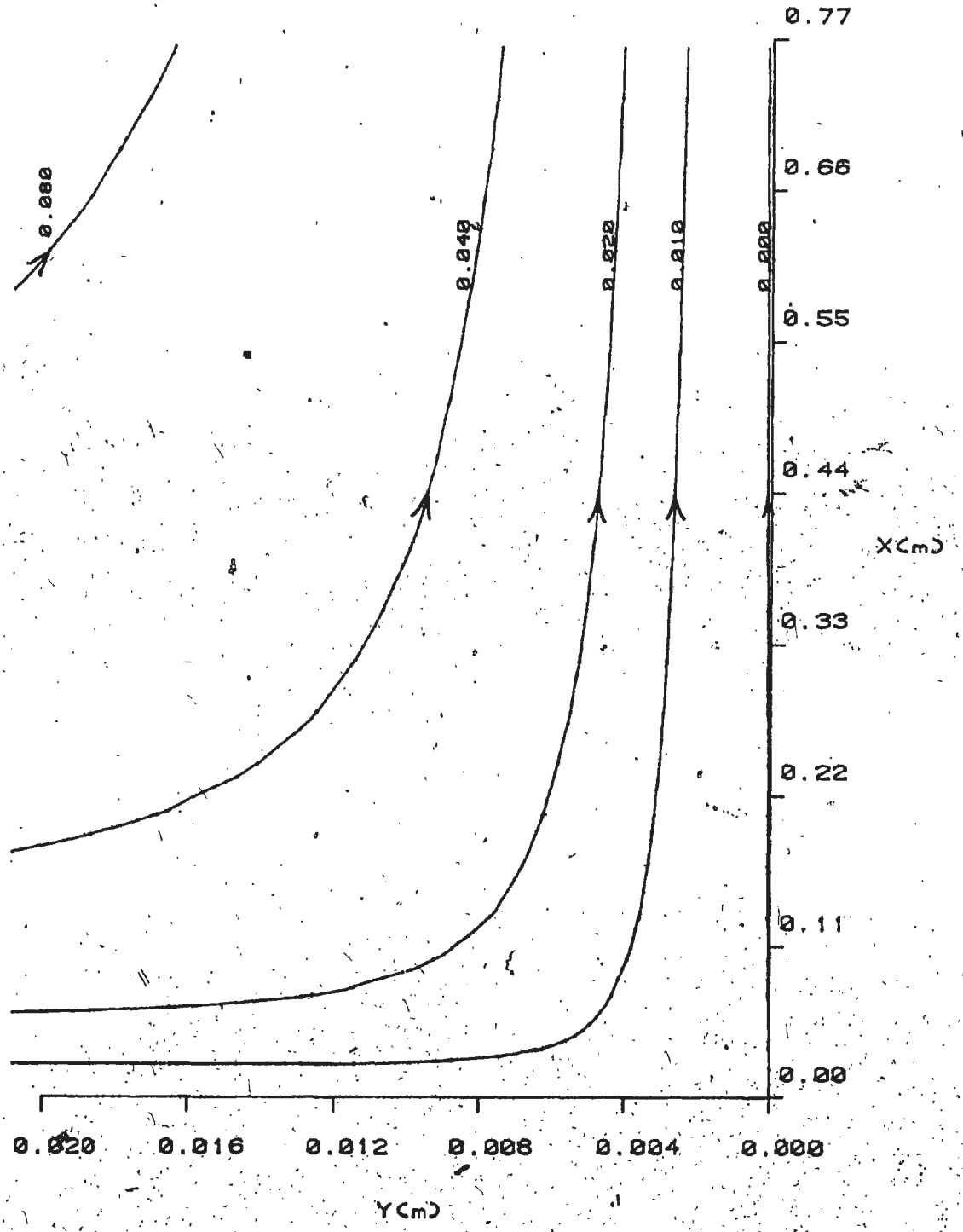

Figure 14(a) Streamlines for T_∞ = 1.00 °C, S_∞ = 5.0‰

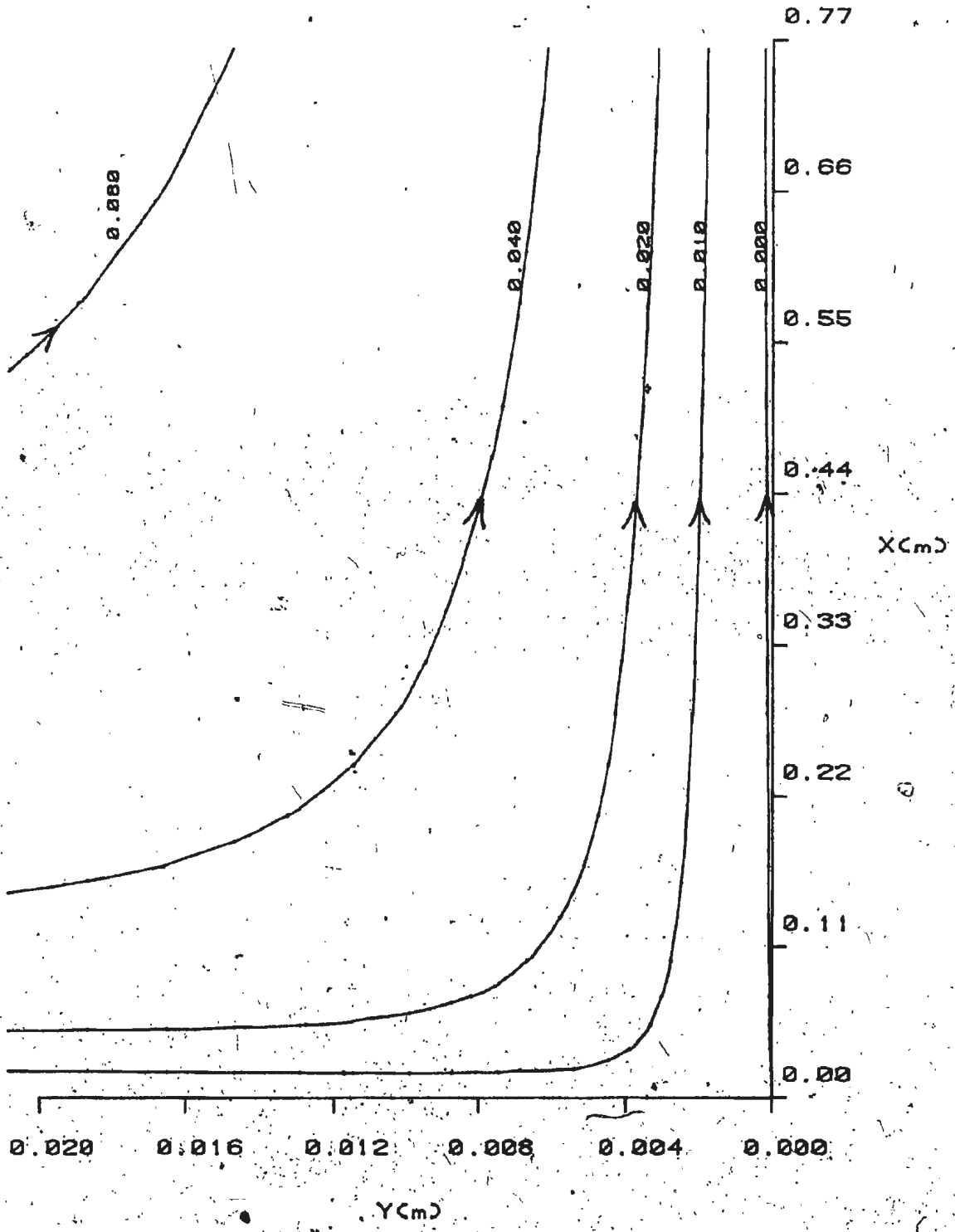

Figure 14(b) Streamlines for T_∞ = 3.00°C, S_∞ = 5.0%

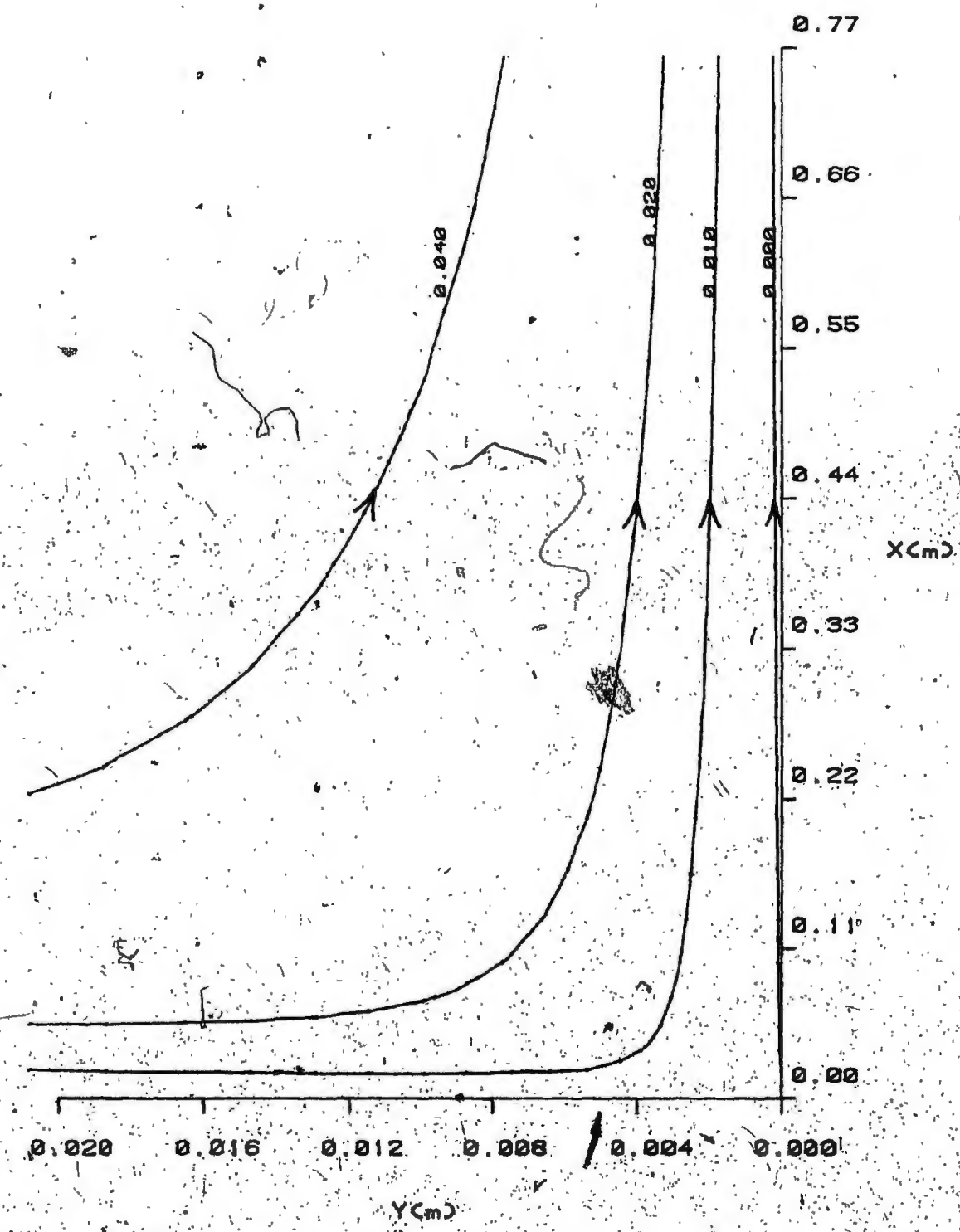

Figure 14(c) Streamlines for T_∞ = 3.87 °C, S_∞ = 5.0%

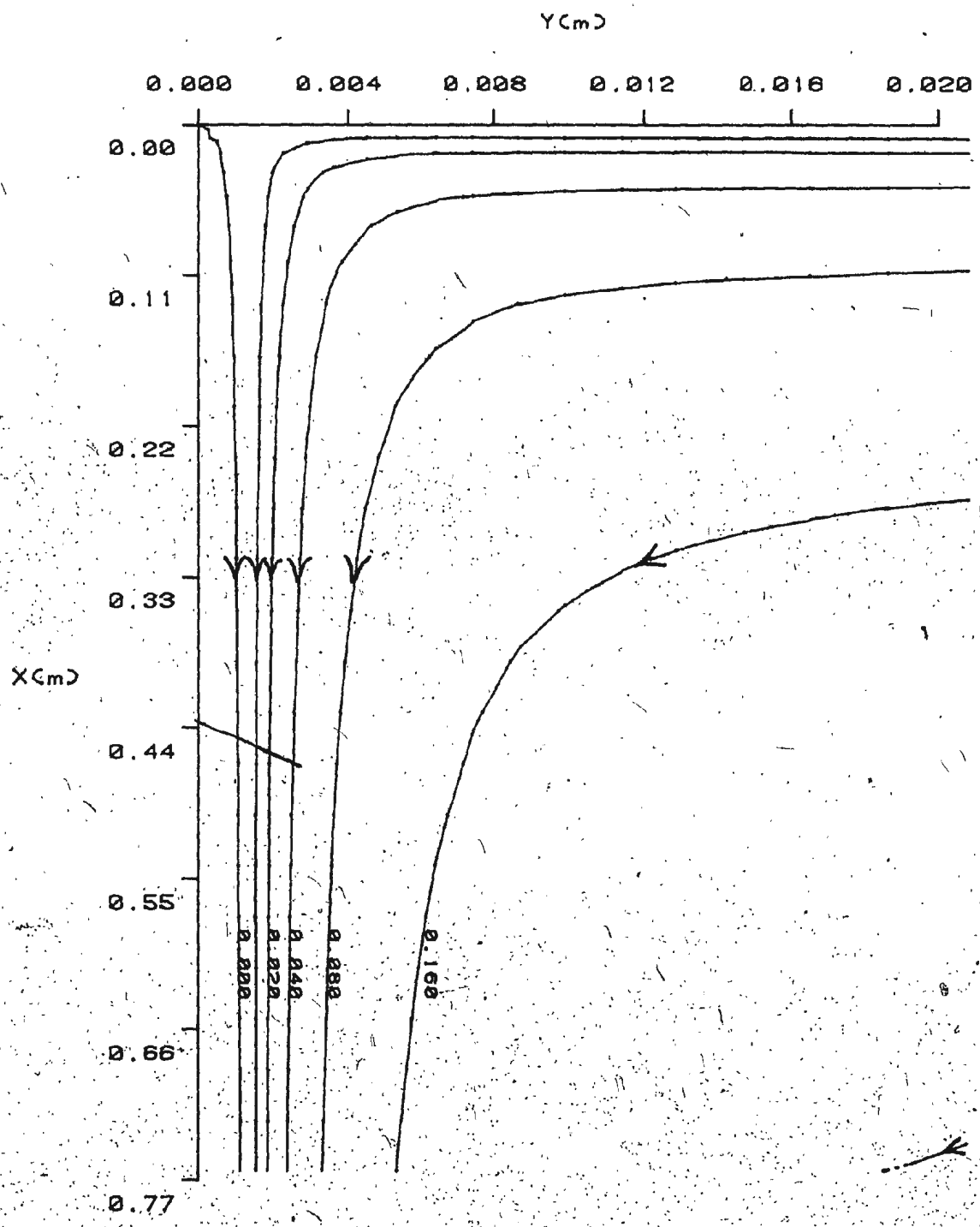

Figure 14(d) Streamlines for $T_\infty = 20.85\ ^\circ c$, $S_\infty = 5.0\ ‰$

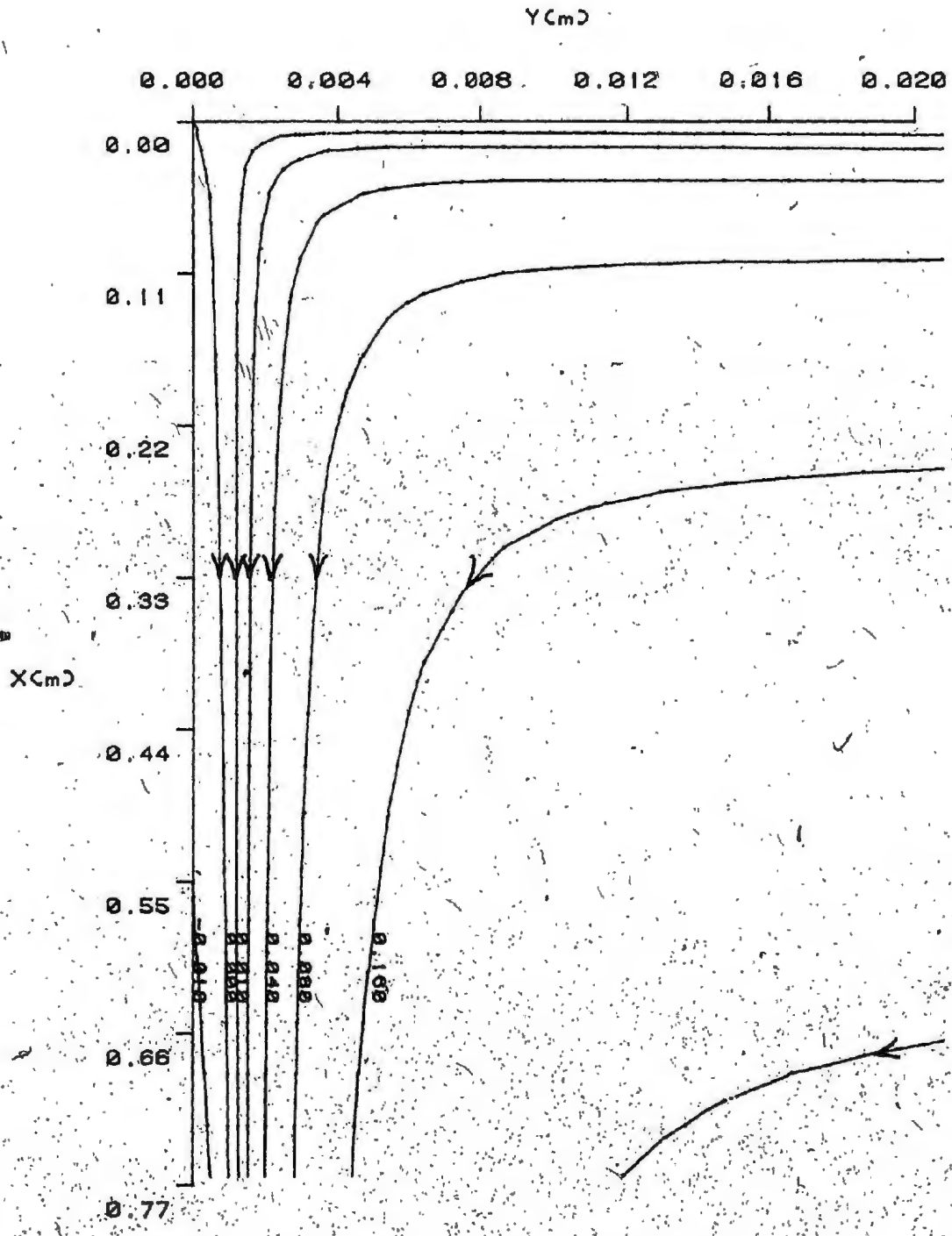

Figure 14(e) Streamlines for $T_\infty = 24.00\ ^\circ C$, $S_\infty = 5.0\ ‰$

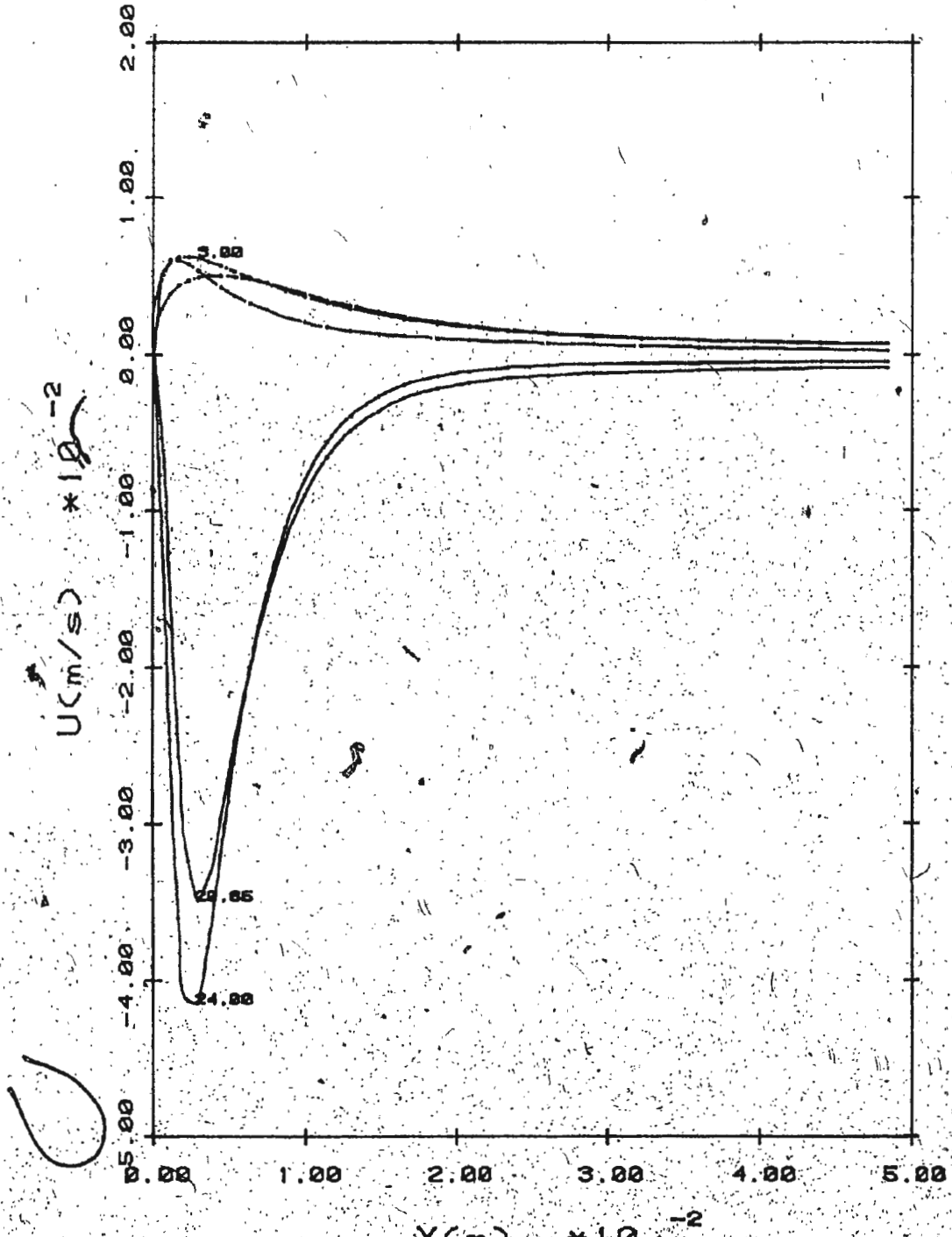

Figure 15 Velocity Profiles of Different T_∞ for $S_\infty = 5.$ at x= 0.0528 m

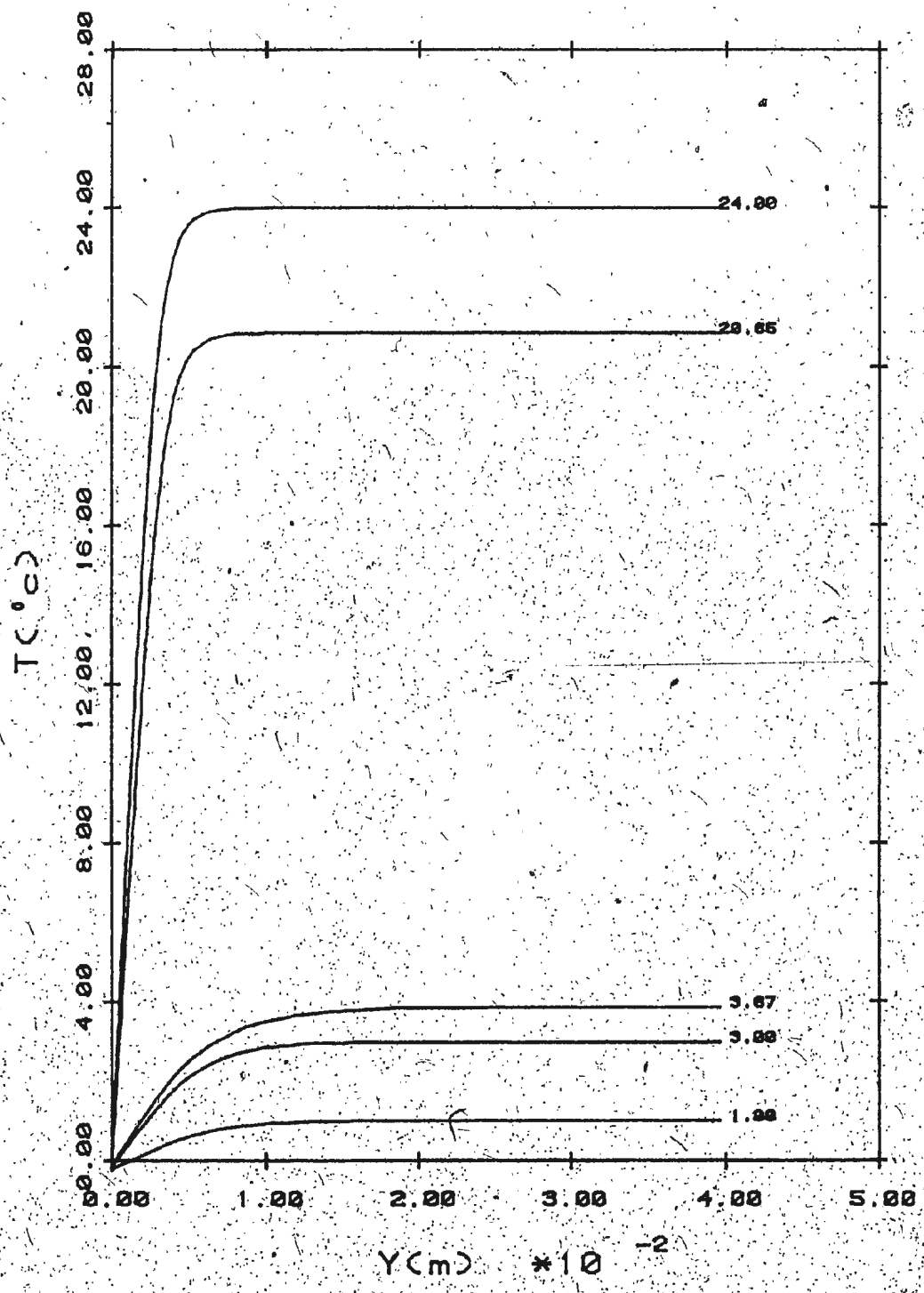

Figure 16 Temperature Profiles of Different T_∞ for S_∞ = 5.‰ at x= 0.5029 m

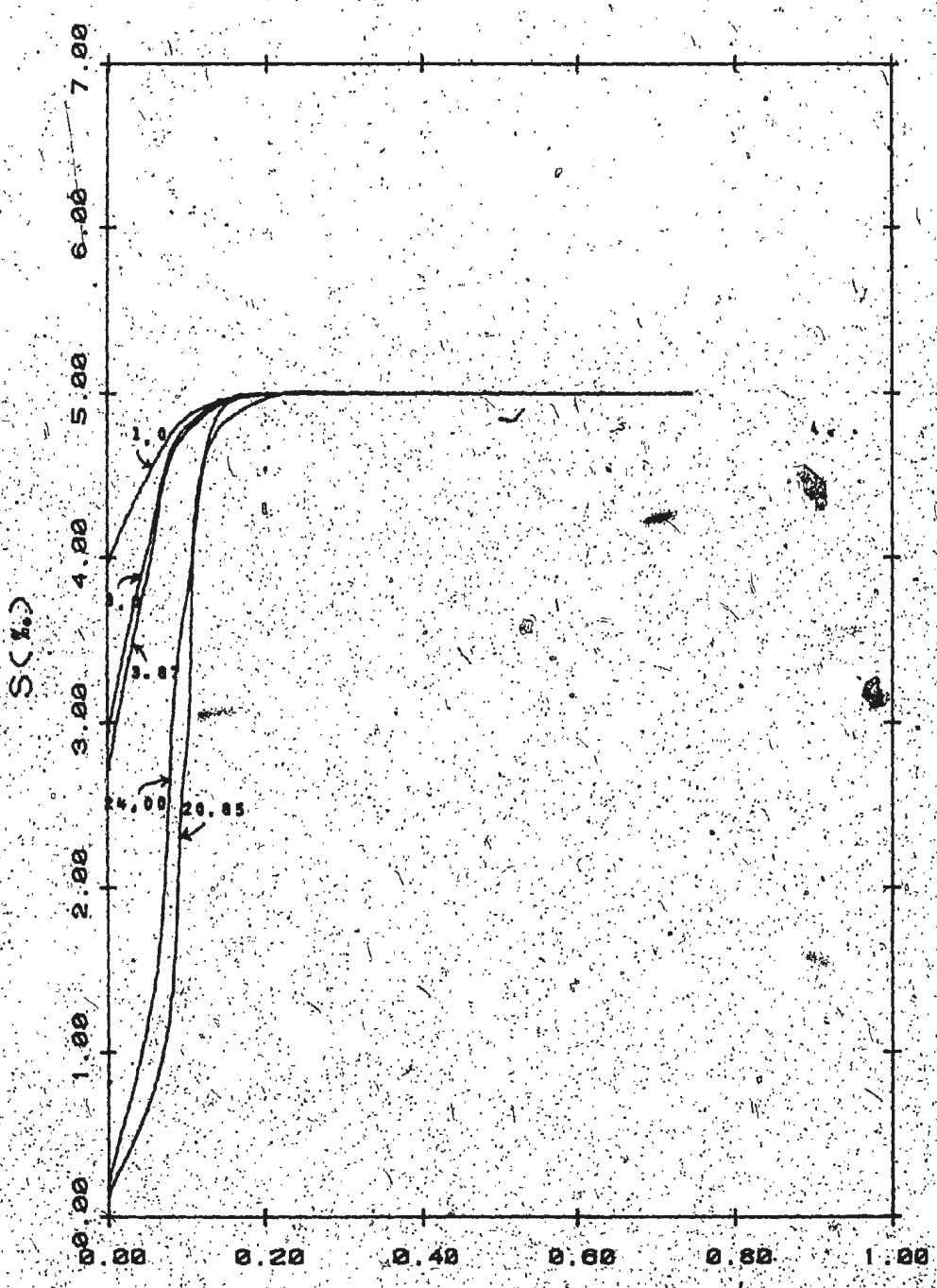

Figure 17(a) Salinity Profiles of Different T_∞ for S_∞ = 5. ‰ at x= 0.5029 m

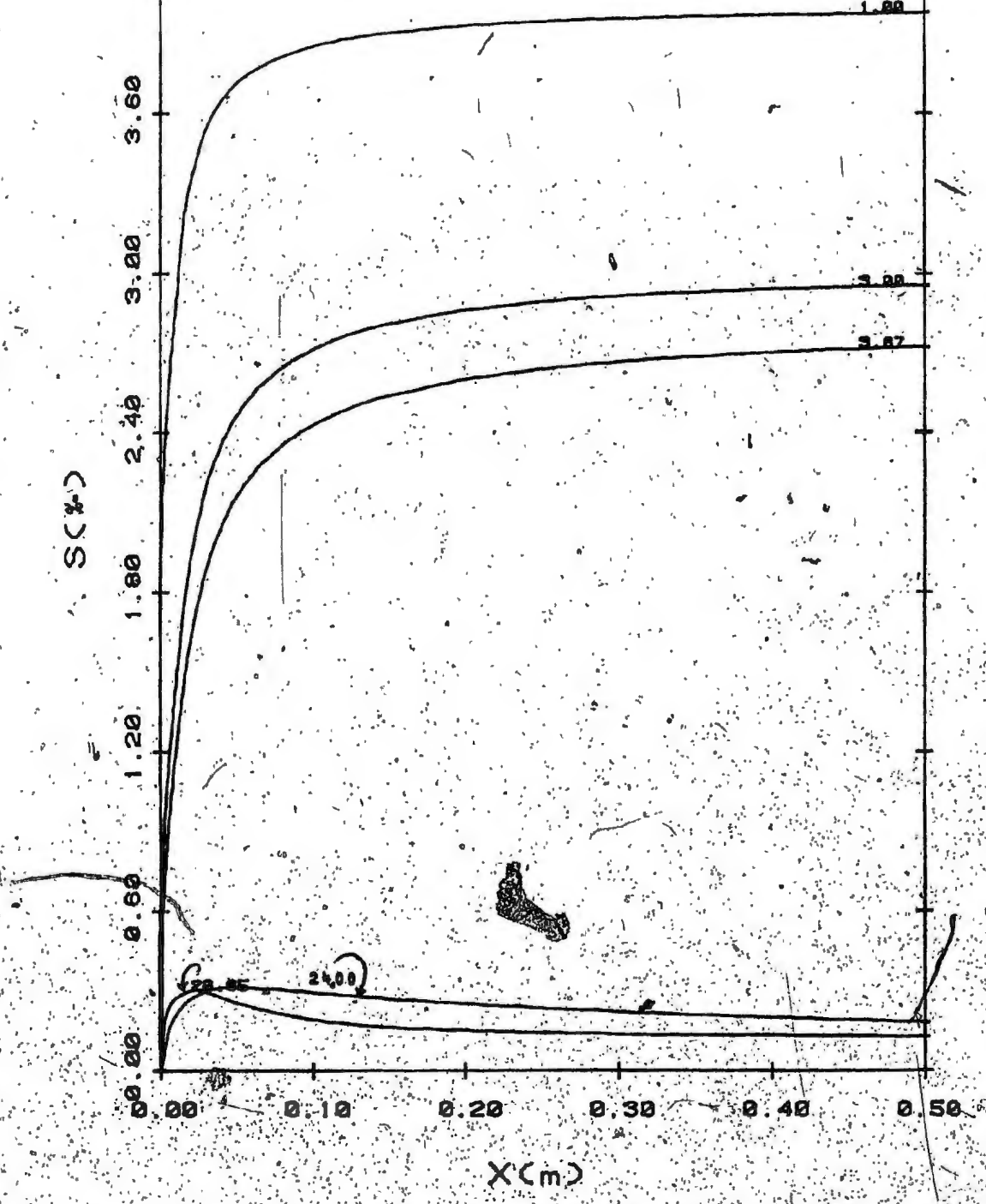

Figure 17(b) Salinity Profiles of Different T_∞ for S_∞ = 5.% at y= 0. m

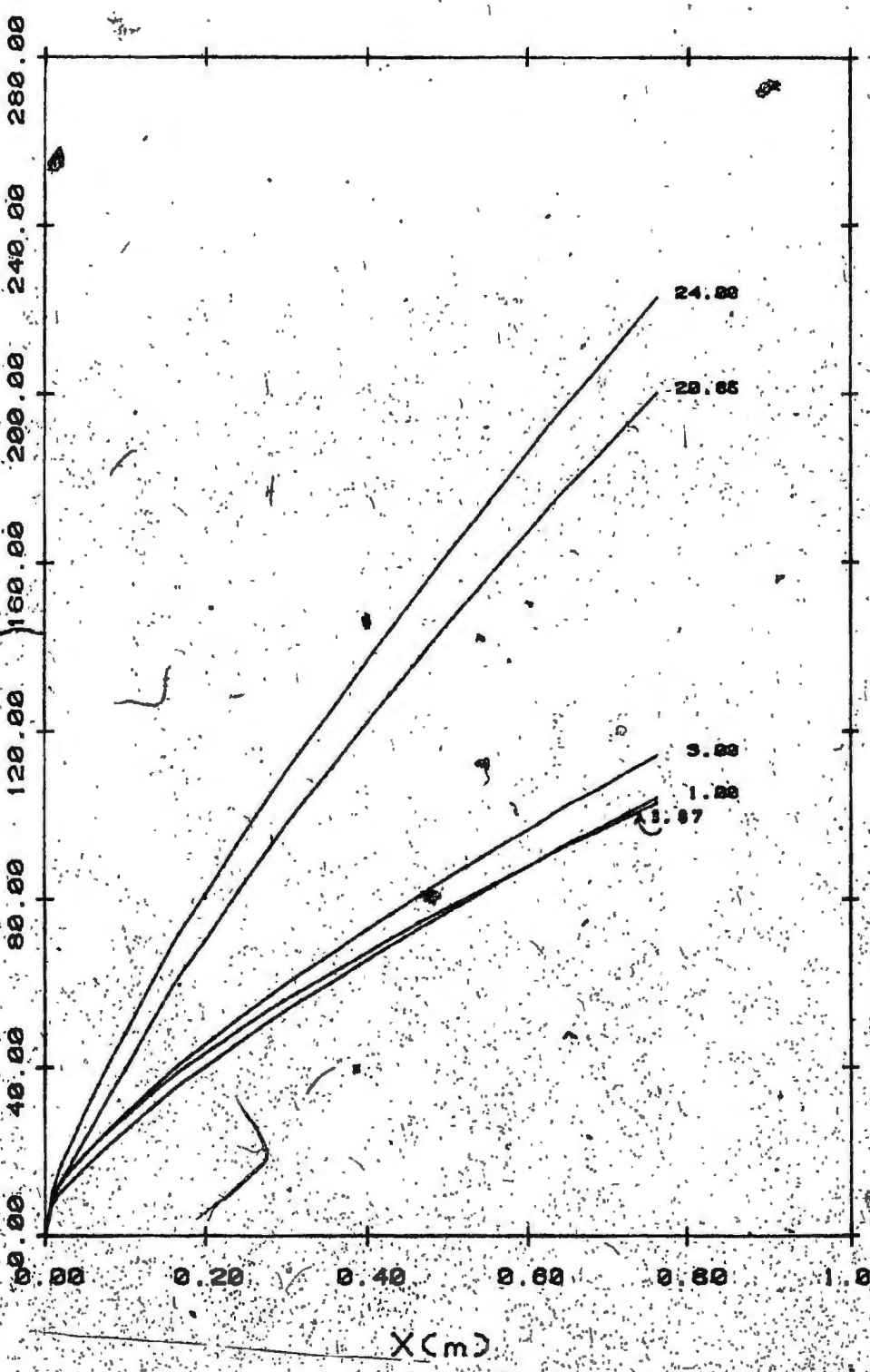

Figure 18 Nu_x of Different T_p as a Function of x for S_a = 5.%

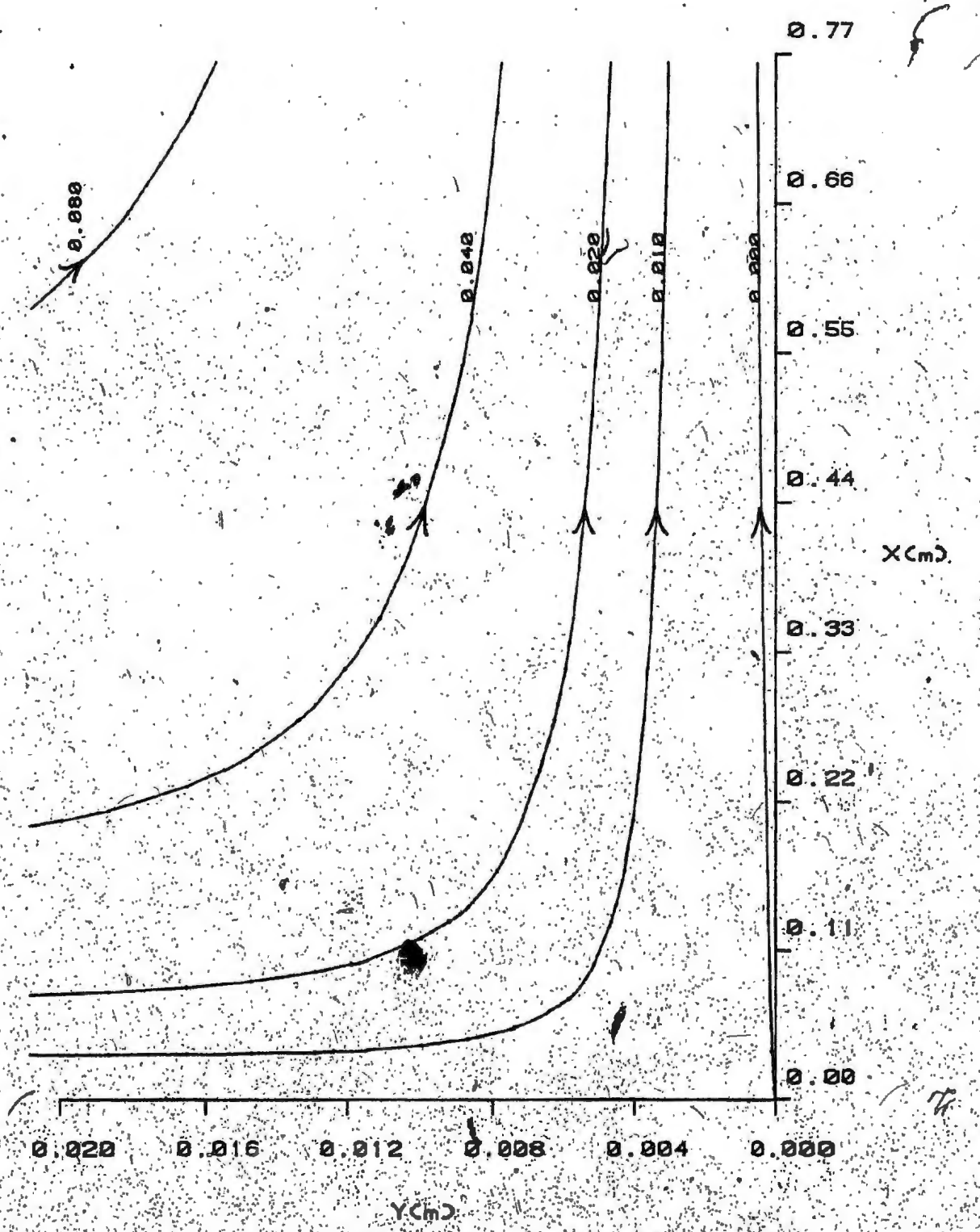

Figure 19(a) Streamlines for T_∞ = 2.00°C, S_∞ = 0.0‰

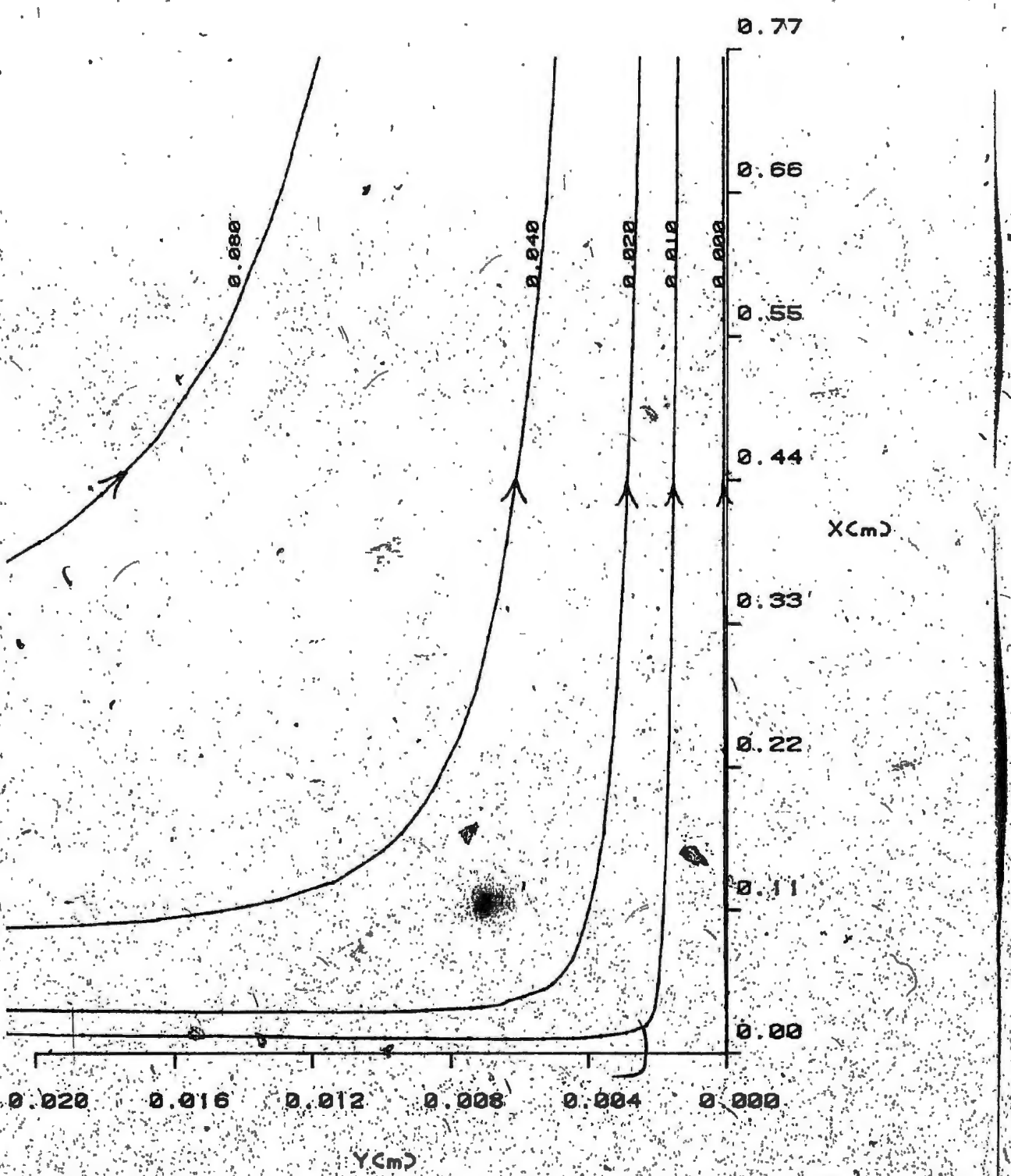

Figure 19(b) Streamlines for T_∞ = 2.00 °C, S_∞ = 10.0 ‰

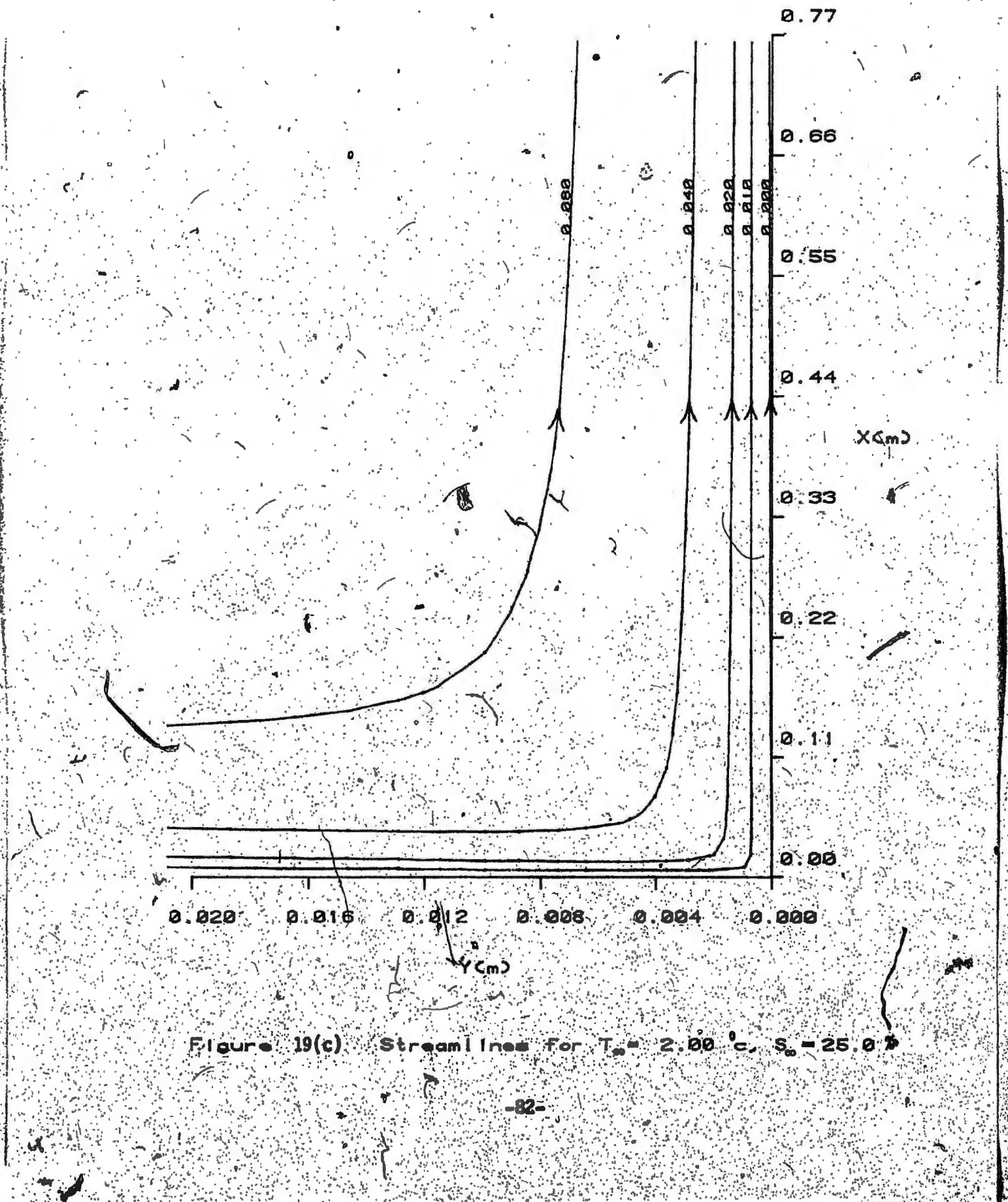

Figure 19(c) Streamlines for T_∞ = 2.00 °C, S_∞ = 25.0 ‰

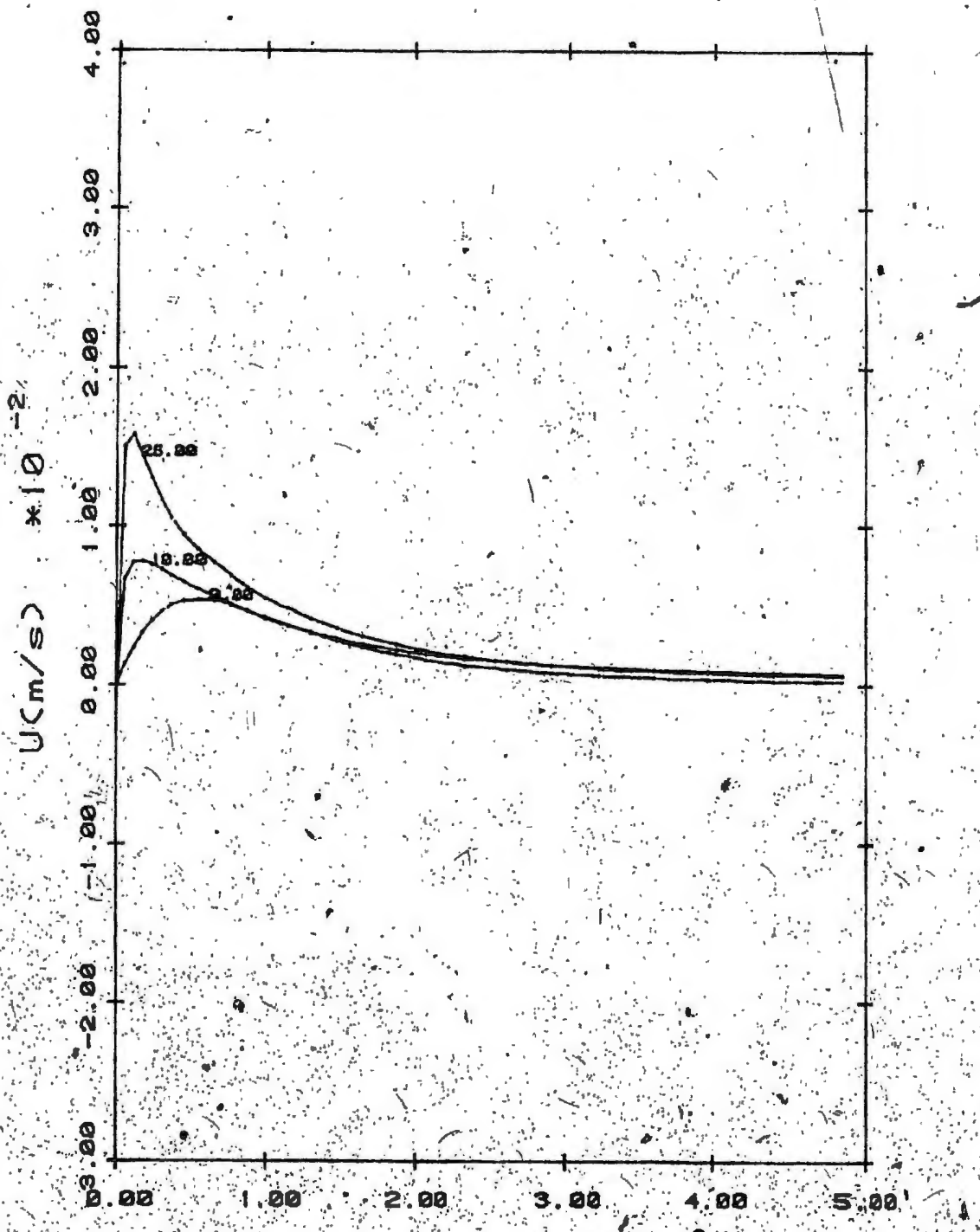

Figure 20 Velocity Profiles of Different S_∞ for T_∞ = 2.°c at x= 0.0528 m

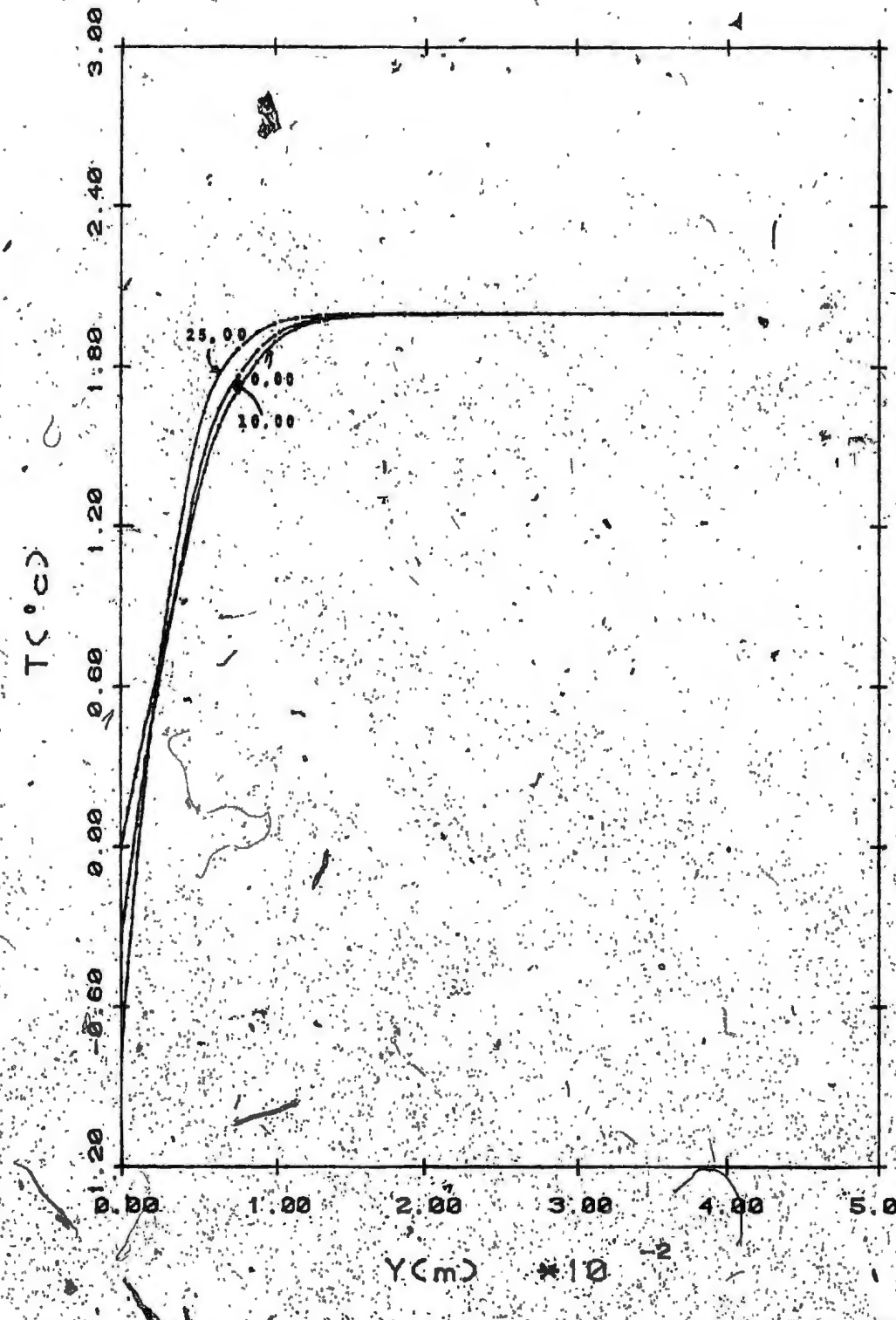

Figure 21 Temperature Profiles of Different S_q for T_∞ = 2.1°c at x= 0.5029 m

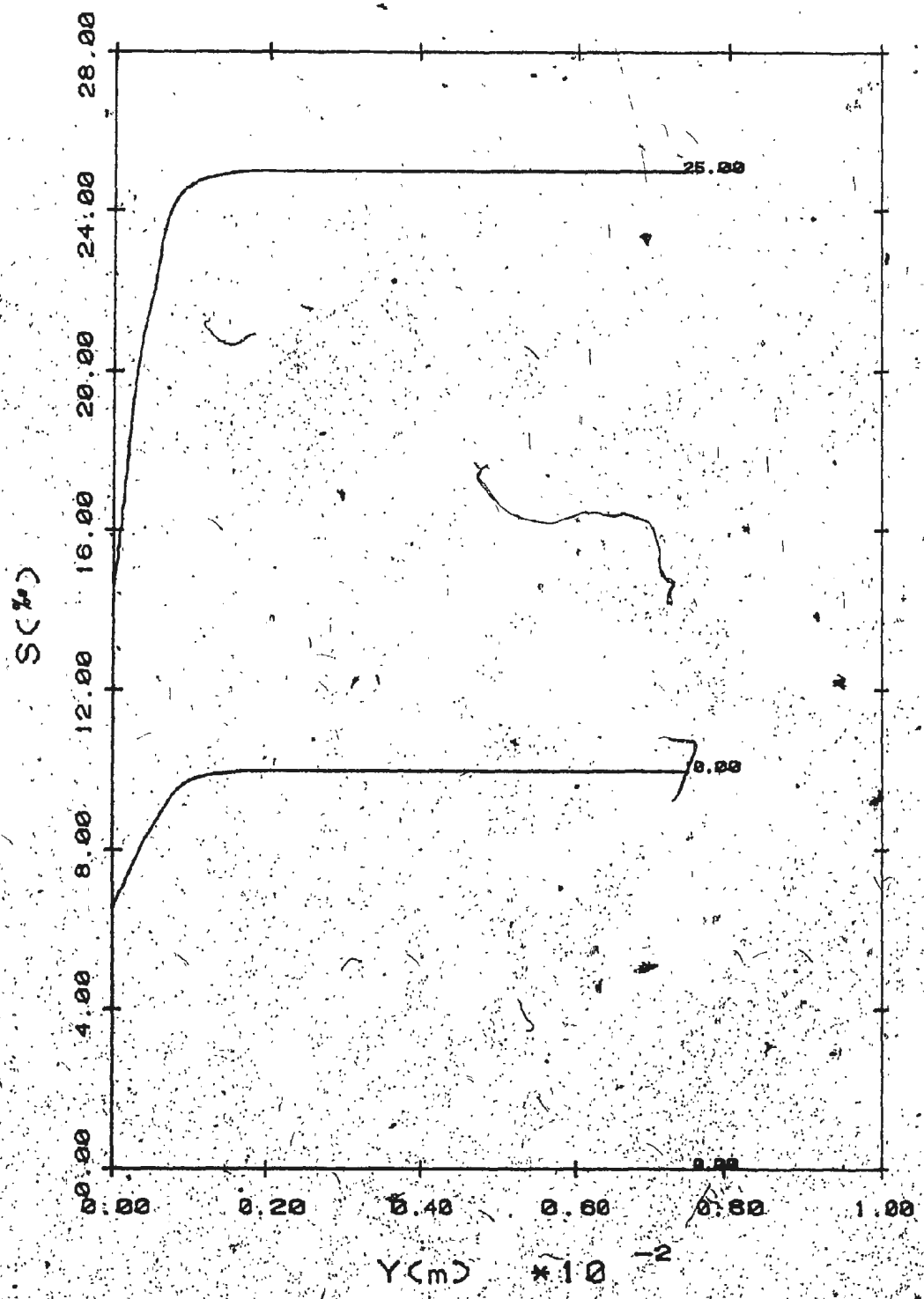

Figure 22. Salinity Profiles of Different S_∞ for T_∞ = 2.°c at x= 0.5029 m

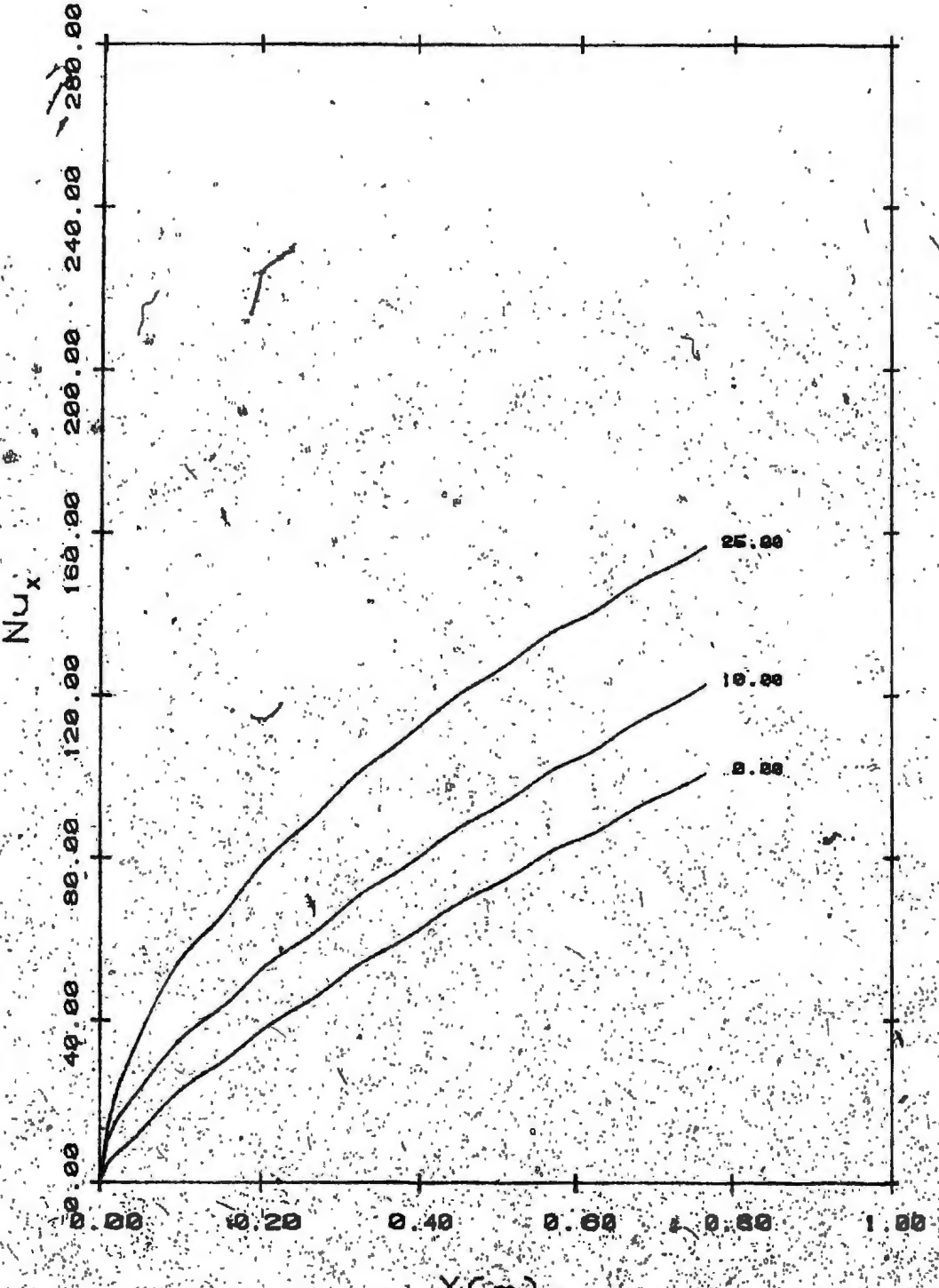

Figure 23 Nu_x of Different S_∞ as a Function of x for $T_\infty = 2.1^\circ C$

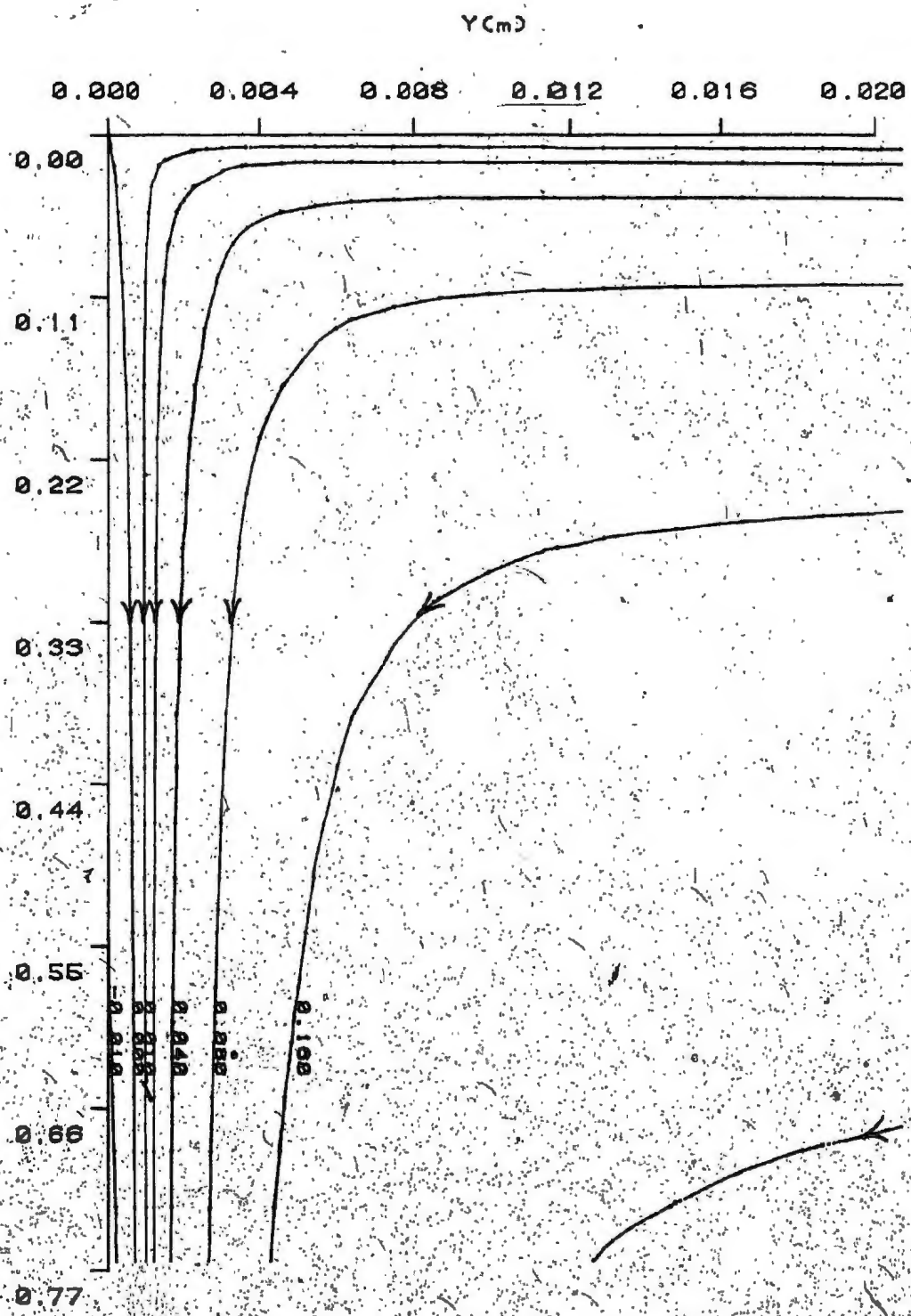

Figure 24(a) Streamlines for T_∞ = 22.00 °c, S_∞ = 0.0‰

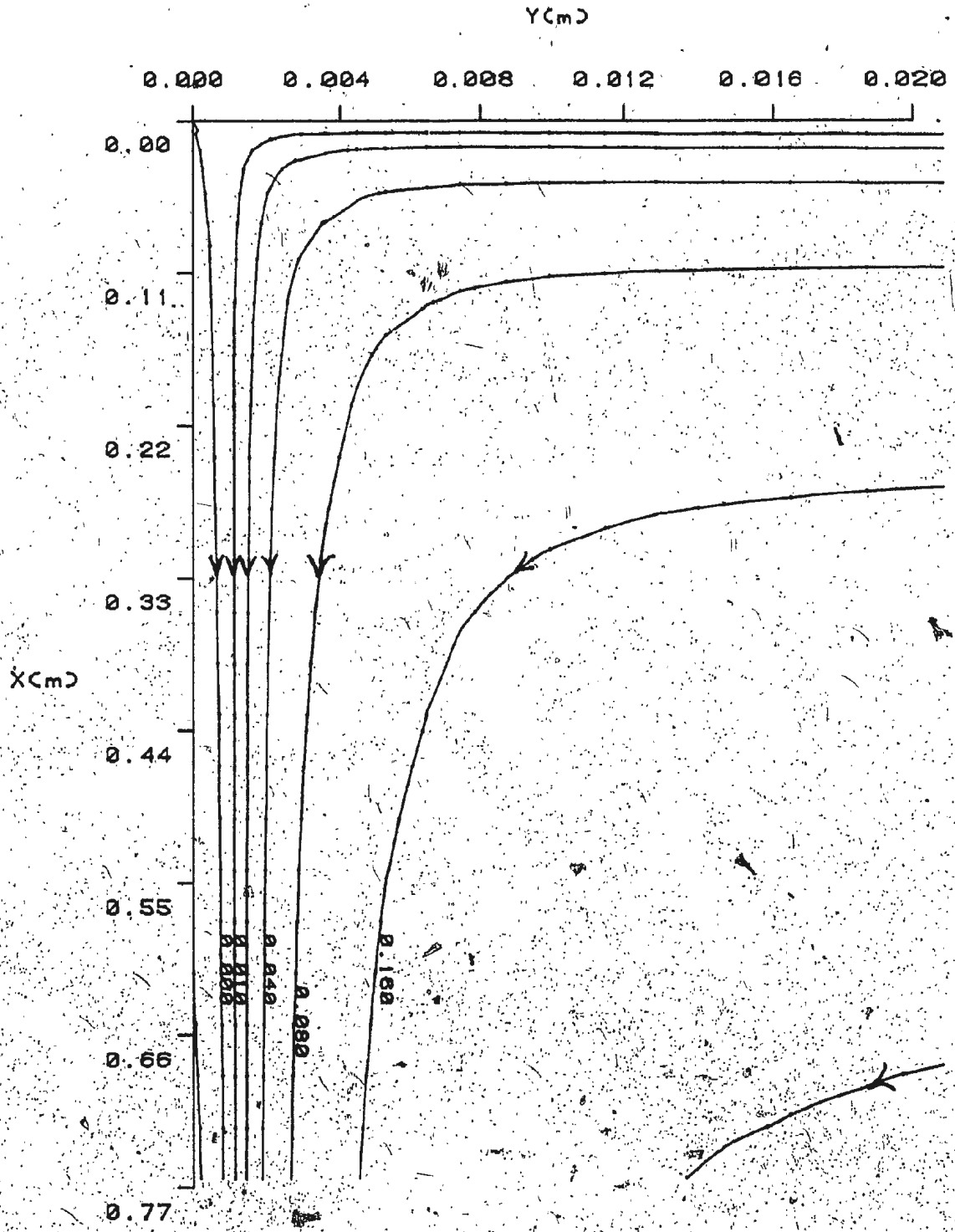

Figure 24(b) Streamlines for $T_\infty = 22.00\ ^\circ C$, $S_\infty = 3.0\ \%$

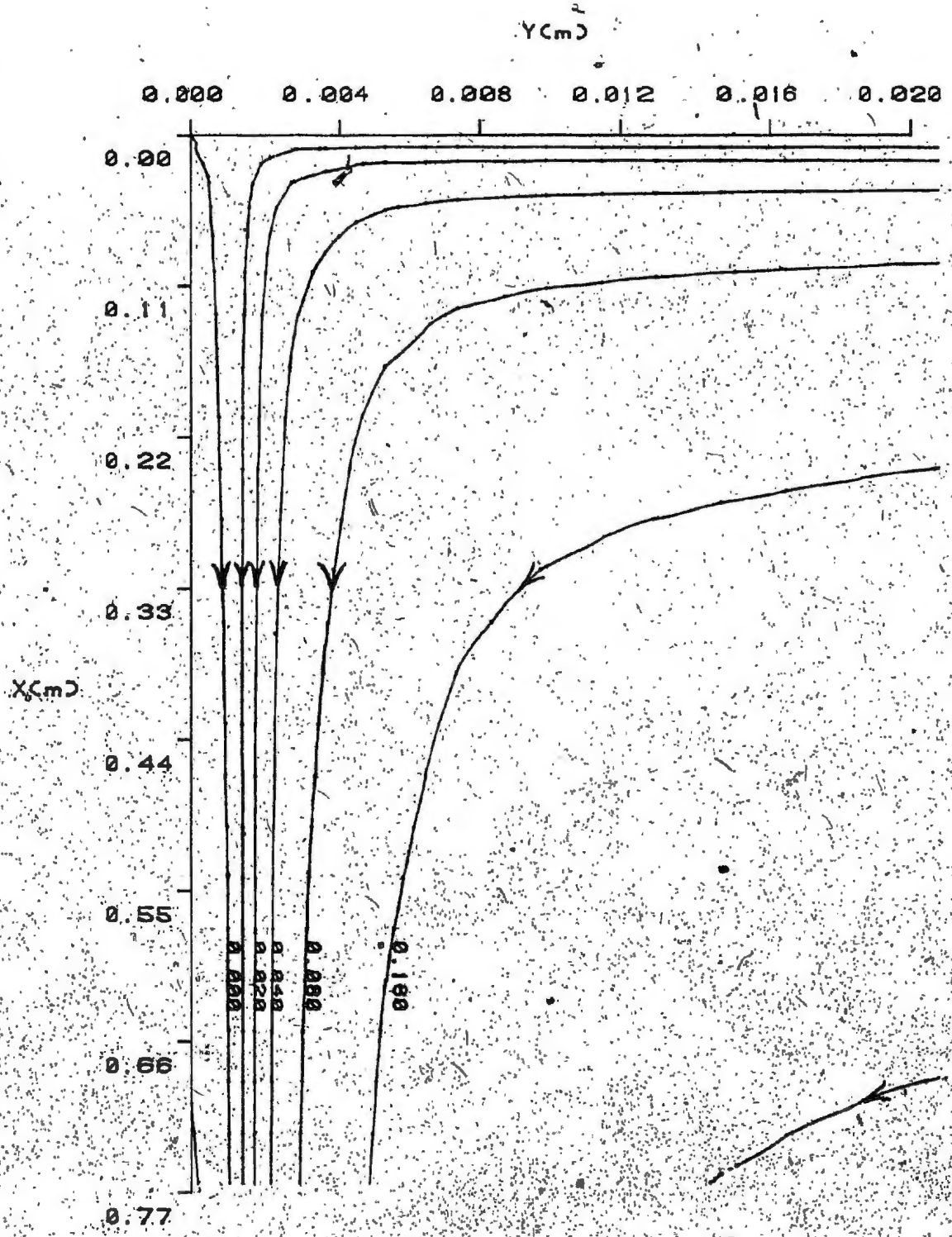

Figure 24(c) Streamlines for $T_\infty = 22.00\ ^\circ C$, $S_\infty = 5.0\ ‰$

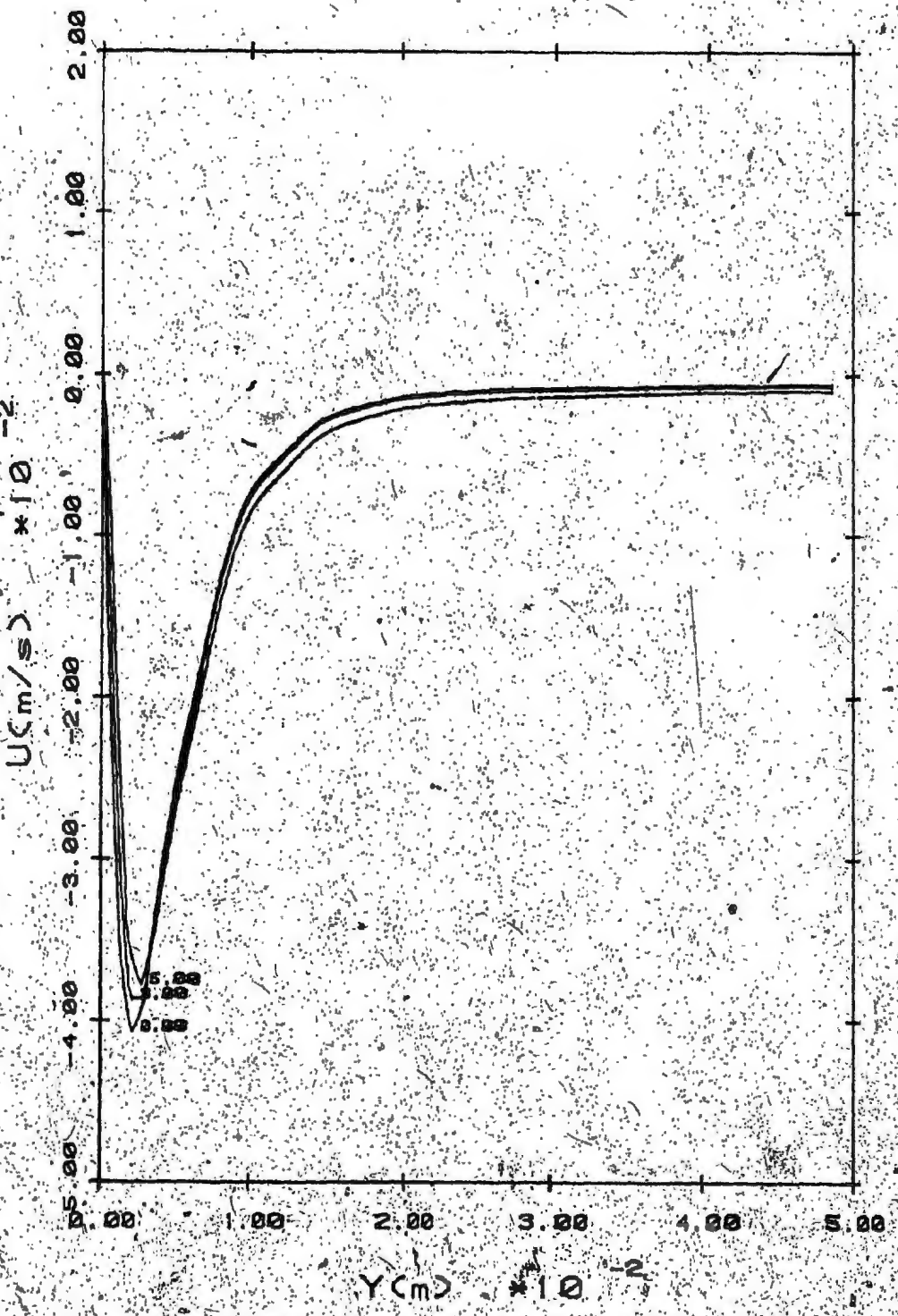

Figure 25 Velocity Profiles of Different S_∞ for $T_\infty = 22.^{\circ}$ c at x= 0.0528 m

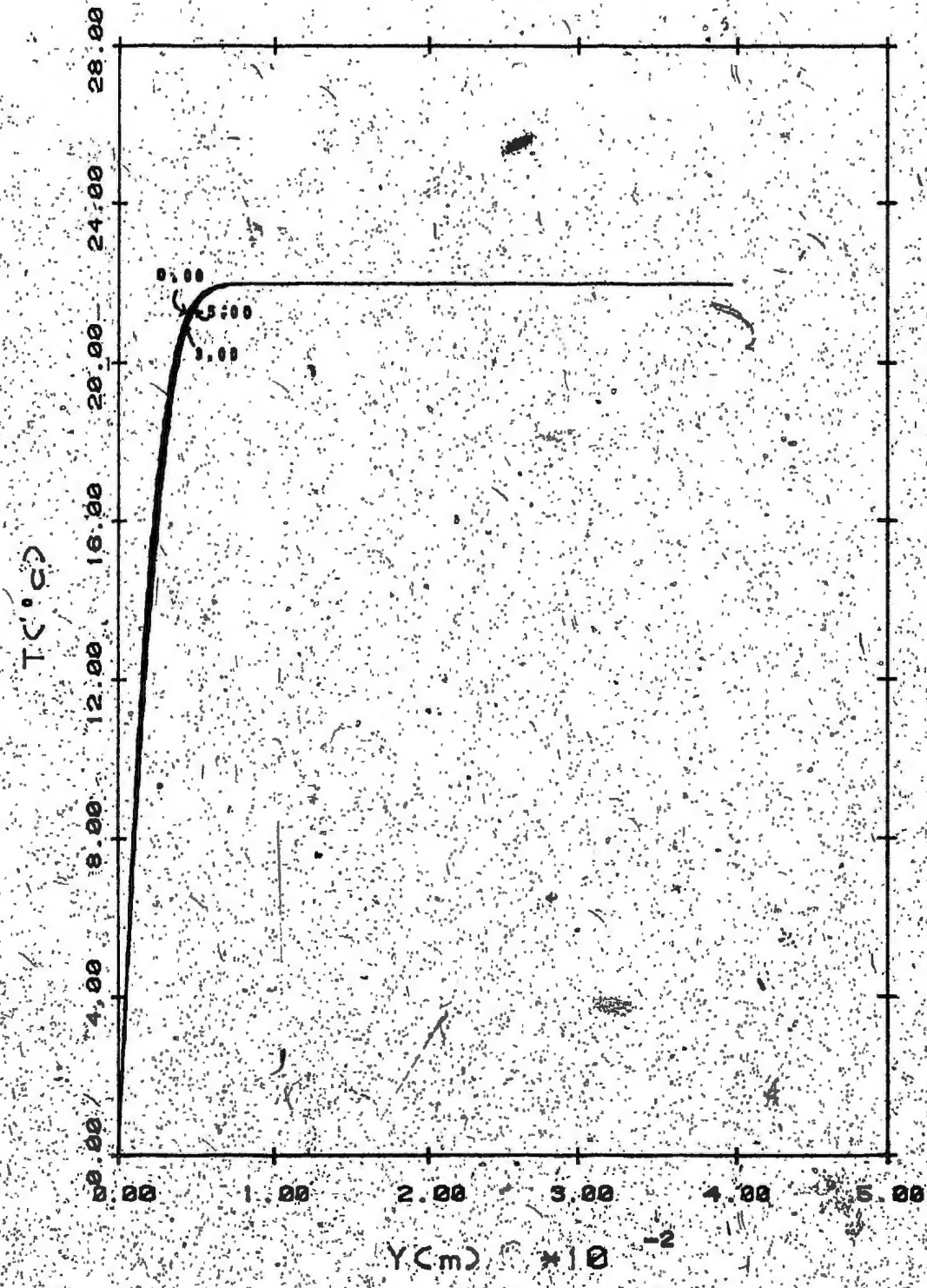

Figure 26 Temperature Profiles of Different S_a for T_a=22; °c at x= 0.5029 m

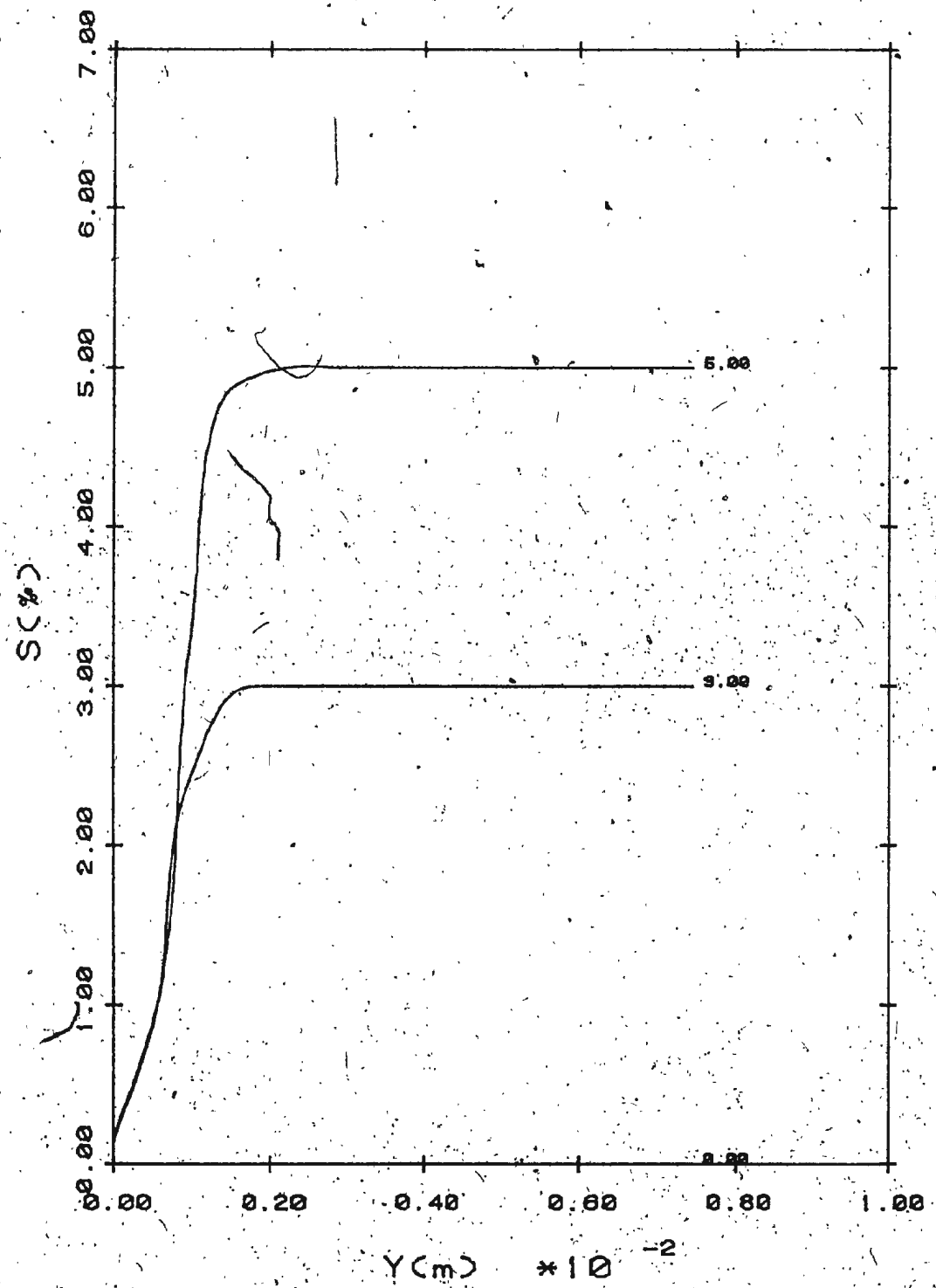

Figure 27 Salinity Profiles of Different S_∞ for T_∞=22.°c at x= 0.5029 m

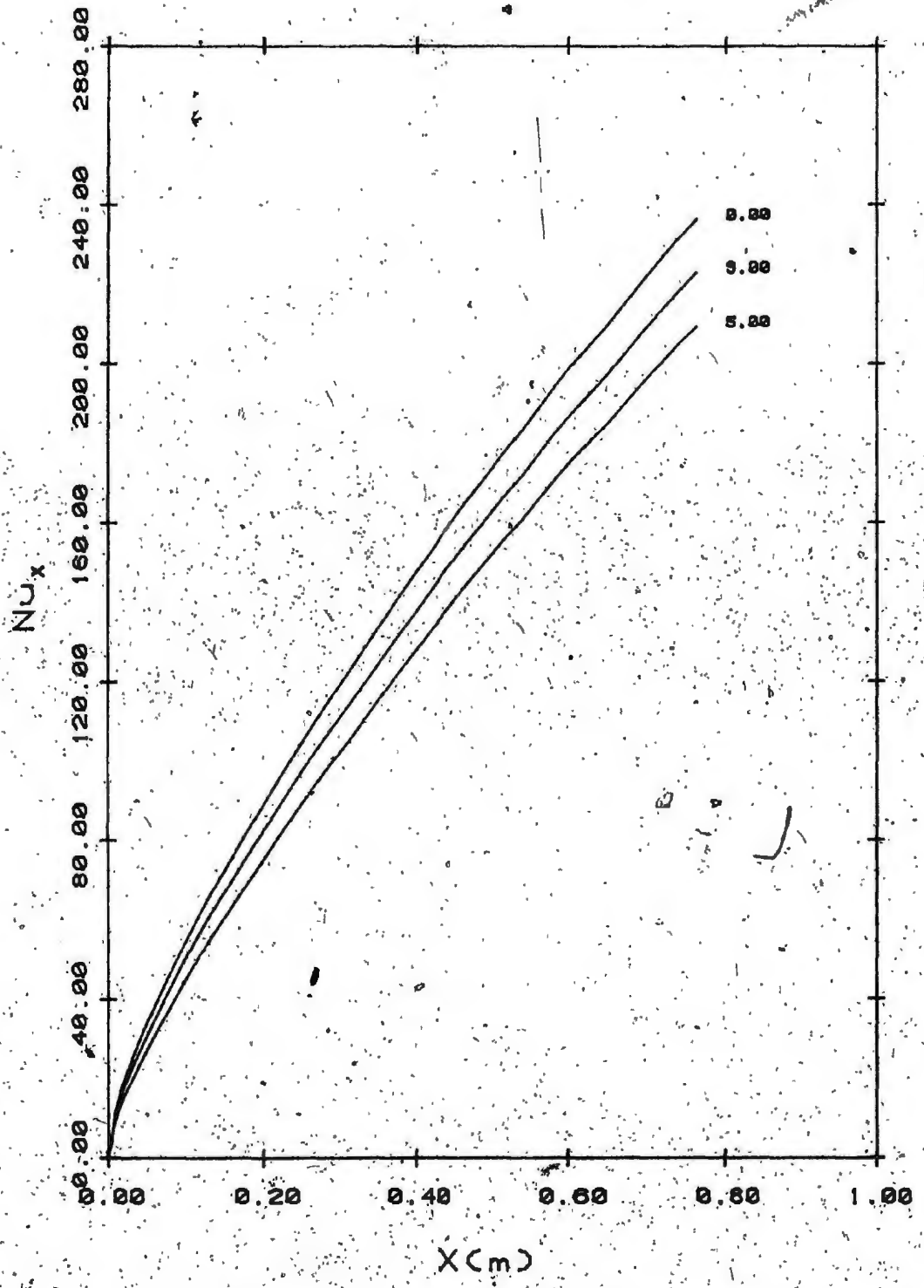

Figure 28 Nu_x of Different S_∞ as a Function of x for T_∞=22.^{0}c

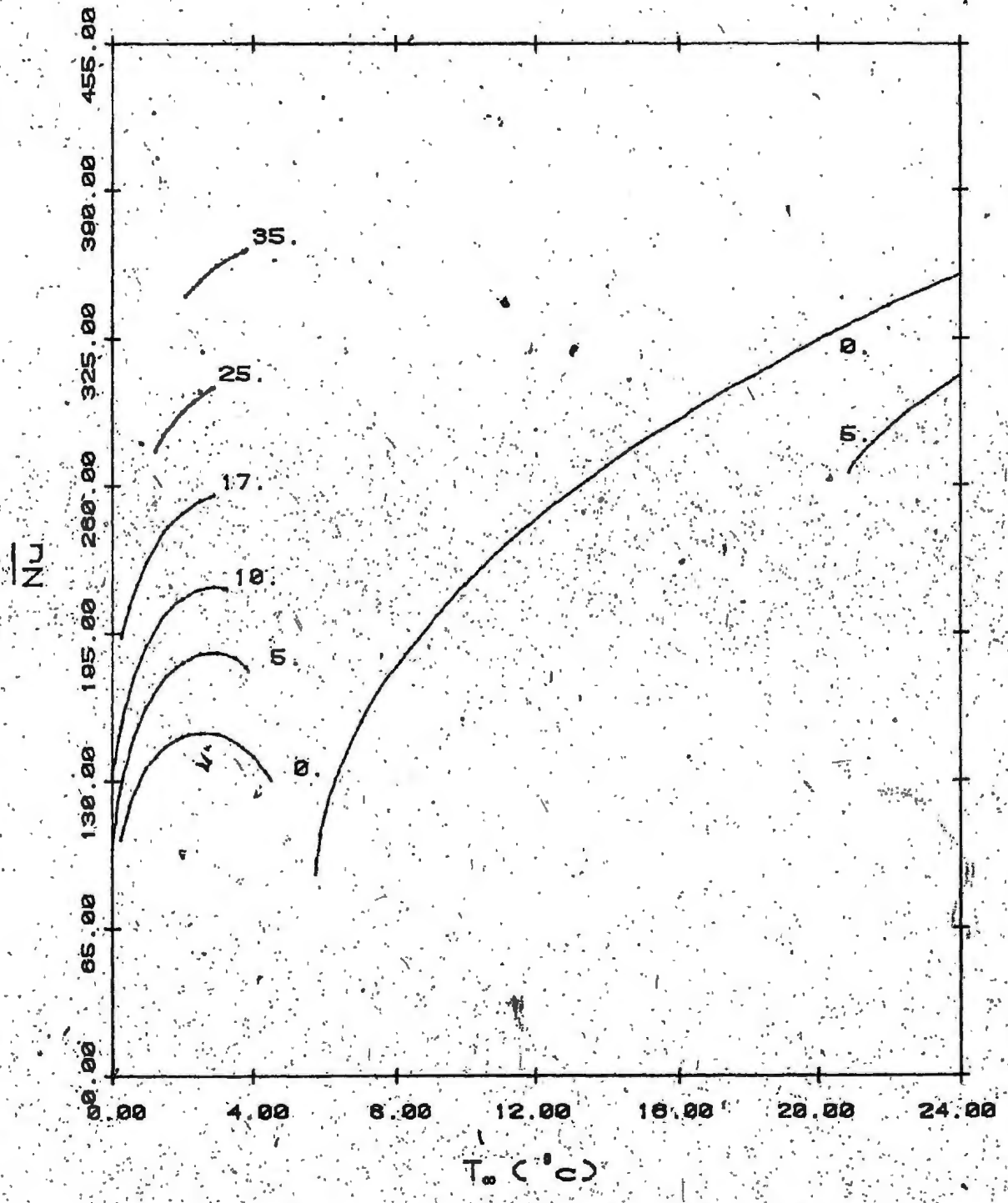

Figure 29 $\overline{Nu}$ Over a Length, 0.7632 m, of a Vertical Plate for Selected Salinities

APPENDICES

APPENDIX A

FORMULATION

Analysis of general two dimensional steady flows with constant viscosity in Cartesian co-ordinates.

Basic differential equations:

(a) The Equation of Continuity

$$\frac{\partial u}{\partial x} + \frac{\partial v}{\partial y} = 0 \qquad \text{(A-1)}$$

(b) The Equation of Momentum

The complete Navier-Stokes equations of motion are

$$\rho u \frac{\partial u}{\partial x} + \rho v \frac{\partial u}{\partial y} = - \frac{\partial P}{\partial x} + \frac{\partial}{\partial x} \left\{ \mu \left[2 \frac{\partial u}{\partial x} - \frac{2}{3} \left(\frac{\partial u}{\partial x} + \frac{\partial v}{\partial y} \right) \right] \right\}$$

$$+ \frac{\partial}{\partial y} \left\{ \mu \left(\frac{\partial u}{\partial y} + \frac{\partial v}{\partial x} \right) \right\} + X \qquad \text{(A-2)}$$

$$\rho u \frac{\partial v}{\partial x} + \rho v \frac{\partial v}{\partial y} = - \frac{\partial P}{\partial y} + \frac{\partial}{\partial y} \left\{ \mu \left[2 \frac{\partial v}{\partial y} - \frac{2}{3} \left(\frac{\partial u}{\partial x} + \frac{\partial v}{\partial y} \right) \right] \right\}$$

$$+ \frac{\partial}{\partial x} \left\{ \mu \left(\frac{\partial u}{\partial y} + \frac{\partial v}{\partial x} \right) \right\} + Y \qquad \text{(A-3)}$$

Using equation (A-1) with μ = constant, equations (A-2) and (A-3) become

$$\rho \left(u \frac{\partial u}{\partial x} + v \frac{\partial u}{\partial y} \right) = - \frac{\partial P}{\partial x} + \mu \left(\frac{\partial^2 u}{\partial x^2} + \frac{\partial^2 u}{\partial y^2} \right) + X \qquad \text{(A-4)}$$

and

$$\rho \left(u \frac{\partial v}{\partial x} + v \frac{\partial v}{\partial y} \right) = - \frac{\partial P}{\partial y} + \mu \left(\frac{\partial^2 v}{\partial x^2} + \frac{\partial^2 v}{\partial y^2} \right) + Y \qquad \text{(A-5)}$$

Differentiating equations (A-4) and (A-5) with respect to y and x, respectively, and using equation (A-1) produces the following equation in which the pressure term disappears:

$$\frac{\partial}{\partial y} \left[\rho \left(u \frac{\partial u}{\partial x} + v \frac{\partial u}{\partial y} \right) \right] - \frac{\partial}{\partial x} \left[\rho \left(u \frac{\partial v}{\partial x} + v \frac{\partial v}{\partial y} \right) \right]$$

$$= \mu \left[\frac{\partial}{\partial y} \left(\frac{\partial^2 u}{\partial x^2} + \frac{\partial^2 u}{\partial y^2} \right) - \frac{\partial}{\partial x} \left(\frac{\partial^2 v}{\partial x^2} + \frac{\partial^2 v}{\partial y^2} \right) \right] + \frac{\partial X}{\partial y} - \frac{\partial Y}{\partial x}$$

or

$$\underbrace{\left[\frac{\partial}{\partial y} \left(\rho u \frac{\partial u}{\partial x} + \rho v \frac{\partial u}{\partial y} \right) - \frac{\partial}{\partial x} \left(\rho u \frac{\partial v}{\partial x} + \rho v \frac{\partial v}{\partial y} \right) \right]}_{(1)}$$

$$\underbrace{- \mu \left[\frac{\partial}{\partial y} \left(\frac{\partial^2 u}{\partial x^2} + \frac{\partial^2 u}{\partial y^2} \right) - \frac{\partial}{\partial x} \left(\frac{\partial^2 v}{\partial x^2} + \frac{\partial^2 v}{\partial y^2} \right) \right]}_{(2)} - \frac{\partial X}{\partial y} + \frac{\partial Y}{\partial x} = 0 \qquad \text{(A-6)}$$

Here we define the stream function and vorticity as

$$\rho u = \frac{\partial \psi}{\partial y}, \quad \rho v = - \frac{\partial \psi}{\partial x}$$

and

$$\omega = \frac{\partial v}{\partial x} - \frac{\partial u}{\partial y}$$

For (1)

$$\frac{\partial}{\partial y}\left(\rho u\frac{\partial u}{\partial x}+\rho v\frac{\partial u}{\partial y}\right)-\frac{\partial}{\partial x}\left(\rho u\frac{\partial v}{\partial x}+\rho v\frac{\partial v}{\partial y}\right)$$

$$=\frac{\partial}{\partial y}\left[\frac{\partial\psi}{\partial y}\frac{\partial u}{\partial x}-\frac{\partial\psi}{\partial x}\left(\frac{\partial v}{\partial x}-\omega\right)\right]-\frac{\partial}{\partial x}\left[\frac{\partial\psi}{\partial y}\left(\omega+\frac{\partial u}{\partial y}\right)-\frac{\partial\psi}{\partial x}\frac{\partial v}{\partial y}\right]$$

$$=\frac{\partial}{\partial y}\left(\omega\frac{\partial\psi}{\partial x}\right)-\frac{\partial}{\partial x}\left(\omega\frac{\partial\psi}{\partial y}\right)+\frac{\partial}{\partial y}\left(\frac{\partial\psi}{\partial y}\frac{\partial u}{\partial x}-\frac{\partial\psi}{\partial x}\frac{\partial v}{\partial x}\right)-\frac{\partial}{\partial x}\left(\frac{\partial\psi}{\partial y}\frac{\partial u}{\partial y}-\frac{\partial\psi}{\partial x}\frac{\partial v}{\partial y}\right)$$

$$=\frac{\partial}{\partial y}\left(\omega\frac{\partial\psi}{\partial x}\right)-\frac{\partial}{\partial x}\left(\omega\frac{\partial\psi}{\partial y}\right)+\frac{\partial}{\partial y}\left(\rho u\frac{\partial u}{\partial x}+\rho v\frac{\partial v}{\partial x}\right)-\frac{\partial}{\partial x}\left(\rho u\frac{\partial u}{\partial y}+\rho v\frac{\partial v}{\partial y}\right)$$

$$=-\frac{\partial}{\partial x}\left(\omega\frac{\partial\psi}{\partial y}\right)+\frac{\partial}{\partial y}\left(\omega\frac{\partial\psi}{\partial x}\right)-\frac{\partial}{\partial x}\left(\rho u\frac{\partial u}{\partial y}\right)+\frac{\partial}{\partial y}\left(\rho u\frac{\partial u}{\partial x}\right)$$

$$-\frac{\partial}{\partial x}\left(\rho v\frac{\partial v}{\partial y}\right)+\frac{\partial}{\partial y}\left(\rho v\frac{\partial v}{\partial x}\right)$$

$$=-\frac{\partial}{\partial x}\left(\omega\frac{\partial\psi}{\partial y}\right)+\frac{\partial}{\partial y}\left(\omega\frac{\partial\psi}{\partial x}\right)-\rho u\frac{\partial^2 u}{\partial x\partial y}-\frac{\partial u}{\partial y}\frac{\partial}{\partial x}(\rho u)+\rho u\frac{\partial^2 u}{\partial y\partial x}$$

$$+\frac{\partial u}{\partial x}\frac{\partial}{\partial y}(\rho u)-\rho v\frac{\partial^2 v}{\partial x\partial y}-\frac{\partial v}{\partial y}\frac{\partial}{\partial x}(\rho v)+\rho v\frac{\partial^2 v}{\partial y\partial x}+\frac{\partial v}{\partial x}\frac{\partial}{\partial y}(\rho v)$$

$$=-\frac{\partial}{\partial x}\left(\omega\frac{\partial\psi}{\partial y}\right)+\frac{\partial}{\partial y}\left(\omega\frac{\partial\psi}{\partial x}\right)+\left(u\frac{\partial u}{\partial x}+v\frac{\partial v}{\partial x}\right)\frac{\partial\rho}{\partial y}-\left(u\frac{\partial u}{\partial y}+v\frac{\partial v}{\partial y}\right)\frac{\partial\rho}{\partial x}$$

$$=-\frac{\partial}{\partial x}\left(\omega\frac{\partial\psi}{\partial y}\right)+\frac{\partial}{\partial y}\left(\omega\frac{\partial\psi}{\partial x}\right)+\frac{\partial}{\partial x}\left(\frac{u^2+v^2}{2}\right)\frac{\partial\rho}{\partial y}-\frac{\partial}{\partial y}\left(\frac{u^2+v^2}{2}\right)\frac{\partial\rho}{\partial x}$$

For (2)

$$-\mu\left[\frac{\partial}{\partial y}\left(\frac{\partial^2 u}{\partial x^2}+\frac{\partial^2 u}{\partial y^2}\right)-\frac{\partial}{\partial x}\left(\frac{\partial^2 v}{\partial x^2}+\frac{\partial^2 v}{\partial y^2}\right)\right]$$

$$=-\mu\left[\frac{\partial}{\partial y}\left(\frac{\partial^2 u}{\partial x^2}+\frac{\partial^2 v}{\partial x\partial y}-\frac{\partial\omega}{\partial y}\right)-\frac{\partial}{\partial x}\left(\frac{\partial\omega}{\partial x}+\frac{\partial^2 u}{\partial x\partial y}+\frac{\partial^2 v}{\partial y^2}\right)\right]$$

$$=\mu\left(\frac{\partial^2\omega}{\partial y^2}+\frac{\partial^2\omega}{\partial x^2}\right)-\mu\left[\frac{\partial}{\partial y}\left(\frac{\partial^2 u}{\partial x^2}+\frac{\partial^2 v}{\partial x\partial y}\right)-\frac{\partial}{\partial x}\left(\frac{\partial^2 u}{\partial x\partial y}+\frac{\partial^2 v}{\partial y^2}\right)\right]$$

$$= \mu \left(\frac{\partial^2 \omega}{\partial x^2} + \frac{\partial^2 \omega}{\partial y^2}\right) - \mu \left(\frac{\partial^3 u}{\partial y \partial x^2} + \frac{\partial^3 v}{\partial y^2 \partial x} - \frac{\partial^3 u}{\partial x^2 \partial y} - \frac{\partial^3 v}{\partial x \partial y^2}\right)$$

$$= \mu \left(\frac{\partial^2 \omega}{\partial x^2} + \frac{\partial^2 \omega}{\partial y^2}\right)$$

Finally, equation (A-6) becomes

$$\frac{\partial}{\partial x}\left(\omega \frac{\partial \psi}{\partial y}\right) - \frac{\partial}{\partial y}\left(\omega \frac{\partial \psi}{\partial x}\right) - \mu \left(\frac{\partial^2 \omega}{\partial x^2} + \frac{\partial^2 \omega}{\partial y^2}\right) - \frac{\partial}{\partial x}\left(\frac{u^2 + v^2}{2}\right) \frac{\partial \rho}{\partial y}$$

$$+ \frac{\partial}{\partial y}\left(\frac{u^2 + v^2}{2}\right) \frac{\partial \rho}{\partial x} + \frac{\partial X}{\partial y} - \frac{\partial Y}{\partial x} = 0 \qquad \text{(A-7)}$$

In a gravitational field oriented as in Figure 1(a) or 1(b), $X = \pm \rho g$, $Y = 0$. Equation (A-7) becomes

$$\frac{\partial}{\partial x}\left(\omega \frac{\partial \psi}{\partial y}\right) - \frac{\partial}{\partial y}\left(\omega \frac{\partial \psi}{\partial x}\right) - \mu \left(\frac{\partial^2 \omega}{\partial x^2} + \frac{\partial^2 \omega}{\partial y^2}\right) - \frac{\partial}{\partial x}\left(\frac{u^2 + v^2}{2}\right) \frac{\partial \rho}{\partial y}$$

$$+ \frac{\partial}{\partial y}\left(\frac{u^2 + v^2}{2}\right) \frac{\partial \rho}{\partial x} \mp g \frac{\partial \rho}{\partial y} = 0 \qquad \text{(A-8)}$$

APPENDIX B

FINITE-DIFFERENCE APPROXIMATION

The differential equations (6), (7), (8) and (9) can be cast into the general form

$$a_\phi \left\{ \frac{\partial}{\partial x} \left(\phi \frac{\partial \psi}{\partial y} \right) - \frac{\partial}{\partial y} \left(\phi \frac{\partial \psi}{\partial x} \right) \right\} - \frac{\partial}{\partial x} \left\{ b_\phi \frac{\partial}{\partial x} \left(c_\phi \phi \right) \right\}$$

$$- \frac{\partial}{\partial y} \left\{ b_\phi \frac{\partial}{\partial y} \left(c_\phi \phi \right) \right\} + e_\phi = 0 \qquad \text{(B-1)}$$

here ϕ is a general dependent variable. Instead of writing the full differential equations for ω, ψ, T and S, we give below the expressions for a_ϕ, b_ϕ, c_ϕ and e_ϕ for these equations.

ϕ	a_ϕ	b_ϕ	c_ϕ	e_ϕ
ω	1	1	μ	$-\left[\frac{\partial}{\partial x}\left(\frac{u^2+v^2}{2}\right)\frac{\partial \rho}{\partial y} - \frac{\partial}{\partial y}\left(\frac{u^2+v^2}{2}\right)\frac{\partial \rho}{\partial x}\right] \mp g \frac{\partial \rho}{\partial y}$
ψ	0	$\frac{1}{\rho}$	1	$-\omega$
T	1	$\frac{k}{Cp}$	1	0
S	1	ρD	1	0

Following the methods of Gosman et al [6], integration of equation (B-1) over a finite rectangular area around the point p (Figure 5) gives the following complete finite-difference equation:

$$A_E (\phi_P - \phi_E) + A_W (\phi_P - \phi_W) + A_N (\phi_P - \phi_N) + A_S (\phi_P - \phi_S)$$

Convection terms

$$- B_E (c_{\phi,E} \phi_E - c_{\phi,P} \phi_P) - B_W (c_{\phi,W} \phi_W - c_{\phi,P} \phi_P)$$

Diffusion terms

$$- B_N (c_{\phi,N} \phi_N - c_{\phi,P} \phi_P) - B_S (c_{\phi,S} \phi_S - c_{\phi,P} \phi_P)$$

Source term

$$+ e_{\phi,P} V_P = 0 \qquad \text{(B-2)}$$

When the finite-difference representation of all the terms in equation (B-2) has been determined the general difference equation can be obtained in the following form:

$$\phi_P = C_E \phi_E + C_W \phi_W + C_N \phi_N + C_S \phi_S + E \qquad \text{(B-3)}$$

where

$$C_E = (A_E + B_E c_{\phi,E}) / \Sigma_{AB}$$

$$C_W = (A_W + B_W c_{\phi,W}) / \Sigma_{AB}$$

$$C_N = (A_N + B_N c_{\phi,N}) / \Sigma_{AB}$$

$$C_S = (A_S + B_S c_{\phi,S}) / \Sigma_{AB}$$

$$E = - e_{\phi,P} V_P / \Sigma_{AB}$$

and

$$\Sigma_{AB} = A_E + A_W + A_N + A_S + c_{\phi,P} (B_E + B_W + B_N + B_S)$$

in which

$$A_E = a_\phi [(\psi_{SE} + \psi_S - \psi_{NE} - \psi_N) + |\psi_{SE} + \psi_S - \psi_{NE} - \psi_N|] / 8$$

$$A_W = a_\phi [(\psi_{NW} + \psi_N - \psi_{SW} - \psi_S) + |\psi_{NW} + \psi_N - \psi_{SW} - \psi_S|] / 8$$

$$A_N = a_\phi [(\psi_{NE} + \psi_E - \psi_{NW} - \psi_W) + |\psi_{NE} + \psi_E - \psi_{NW} - \psi_W|] / 8$$

$$A_S = a_\phi [(\psi_{SW} + \psi_W - \psi_{SE} - \psi_E) + |\psi_{SW} + \psi_W - \psi_{SE} - \psi_E|] / 8$$

$$B_E = \frac{b_{\phi,E} + b_{\phi,P}}{4} \frac{y_N - y_S}{x_E - x_P}$$

$$B_W = \frac{b_{\phi,W} + b_{\phi,P}}{4} \frac{y_N - y_S}{x_P - x_W}$$

$$B_N = \frac{b_{\phi,N} + b_{\phi,P}}{4} \frac{x_E - x_W}{y_N - y_P}$$

$$B_S = \frac{b_{\phi,S} + b_{\phi,P}}{4} \frac{x_E - x_W}{y_P - y_S}$$

$$V_P = \left(\frac{x_E - x_W}{2}\right)\left(\frac{y_N - y_S}{2}\right)$$

The complexities in solving equation (B-3) result primarily from the possible variation of fluid properties. In order to simplify the equation, it is assumed that the variation of the fluid properties can be ignored except for the density variation in body forces during the processes of calculation. Therefore, the final general difference equation will becomes:

$$\phi_p = \frac{[(a_\phi A'_E + f_\phi B'_E)\omega_E + (a_\phi A'_W + f_\phi B'_W)\omega_W + (a_\phi A'_N + f_\phi B'_N)\omega_N + (a_\phi A'_S + f_\phi B'_S)\omega_S] + h_\phi}{a_\phi (A'_E + A'_W + A'_N + A'_S) + f_\phi (B'_E + B'_W + B'_N + B'_S)} \qquad \text{(B-4)}$$

Instead of writing the difference equations for ω, ψ, T and S, the expressions for a_ϕ, f_ϕ and h_ϕ are given below for these equations.

ϕ	a_ϕ	f_ϕ	h_ϕ
ω	0	μ	$\frac{\partial}{\partial x}\left(\frac{u^2+v^2}{2}\right)\frac{\partial \rho}{\partial y} - \frac{\partial}{\partial y}\left(\frac{u^2+v^2}{2}\right)\frac{\partial \rho}{\partial x} \pm g\frac{\partial \rho}{\partial y}$
ψ	0	1	$\rho_p \omega_p$
T	1	$\frac{\mu}{Pr}$	0
S	1	$\frac{\mu}{Sc}$	0

In equation (B-4), A'_E, A'_W, A'_N, A'_S, B'_E, B'_W, B'_N and B'_S are given by

$$A'_E = \frac{|\psi_N - \psi_S + \psi_{NE} - \psi_{SE}| - (\psi_N - \psi_S + \psi_{NE} - \psi_{SE})}{2(x_E - x_W)(y_N - y_S)}$$

$$A'_W = \frac{|\psi_N - \psi_S + \psi_{NW} - \psi_{SW}| + (\psi_N - \psi_S + \psi_{NW} - \psi_{SW})}{2(x_E - x_W)(y_N - y_S)}$$

$$A'_N = \frac{|\psi_W - \psi_E + \psi_{NW} - \psi_{NE}| - (\psi_W - \psi_E + \psi_{NW} - \psi_{NE})}{2(x_E - x_W)(y_N - y_S)}$$

$$A'_S = \frac{|\psi_W - \psi_E + \psi_{SW} - \psi_{SE}| + (\psi_W - \psi_E + \psi_{SW} - \psi_{SE})}{2(x_E - x_W)(y_N - y_S)}$$

$$B'_E = \frac{2}{(x_E - x_P)(x_E - x_W)}$$

$$B'_W = \frac{2}{(x_P - x_W)(x_E - x_W)}$$

$$B'_N = \frac{2}{(y_N - y_P)(y_N - y_S)}$$

$$B'_S = \frac{2}{(y_P - y_S)(y_N - y_S)}$$

Equation (B-4) shows that the value of ϕ at the central point p is related to the value of ϕ at the four neighbour points. The gradients of ρ, u, v and $\frac{u^2+v^2}{2}$ in equation (B-4) when applied to ω are given as follows.

Consider a gradient of ϕ at the central point p in x direction as shown below

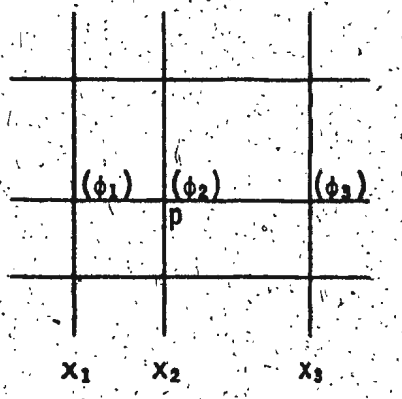

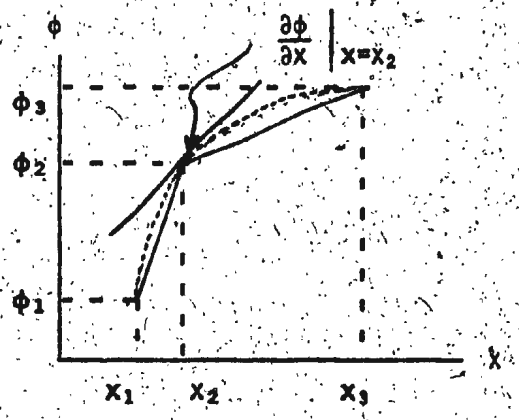

The simplest function which we can choose to satisfy (x_1, ϕ_1), (x_2, ϕ_2) and (x_3, ϕ_3) is a polynomial with three arbitrary constants. Thus

$$\phi = ax^2 + bx + c \qquad \text{(B-5)}$$

or

$$\phi_1 = ax_1^2 + bx_1 + c \qquad \text{(B-6)}$$

$$\phi_2 = ax_2^2 + bx_2 + c \qquad \text{(B-7)}$$

$$\phi_3 = ax_3^2 + bx_3 + c \qquad \text{(B-8)}$$

Differentiating equation (B-5) with respect to x gives

$$\frac{\partial \phi}{\partial x} = 2ax + b$$

Carrying out the elimination of c from equations (B-6), (B-7) and (B-8) leads to

$$a = \frac{(\phi_3 - \phi_1)(x_2 - x_1)(\phi_2 - \phi_1)(x_3 - x_1)}{(x_2 - x_1)(x_3 - x_2)(x_3 - x_1)}$$

and

$$b = \frac{(\phi_3 - \phi_2) - a(x_3^2 - x_2^2)}{(x_3 - x_2)}$$

So that the gradient of ϕ at the central point p becomes

$$\left.\frac{\partial \phi}{\partial x}\right|_{x=x_2} = 2ax_2 + b$$

$$= \frac{\phi_3 - \phi_2}{x_3 - x_2} - \frac{\phi_3 - \phi_1}{x_3 - x_1} + \frac{\phi_2 - \phi_1}{x_2 - x_1}$$

$$\frac{(\phi_3 - \phi_2)(x_2 - x_1) + (\phi_2 - \phi_1)(x_3 - x_2)}{(x_3 - x_1)}$$

In order to obtain adequate convergence, nodes should be closely spaced in regions of rapid change of variables. The rectangular enclosure employed for calculation should have a large enough area so that the velocity, temperature and salinity distributions can reach their final shapes. All results presented in this report were obtained using the mesh sizes as shown in Table 1(a). Since we have formed finite-difference equations for all the nodes in the calculation domain, the next task we have to do is to solve this set of equations. A calculation procedure is summarized as the following steps:

(i) Provide initial estimates of the values of all the variables including fluid properties u, v and source (h_ϕ).

(ii) Calculate the density ρ from equation (10).

(iii) Solve the finite-difference equation (B-4) for all dependent variables, ω, ψ, T and S with associated boundary conditions.

(iv) Regard the new values of the variables as improved estimates and return to step (ii). Repeat the process until convergence.

In order to minimize the computing time, a technique called underrelaxation must be used in step (iii) to speed up convergence. The relationship between a new value and an old value of the dependent variable ϕ_p is given by

$$\phi_{p_{new}} = \phi_{p_{old}} + RP \left(\phi_p - \phi_{p_{old}} \right)$$

where RP is called the relaxation parameter which lies between 0 and

1, and ϕ_p is given by equation (B-4). The source term in equation (B-4) can also be underrelaxed separately in the cyclic repetion of the above steps as shown in main programme.

APPENDIX C

COMPUTER PROGRAMMES

```
C     ****************************************************************
C     *              BLOCK ' 41BL.FTN '---: DATA                     *
C     ****************************************************************
      BLOCK DATA
      COMMON/VORTIC/W1(41),W2(41),W3(41),RPW,RSDUW
      COMMON/STRFN/F1(41),F2(41),F3(41),RPF,RSDUF
      COMMON/TEM/T1(41),T2(41),T3(41),RPT,RSDUT
      COMMON/SAL/S1(41),S2(41),S3(41),RPS,RSDUS
      COMMON/VSQ/VSQ1(41),VSQ2(41),VSQ3(41),V2
      COMMON/SOR/SOR1(41),SOR2(41),SOR3(41),RPSOR
      COMMON/CONVE/AE(41),AW(41),AN(41),AS(41),AT(41)
      COMMON/DEN/RO1(41),RO2(41),RO3(41)
      COMMON/BW/BWE,BWW,BWEW,BWN(41),BWS(41),BWNS(41)
      COMMON/BF/BFE,BFW,BFEW,BFN(41),BFS(41),BFNS(41)
      COMMON/BT/BTE,BTW,BTEW,BTN(41),BTS(41),BTNS(41)
      COMMON/BS/BSE,BSW,BSEW,BSN(41),BSS(41),BSNS(41)
      COMMON/XY/Y(41),DDY(41),Y32,Y22,DY,DYY,X1,X2,X3
      COMMON/PROP/THECON,FUSION,DIFCL
      COMMON/VAR/JJ,JNM,JN,TINF,SALINF
      COMMON/VEL/U1(41),U2(41),U3(41)
      DATA RPW,RPF,RPT,RPS,RPSOR/.5,.8,.8,.8,.2/
      DATA RSDUW,RSDUF,RSDUT,RSDUS/4*0./
      DATA Y/0.,.0005,.001,.0016,.0022,.00292,.00364,.0045,
     *.00536,.0064,.00744,.00868,.00992,.01142,.01292,.01471,.0165,
     *.01865,.0208,.0234,.026,.0291,.0322,.0359,.0396,.044,.0484,
     *.0538,.0592,.0656,.072,.0797,.0874,.0967,.106,.1155,.125,
     *.1375,.15,.1625,.175/
      DATA THECON,FUSION,DIFCL/.596,334944.,12.9E-10/
      DATA JJ,JNM,JN/2,40,41/
      DATA BWE,BWW,BWEW,BFE,BFW,BFEW,BTE,BTW,
     *  BTEW,BSE,BSW,BSEW/12*0./
      END
```

```
C     ***************************************************************
C     *     PROGRAM ' 41GR.FTN '---: INITIAL VALUES                 *
C     ***************************************************************
      DIMENSION X(51)
      BYTE ANAME(80)
      COMMON/VORTIC/W1(41),W2(41),W3(41),RPW,RSDUW
      COMMON/STRFN/F1(41),F2(41),F3(41),RPF,RSDUF
      COMMON/TEM/T1(41),T2(41),T3(41),RPT,RSDUT
      COMMON/SAL/S1(41),S2(41),S3(41),RPS,RSDUS
      COMMON/VSQ/VSQ1(41),VSQ2(41),VSQ3(41),V2
      COMMON/SOR/SOR1(41),SOR2(41),SOR3(41),RPSOR
      COMMON/CONVE/AE(41),AW(41),AN(41),AS(41),AT(41)
      COMMON/DEN/RO1(41),RO2(41),RO3(41)
      COMMON/BW/BWE,BWW,BWEW,BWN(41),BWS(41),BWNS(41)
      COMMON/BF/BFE,BFW,BFEW,BFN(41),BFS(41),BFNS(41)
      COMMON/BT/BTE,BTW,BTEW,BTN(41),BTS(41),BTNS(41)
      COMMON/BS/BSE,BSW,BSEW,BSN(41),BSS(41),BSNS(41)
      COMMON/XY/Y(41),DDY(41),Y32,Y22,DY,DYY,X1,X2,X3
      COMMON/PROP/THECON,FUSION,DIFCL
      COMMON/VAR/JJ,JNM,JN,TINF,SALINF
      COMMON/VEL/U1(41),U2(41),U3(41)
      DATA W1,F1,T1,S1,VSQ1,SOR1,RO1,U1/328*0./
      DATA X/0.,.00953,.0212,.0353,.0526,.0738,.0995,.131
     *,.169,.2054,.2426,.2798,.3169,.3541,.3913,.4285,.4657
     *,.5029,.5401,.5772,.6144,.6516,.6888,.726,.7632,.8004
     *,.8376,.8748,.9120,.9492,.9863,1.0235,1.0607,1.0979
     *,1.1351,1.1723,1.2102,1.2474,1.2846,1.3218,1.359,1.396
     *,1.433,1.470,1.508,1.545,1.582,1.619,1.657,1.694,1.731/
      DATA PR,SC,ZMUREF/7.0,813.2,.001075/
      TYPE *,' ENTER NAME OF FILE'
      READ(5,10)ANAME
10    FORMAT(80A1)
      ANAME(80)=0.
      OPEN(UNIT=1,TYPE='NEW',ACCESS='DIRECT',INITIALSIZE=53,
     *  RECORDSIZE=346,ASSOCIATEVARIABLE=III,NAME=ANAME)
      TYPE *,' II,IN'
      READ(5,20)II,IN
20    FORMAT(I5)
      TYPE *,' TINF, SALINF, CC'
      READ(5,30)TINF,SALINF,CC
30    FORMAT(F10.0)
      DO 40 J=2,JNM
      D=2./(Y(J+1)-Y(J-1))
      BFS(J)=D/(Y(J)-Y(J-1))
      BFN(J)=D/(Y(J+1)-Y(J))
      BFNS(J)=BFS(J)+BFN(J)
      BWS(J)=ZMUREF*BFS(J)
      BWN(J)=ZMUREF*BFN(J)
```

```
      BWNS(J)=BWN(J)+BWS(J)
      BTS(J)=BWS(J)/PR
      BTN(J)=BWN(J)/PR
      BTNS(J)=BTS(J)+BTN(J)
      BSS(J)=BWS(J)/SC
      BSN(J)=BWN(J)/SC
      BSNS(J)=BSS(J)+BSN(J)
40    DDY(J)=Y(J+1)-Y(J-1)
      Y32=Y(3)**2
      Y22=Y(2)**2
      DY=Y(2)*Y32-Y(3)*Y22
      DYY=Y(JN)-Y(JNM)
      K=0
      III=1
      INM=IN-1
      WRITE(1,'III)II,INM,IN,PR,SC,ZMUREF,TINF,SALINF
     *,JJ,JNM,JN,THECON,FUSION,DIFCL,BWN,BWS,BWNS,BFN,BFS,BFNS,Y
      WRITE(1,'III)DDY,BTN,BTS,BTNS,BSN,BSS,BSNS,Y32,Y22,DY,DYY
     *,RPW,RPF,RPT,RPS,RPSOR,CC
      III=3
      CALL DENSIT(SALINF,TINF,ROINF)
      X1=0.
      DO 70 I=1,IN
      IF(I.EQ.1.OR.I.EQ.IN)GOTO50
      DX=2./(X(I+1)-X(I-1))
      BFW=DX/(X(I)-X(I-1))
      BFE=DX/(X(I+1)-X(I))
      BFEW=BFW+BFE
      BWW=ZMUREF*BFW
      BWE=ZMUREF*BFE
      BWEW=BWE+BWW
      BTE=BWE/PR
      BTW=BWW/PR
      BTEW=BTE+BTW
      BSW=BWW/SC
      BSE=BWE/SC
      BSEW=BSW+BSE
50    X1=X(I)
      T1(I)=-.003-.0527*S1(I)-.00004*S1(I)**2
      S1(I)=0.
      F1(I)=0.
      CALL DENSIT(0.,0.,RO1(I))
      DO 60 J=2,JN
      T1(J)=TINF
      S1(J)=SALINF
      F1(J)=0.
      W1(J)=0.
      VSQ1(J)=0.
```

```
      SOR1(J)=0.
      U1(J)=0.
      CALL DENSIT(S1(J),T1(J),RO1(J))
60    CONTINUE
70    WRITE(1,111)W1,F1,T1,S1,VSQ1,SOR1,RO1,BWE,BWW,BWEW,
     *BFE,BFW,BFEW,BTE,BTW,BTEW,BSE,BSW,BSEW,RSDUW,RSDUF
     *,RSDUT,RSDUS,X1,K,U1
      CLOSE(UNIT=1)
      STOP
      END
```

```
C     ***************************************************************
C     *        PROGRAM ' 41MA.FTN '---: MAIN PROGRAM.               *
C     ***************************************************************
      BYTE ANAME(80)
      COMMON/VORTIC/W1(41),W2(41),W3(41),RPW,RSDUW
      COMMON/STRFN/F1(41),F2(41),F3(41),RPF,RSDUF
      COMMON/TEM/T1(41),T2(41),T3(41),RPT,RSDUT
      COMMON/SAL/S1(41),S2(41),S3(41),RPS,RSDUS
      COMMON/VSQ/VSQ1(41),VSQ2(41),VSQ3(41),V2
      COMMON/SOR/SOR1(41),SOR2(41),SOR3(41),RPSOR
      COMMON/CONVE/AE(41),AW(41),AN(41),AS(41),AT(41)
      COMMON/DEN/RO1(41),RO2(41),RO3(41)
      COMMON/BW/BWE,BWW,BWEW,BWN(41),BWS(41),BWNS(41)
      COMMON/BF/BFE,BFW,BFEW,BFN(41),BFS(41),BFNS(41)
      COMMON/BT/BTE,BTW,BTEW,BTN(41),BTS(41),BTNS(41)
      COMMON/BS/BSE,BSW,BSEW,BSN(41),BSS(41),BSNS(41)
      COMMON/XY/Y(41),DDY(41),Y32,Y22,DY,DYY,X1,X2,X3
      COMMON/PROP/THECON,FUSION,DIFCL
      COMMON/VAR/JJ,JNM,JN,TINF,SALINF
      COMMON/VEL/U1(41),U2(41),U3(41)
      DATA RSW,RSF,RST,RSS/4*0./
      DATA RSDUW,RSDUF,RSDUT,RSDUS/4*0./
      DATA V1/0./
      TYPE *,' ENTER NAME OF DATA FILE'
      READ(5,10)ANAME
10    FORMAT(80A1)
      ANAME(80)=0
      OPEN(UNIT=1,TYPE='OLD',ACCESS='DIRECT',
     *  ASSOCIATEVARIABLE=III,FORM='UNFORMATTED',NAME=ANAME)
      III=1
      READ(1'III)II,INM,IN,PR,SC,ZMUREF,TINF,SALINF,
     *JJ,JNM,JN,THECON,FUSION,DIFCL,BWN,BWS,BWNS,BFN,BFS,BFNS,Y
      READ(1'III)DDY,BTN,BTS,BTNS,BSN,BSS,BSNS,Y32,Y22,DY,DYY
     *,RPW,RPF,RPT,RPS,RPSOR,CC
      TYPE *,' ENTER NMAX'
      READ(5,15)NMAX
15    FORMAT(I5)
      WREF=10.
      FREF=10.
      TREF=TINF
      SREF=SALINF
      IF(TINF.EQ.0.)TREF=1.
      IF(SALINF.EQ.0.)SREF=1.
      POM=1.
      TLEE=5.3+SALINF
      IF(TINF.GE.TLEE)POM=-1.
20    III=3
      READ(1'III)W1,F1,T1,S1,VSQ1,SOR1,RO1,BWE,BWW,BWEW
```

```
     *,BFE,BFW,BFEW,BTE,BTW,BTEW,BSE,BSW,BSEW,RW,RF,RT,RS
     *,X1,K,U1
        READ(1'III)W2,F2,T2,S2,VSQ2,SOR2,RO2,BWE,BWW,BWEW
     *,BFE,BFW,BFEW,BTE,BTW,BTEW,BSE,BSW,BSEW,RW,RF,RT,RS
     *,X2,K,U2
        I=II
        V1=0.
30      III=I+3
        READ(1'III)W3,F3,T3,S3,VSQ3,SOR3,RO3,BWE3,BWW3,BWEW3
     *,BFE3,BFW3,BFEW3,BTE3,BTW3,BTEW3,BSE3,BSW3,BSEW3,
     *RSDUW3,RSDUF3,RSDUT3,RSDUS3,X3,K,U3
        K=K+1
        DX=(X3-X1)*2.
        J=JJ
35      JP=J+1
        JM=J-1
        DV=DX*DDY(J)
        STNW=F1(JP)
        STWME=F1(J)-F3(J)
        STSW=F1(JM)
        STNMS=F2(JP)-F2(JM)
        STSE=F3(JM)
        STNE=F3(JP)
        G1PW=(STNMS+STNW-STSW)/DV
        G1PE=(STNMS+STNE-STSE)/DV
        G2PS=(STWME+STSW-STSE)/DV
        G2PN=(STWME+STNW-STNE)/DV
        AE(J)=ABS(G1PE)-G1PE
        AW(J)=ABS(G1PW)+G1PW
        AS(J)=ABS(G2PS)+G2PS
        AN(J)=ABS(G2PN)-G2PN
        AT(J)=AE(J)+AW(J)+AN(J)+AS(J)
        IF(J.EQ.JNM)GOTO 40
        J=J+1
        GOTO 35
40      CONTINUE
        J=JJ
50      ANUM=(AE(J)+BWE)*W3(J)+(AW(J)+BWW)*W1(J)
     * +(AN(J)+BWN(J))*W2(J+1)+(AS(J)+BWS(J))*W2(J-1)
     * +SOR2(J)
        ADNM=AT(J)+BWEW+BWNS(J)
        IF(ADNM.EQ.0.)GOTO 51
        CALL RESID(W2(J),ANUM,ADNM,WREF,RPW,RSDUW)
51      IF(J.EQ.JNM)GOTO 52
        J=J+1
        GOTO 50
52      CONTINUE
        J=JJ
```

```
   60     ANUM=BFE*F3(J)+BFW*F1(J)
     *  +BFN(J)*F2(J+1)+BFS(J)*F2(J-1)+W2(J)*RO2(J)
          ADNM=BFEW+BFNS(J)
          IF(ADNM.EQ.0.)GOTO 61
          CALL RESID(F2(J),ANUM,ADNM,FREF,RPF,RSDUF)
   61     IF(J.EQ.JNM)GOTO 62
          J=J+1
          GOTO 60
   62     CONTINUE
          J=JJ
   70     ANUM=(AE(J)+BTE)*T3(J)+(AW(J)+BTW)*T1(J)
     *  +(AN(J)+BIN(J))*T2(J+1)+(AS(J)+BTS(J))*T2(J-1)
          ADNM=AT(J)+BTEW+BTNS(J)
          IF(ADNM.EQ.0.)GOTO 71
          CALL RESID(T2(J),ANUM,ADNM,TREF,RPT,RSDUT)
   71     IF(J.EQ.JNM)GOTO 72
          J=J+1
          GOTO 70
   72     CONTINUE
          J=JJ
   80     ANUM=(AE(J)+BSE)*S3(J)+(AW(J)+BSW)*S1(J)
     *  +(AN(J)+BSN(J))*S2(J+1)+(AS(J)+BSS(J))*S2(J-1)
          ADNM=AT(J)+BSEW+BSNS(J)
          IF(ADNM.EQ.0.)GOTO 81
          CALL RESID(S2(J),ANUM,ADNM,SREF,RPS,RSDUS)
   81     IF(J.EQ.JNM)GOTO 82
          J=J+1
          GOTO 80
   82     CONTINUE
          DX=X2-X1
          DTDY=(Y32*(T2(2)-T2(1))-Y22*(T2(3)-T2(1)))/DY
          V2=THECON/RO2(1)/FUSION*DTDY
          S2(1)=DIFCL*S2(2)/(V2*Y(2)+DIFCL)
          IF(S2(1).LT.0.)S2(1)=0.
          T2(1)=-.003-.0527*S2(1)-.00004*S2(1)**2
          F2(1)=F1(1)-(RO1(1)*V1+RO2(1)*V2)/2.*DX
          U2(2)=DIFF(F2(3),F2(2),F2(1),Y(3),Y(2),Y(1))/RO2(2)
          W2(1)=(V2-V1)/DX-U2(2)/Y(2)
          F2(JNM)=F2(JN-2)
          F2(JN)=F2(JNM)
          DO 90 J=1,JN
   90     CALL DENSIT(S2(J),T2(J),RO2(J))
          VSQ2(1)=V2**2/2.
          DO 100 J=2,JNM
          JP=J+1
          JM=J-1
          U2(J)=DIFF(F2(JP),F2(J),F2(JM),Y(JP),Y(J),Y(JM))/RO2(J)
          V=-DIFF(F3(J),F2(J),F1(J),X3,X2,X1)/RO2(J)
```

```
      VSQ2(J)=(U2(J)*U2(J)+V*V)/2.
100   CONTINUE
      J=JJ
110   JP=J+1
      JM=J-1
      Y1=Y(JM)
      Y2=Y(J)
      Y3=Y(JP)
      SR1=DIFF(RO2(JP),RO2(J),RO2(JM),Y3,Y2,Y1)
      SR2=DIFF(RO3(JP),RO2(J),RO1(JM),X3,X2,X1)
      SS1=DIFF(VSQ3(JP),VSQ2(J),VSQ1(JM),X3,X2,X1)*SR1
      SS2=DIFF(VSQ2(JP),VSQ2(J),VSQ2(JM),Y3,Y2,Y1)*SR2
      SOROLD=SOR2(J)
      SOR2(J)=SOROLD+RPSOR*(SS1-SS2+POM*9.81*SR1-SOROLD)
      IF(J.EQ.JNM)GOTO 115
      J=J+1
      GOTO 110
115   CONTINUE
      III=I+2
      WRITE(1,'III)W2,F2,T2,S2,VSQ2,SOR2,RO2,BWE,BWW,
     *BWEW,BFE,BFW,BFEW,BTE,BTW,BTEW,BSE,BSW,BSEW,
     *RSDUW,RSDUF,RSDUT,RSDUS,X2,K,U2
      IF(I.EQ.INM)GOTO 130
      J=1
120   W1(J)=W2(J)
      W2(J)=W3(J)
      F1(J)=F2(J)
      F2(J)=F3(J)
      T1(J)=T2(J)
      T2(J)=T3(J)
      S1(J)=S2(J)
      S2(J)=S3(J)
      VSQ1(J)=VSQ2(J)
      VSQ2(J)=VSQ3(J)
      SOR1(J)=SOR2(J)
      SOR2(J)=SOR3(J)
      RO1(J)=RO2(J)
      RO2(J)=RO3(J)
      U1(J)=U2(J)
      U2(J)=U3(J)
      IF(J.EQ.JN)GOTO 125
      J=J+1
      GOTO 120
125   BWE=BWE3
      BWW=BWW3
      BWEW=BWEW3
      BFE=BFE3
      BFW=BFW3
```

```
      BFEW=BFEW3
      BTE=BTE3
      BTW=BTW3
      BTEW=BTEW3
      BSE=BSE3
      BSW=BSW3
      BSEW=BSEW3
      X1=X2
      X2=X3
      V1=V2
      RSW=AMAX1(RSW,RSDUW)
      RSF=AMAX1(RSF,RSDUF)
      RST=AMAX1(RST,RSDUT)
      RSS=AMAX1(RSS,RSDUS)
      RSDUW=0.
      RSDUF=0.
      RSDUT=0.
      RSDUS=0.
      I=I+1
      GOTO 30
130   DX=X2-X1
      DXX=X3-X2
      DO 140 J=1,JN
      W3(J)=W2(J)+((W2(J)-W1(J))/DX)*DXX
      F3(J)=F2(J)+((F2(J)-F1(J))/DX)*DXX
      T3(J)=T2(J)+((T2(J)-T1(J))/DX)*DXX
      S3(J)=S2(J)+((S2(J)-S1(J))/DX)*DXX
      U3(J)=U2(J)+((U2(J)-U1(J))/DX)*DXX
      RO3(J)=RO2(J)+((RO2(J)-RO1(J))/DX)*DXX
      VSQ3(J)=VSQ2(J)+((VSQ2(J)-VSQ1(J))/DX)*DXX
140   SOR3(J)=SOR2(J)+((SOR2(J)-SOR1(J))/DX)*DXX
      WRITE(1,'III)W3,F3,T3,S3,VSQ3,SOR3,RO3,BWE3,BWW3,
     *BWEW3,BFE3,BFW3,BFEW3,BTE3,BTW3,BTEW3,BSE3,BSW3,
     *BSEW3,RSW,RSF,RST,RSS,X3,K,U3
      WRITE(5,145)K,RSW,RSF,RST,RSS
145   FORMAT(I5,4E11.4)
      IF(AMAX1(RSW,RSF,RST,RSS).LT.CC.OR.K.GE.NMAX)
     *GOTO 150
      RSW=0.
      RSF=0.
      RST=0.
      RSS=0.
      GOTO 20
150   CONTINUE
      STOP
      END
```